NAVAL POSTGRADUATE SCHOOL

MONTEREY, CALIFORNIA

THESIS

THE ROLE AND VARIABILITY OF OCEAN HEAT CONTENT IN THE ARCTIC OCEAN: 1948–2009

by

Dominic F. DiMaggio

June 2014

Thesis Co-Advisors: Wieslaw Maslowski
Andrew Roberts

Approved for public release; distribution is unlimited

THIS PAGE INTENTIONALLY LEFT BLANK

REPORT DOCUMENTATION PAGE

Form Approved OMB No. 0704-0188

1. AGENCY USE ONLY ***(Leave blank)***	**2. REPORT DATE** June 2014	**3. REPORT TYPE AND DATES COVERED** Master's Thesis

4. TITLE AND SUBTITLE
THE ROLE AND VARIABILITY OF OCEAN HEAT CONTENT IN THE ARCTIC OCEAN: 1948–2009

5. FUNDING NUMBERS

6. AUTHOR(S) Dominic DiMaggio

7. PERFORMING ORGANIZATION NAME(S) AND ADDRESS(ES)
Naval Postgraduate School
Monterey, CA 93943-5000

8. PERFORMING ORGANIZATION REPORT NUMBER

9. SPONSORING /MONITORING AGENCY NAME(S) AND ADDRESS(ES)
N/A

10. SPONSORING/MONITORING AGENCY REPORT NUMBER

11. SUPPLEMENTARY NOTES The views expressed in this thesis are those of the author and do not reflect the official policy or position of the Department of Defense or the U.S. Government. IRB protocol number ____N/A____.

12a. DISTRIBUTION / AVAILABILITY STATEMENT
Approved for public release; distribution is unlimited

12b. DISTRIBUTION CODE
A

13. ABSTRACT (maximum 200 words)
The observed rate of sea ice cover decline in the Arctic for the past decades is faster than those projected by the recent Coupled Model Intercomparison Project (CMIP5). I hypothesize that a critical source of energy in the Arctic Ocean, heat content accumulating below the surface mixed layer and above the halocline, has been increasing in magnitude and area, and may be contributing to the recent decline in the ice cover. Consistent with observations, model results from a subset of the Regional Arctic System Model (RASM) indicate that heat has been stored between the mixed layer and the halocline, and that it has increased during the period of 1948 to 2009. Ongoing analyses show that the total amount and rate of increase of heat content has been largest in the western Arctic, and there is a causal relationship between the accumulation of heat content and the reduction of sea ice volume. Future studies involving new observations of physical processes and feedbacks in the western Arctic Ocean, and higher resolution and coupled climate models with improved representation of such processes and feedbacks are needed to advance understanding, realistic modeling, and improved prediction of the Arctic System and its variability and change.

14. SUBJECT TERMS Arctic oceanography, ocean heat content, climate change and prediction, Regional Arctic System Model, Ice-Tethered Profiler

15. NUMBER OF PAGES
159

16. PRICE CODE

17. SECURITY CLASSIFICATION OF REPORT	**18. SECURITY CLASSIFICATION OF THIS PAGE**	**19. SECURITY CLASSIFICATION OF ABSTRACT**	**20. LIMITATION OF ABSTRACT**
Unclassified	Unclassified	Unclassified	UU

NSN 7540-01-280-5500

Standard Form 298 (Rev. 2-89)
Prescribed by ANSI Std. 239-18

THIS PAGE INTENTIONALLY LEFT BLANK

Approved for public release; distribution is unlimited

THE ROLE AND VARIABILITY OF OCEAN HEAT CONTENT IN THE ARCTIC OCEAN: 1948–2009

Dominic F. DiMaggio
Lieutenant, United States Navy
B.S., University of Arkansas, 2004

Submitted in partial fulfillment of the
requirements for the degree of

MASTER OF SCIENCE IN METEOROLOGY AND PHYSICAL OCEANOGRAPHY

from the

NAVAL POSTGRADUATE SCHOOL
June 2014

Author: Dominic F. DiMaggio

Approved by: Wieslaw Maslowski
Thesis Co-Advisor

Andrew Roberts
Thesis Co-Advisor

Peter Chu
Chair, Department of Oceanography

THIS PAGE INTENTIONALLY LEFT BLANK

ABSTRACT

The observed rate of sea ice cover decline in the Arctic for the past decades is faster than those projected by the recent Coupled Model Intercomparison Project (CMIP5). I hypothesize that a critical source of energy in the Arctic Ocean, heat content accumulating below the surface mixed layer and above the halocline, has been increasing in magnitude and area, and may be contributing to the recent decline in the ice cover. Consistent with observations, model results from a subset of the Regional Arctic System Model (RASM) indicate that heat has been stored between the mixed layer and the halocline, and that it has increased during the period of 1948 to 2009. Ongoing analyses show that the total amount and rate of increase of heat content has been largest in the western Arctic, and there is a causal relationship between the accumulation of heat content and the reduction of sea ice volume. Future studies involving new observations of physical processes and feedbacks in the western Arctic Ocean, and higher resolution and coupled climate models with improved representation of such processes and feedbacks are needed to advance understanding, realistic modeling, and improved prediction of the Arctic System and its variability and change.

THIS PAGE INTENTIONALLY LEFT BLANK

TABLE OF CONTENTS

LIST OF FIGURES

THIS PAGE INTENTIONALLY LEFT BLANK

LIST OF TABLES

THIS PAGE INTENTIONALLY LEFT BLANK

LIST OF ACRONYMS AND ABBREVIATIONS

AC	Arctic Council
ASM	Arctic System Model
AWPPA	Arctic Waters Pollution Prevention Act
CAA	Canadian Arctic Archipelago
CESM	Community Earth System Model
CICE	Sea Ice model
CORE2	Common Ocean Reference Experiment version 2
CTD	conductivity, temperature, and depth sensor
DOD	Department of Defense
FAO	Food and Agriculture Organization of the United Nations
GCMs	General Circulation Models
HD	halocline depth
IASC	International Arctic Science Committee
IPCC	Intergovernmental Panel on Climate Change
ITP	Ice-Tethered Profiler
JCOMM	Joint World Meteorological Organization-Intergovernmental Oceanographic Commission Technical Commission for Oceanography and Marine Meteorology
LANL	Los Alamos National Laboratory
MLD	mixed layer depth
N^2	Buoyancy frequency
NAME	NPS Arctic Modeling Effort
NCAR	National Center for Atmospheric Research
NPS	Naval Postgraduate School
NSIDC	National Snow and Ice Data Center
NSR	Northern Sea Route
NSRIO	Northern Sea Route Information Office
NSTM	Near Surface Temperature Maximum
NWP	Northwest Passage
ONR	Office of Naval Research

OSD	Office of the Secretary of Defense
POP	Parallel Ocean Program model
RASM	Regional Arctic System Model
RSM	Regional System Model
SSM/I	Special Sensor Microwave/Imager
TFCC	Task Force Climate Change
TPR	Trans-Polar Route
UNCLOS	United Nations Convention on the Law of the Sea
USGS	United States Geological Survey
VIC	Variable Infiltration Capacity land hydrology model
PSU	practical salinity units
WHOI	Woods Hole Oceanographic Institution
WMO	World Meteorological Office
WRF	Weather Research and Forecasting model

ACKNOWLEDGMENTS

I would like to acknowledge the great deal of support I have received during these past years while working on this research. First, I thank my advisors, Wieslaw Maslowski and Andrew Roberts. Wieslaw's dedication to the highest standards and ability to focus my efforts have been instrumental to my work. Andrew has shown me great patience and understanding, all the while showing me the inner workings of how to conduct top-quality research. I have greatly enjoyed working with these two intelligent and passionate scientists. Jackie Clement-Kinney and Robert Osinski have also been key contributors to my research, and I want to acknowledge their assistance in using and understanding the group's models.

I would like to thank all of the faculty and staff at Naval Postgraduate School for such an amazing education. I have also received a great deal of advice and mentorship from a number of men and women in the Naval Oceanography team and my current and former communities. I would especially like to thank Captain Tony Miller, Commander Nick Vincent, Commander William Sommer, Commander Micah Weltmer, Lieutenant Commander Doug Pearman, Dr. Gay Stewart, Mr. Mike Cook, and Mr. Warren Finch for all of their advice, mentorship, and support. My classmates and fellow students have also been a big help these past two years, and I am grateful to call them all friends.

My mother and father, and my brothers and sisters have all been an inspiration to me. They set the bar high with their actions, and motivate me to achieve beyond my own expectations. Finally, I wish to thank my wife, Cassidy, and our children, Michael and Ivy. They deserve my deepest gratitude and admiration for their patience during these especially grueling last months. All of my hard work and effort is enabled by their love and support.

THIS PAGE INTENTIONALLY LEFT BLANK

I. INTRODUCTION

A. BACKGROUND: GLOBAL CLIMATE CHANGE AND THE ARCTIC

The global climate system is changing. There is overwhelming evidence that our planet has entered a period of significant change with respect to a number of climate indicators (IPCC 2013). The average global surface temperature has increased by about 1^{o}C since the 1800s, upper ocean heat content has increased linearly by 17×10^{22} J since 1971, and average sea level has risen by 0.19 m (IPCC 2013). The polar regions especially have undergone significant change as part of the global system. Ice sheets on Greenland and Antarctica have been losing mass on the order of tens of gigatons per year since the early 1990s, Northern Hemisphere snow cover has decreased by 1.6 to 11.7 percent per decade in the last six decades (IPCC 2013), and as much as 17.8 percent decrease per decade for the month of June indicating an earlier onset of spring melt in the Arctic (Derksen and Brown 2012). Air temperatures near the surface in the Arctic have increased almost twice as much as at lower latitudes (IPCC 2013), and this so-called "polar amplification" is an active field of research. As lower latitudes experience warming, poleward transport of sensible and latent heat is increased, thereby amplifying the net warming in the Arctic (e.g., Langen and Alexeev 2007). Similarly, Screen and Simmonds (2010) concluded that diminishing Arctic sea ice is also a key contributor to polar amplification. They suggest that a larger open ocean fraction is increasing the humidity of the lower atmosphere, which then traps more heat (Screen and Simmonds 2010). Northern Hemisphere permafrost has warmed by more than 2^{o}C since 1975 (IPCC 2013). Melting of all permafrost in Northern Hemisphere could release up to 1650 petagrams of carbon, with potential large positive feedbacks to atmospheric "greenhouse gases" (Treat and Frolking 2013).

Perhaps the most noticeable regional change anywhere on Earth has been in Arctic sea ice volume. To exclude the influence of glaciers, ice sheets, and other land-based sources of ice, sea ice is defined as water of oceanic origin that has frozen into ice. Sea ice in the Arctic varies seasonally and is heavily influenced by both short-scale weather events as well as longer duration climate variations. Generally, Arctic sea ice

melts in the summer and reaches a minimum extent of about 5 to 8 million square kilometers in September, and regrows during the winter to a maximum extent of about 14 to 16 million square kilometers in March (NSIDC 2014). Since 1979 the Northern Hemisphere summer minimum ice extent, defined as the ocean area with at least 15% ice concentration, has decreased by about 11% per decade, reaching a record minimum of only 3.1 million square kilometers (Stroeve et al. 2011; Polyakov et al. 2013; IPCC 2013). Sea ice also drifts and deforms under atmospheric and oceanic forcing, so thickness is not uniform temporally or spatially. However, sea ice generally thickens during the winter and thins during the summer. Since 1979, limited observations by submarine and satellite show that sea ice thickness has decreased by an average of 1.8m (e.g., Wadhams and Davis 2000; Kwok and Rothrock 2009). Arctic sea ice is retreating non-uniformly in space. The western Arctic has shown a greater loss of sea ice than the eastern Arctic. Figure 1 provides the Arctic sea ice concentration as measured by the special sensor microwave/imager (SSM/I) during three summer sea ice minima, September 1980, 2002, 2005, 2007, and 2012. The ice extent in September 1980 was 7.5 million km^2 and was representative of the long term mean over 1979–2000. Since the late 1990s, a new record summer minimum has been set every 2–5 years, starting in 2002, through 2005, followed by 2007 with the latest record broken again in 2012. This figure illustrates how the western Arctic sea ice is retreating at a much greater rate than in the east, and understanding the cause of this asymmetrical change is a yet unresolved issue.

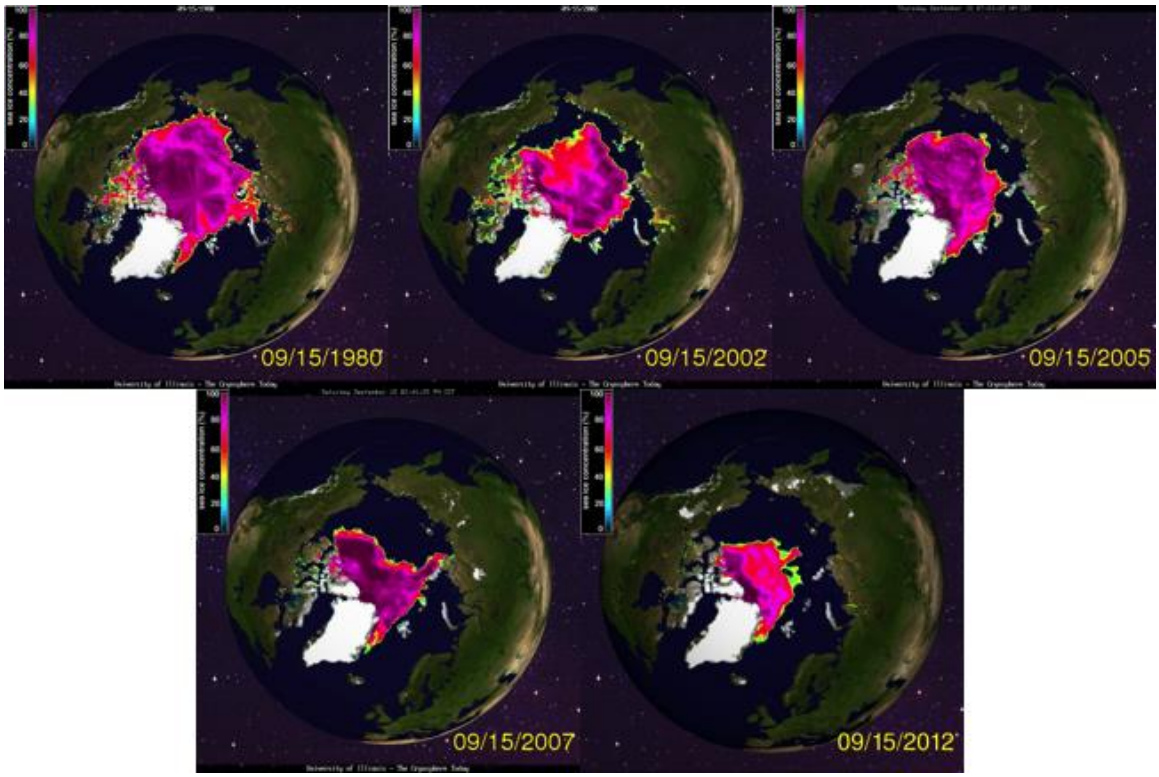

Figure 1. Arctic sea ice concentrations for September 15, 1980, 2002, 2005, 2007, and 2012 as measured by SSM/I (from The Cryosphere Today 2014).

Changes in Arctic sea ice may have a significant impact on the global climate, possibly amplifying global warming. The global linkage is best explained starting with a discussion of a set of processes contributing to the so-called ice-albedo feedback loop. The thermal conductivity of ice is quite low (~2 W/mK; Wadhams 2000), and that of snow is even lower (~0.3 W/mK; Lecomte et al. 2013). Sea ice albedo values range from 0.5 to 0.7, with older ice having higher values. Additionally, sea ice is usually covered with snow, increasing the albedo to over 0.8 (Perovich 1998). Therefore, the snow and ice covered ocean is well insulated from both atmospheric heating and solar radiation. During the melt season, between March and September, the relatively warm atmosphere provides a source of heating to the surface of the snow and ice. During the melt cycle, sea ice undergoes a broad spectrum of albedo values from approximately 0.77 to less than 0.1 (Briegleb and Light 2007). As the albedo decreases, the amount of solar radiation absorbed increases, accelerating the melting process, leading to a larger open water

fraction, which further lowers the surface albedo (open water has an albedo of 0.06, Perovich 1998), resulting in a positive ice-albedo feedback loop. For example, during the extreme minimum ice extent of 2007, Perovich et al. (2008) showed that there was an increase of 500% of solar heating to the upper ocean. Warming is not the only factor in the ice-albedo feedback loop. Momentum flux from the atmosphere or ocean may deform ice to the point of opening of leads. These areas of open ocean between ice floes reduce the overall ice concentration. This lowers the area-averaged albedo of the surface due to an increased open water fraction, and in the presence of solar radiation, contributes to the ice-albedo feedback.

Changes in the surface albedo driven by small-scale processes, when integrated over the Arctic Ocean, can play a role at global scales as well. Perovich et al. (2007) showed that as the Arctic sea ice has decreased in concentration, the increased open water fraction and subsequent decrease in overall albedo in the Arctic Ocean has resulted in an increase of solar heat input to the global ocean by as much as 4% a year. This has allowed for an additional 2.9 ZJ (or 2.9×10^{21} J) of heat being input to the Arctic directly from the sun between 1979 and 2005. This amount is considered a lower limit because it ignores solar radiation that penetrates thin ice and melt ponds as well as laterally advected heat from lower latitudes (Perovich et al. 2007). This additional heat has the potential to melt additional sea ice and effectively increase the net global heating of Earth by the sun. Understanding both the small-scale and large-scale thermodynamic and dynamic processes associated with melting ice is key to understanding both regional and global climate change.

B. MODELING THE GLOBAL AND ARCTIC SYSTEMS

To better understand how and why the Arctic is changing, and the implications for the global climate system, there is a large multinational effort to better match computer simulations and measurements of Arctic changes. These models can roughly be grouped into three categories: process studies, circulation models, and Earth system models. Models used in process studies typically have a small enough temporal and spatial domain that allows for resolutions high enough to resolve, or at least well-represent,

small scale processes such as turbulent mixing, which in the ocean occurs on horizontal and vertical length scales on the order of 1 m and temporal scales of 1 minute (McPhee 2008). In certain configurations, this type of model can be run in large ensembles, allowing for the exploration of parameter space and sensitivities. However, these types of models are generally too simple or too narrow in scope to capture all of the dynamics and exchanges of multiple variables across spatial scales and components of the Earth system.

General circulation models (GCMs) are larger in scale, and often couple multiple components, such as the atmosphere, cryosphere, or ocean, though some are still stand-alone, i.e., dedicated solely to a single component. These models simulate either the entire globe or a region, typically only with boundary conditions provided for the top of the atmosphere, and via atmospheric constituents, including methane and carbon dioxide. The strength of these models lies in their ability to represent the dynamics of the physical processes in the climate system on timescales allowing a centennial signal, such as greenhouse gas forcing. The choice of model domain, complexity and length of simulation comes with a cost, however. The more complex models are, the more computationally resources they require to run. In order to represent the climate system across many years for the entire globe, GCMs run at resolutions that are lower than what might be necessary to completely represent significant processes. For example, the general circulation components of the Community Climate System Model (CCSM) resolve the atmosphere and ocean resolution of about 1^{o}, which equates to approximately 111 km between resolved grid points. The Max Planck Institute for Meteorology circulation model is also considered to be well performing, though its atmospheric spatial resolution is only 1.8^{o}, approximately 200 km (Stevens et al. 2012). It has been demonstrated that mesoscale processes are not well represented in the Arctic region at resolutions lower than 10km in the atmosphere and a few km in the ocean (DuVivier and Cassano 2013; Maslowski et al. 2008). At resolutions below these, process such as oceanic mesoscale eddies, buoyancy-driven coastal and boundary currents, vertical stratification, surface and bottom mixed layers, sea ice thickness distribution, concentration, deformation, drift and export, and air-ice-sea interactions and coupling can all be misrepresented or even completely omitted (Maslowski et al. 2012).

Giorgi (2005) argued that models used to understand climate change must include all important climate system processes and feedbacks, and they must be configured at high enough resolution and with high enough efficiency to allow ensemble runs to generate robust statistics. Consequently, Earth System Models (ESMs) expand on GCMs to include ice sheets and glaciers as well as biological, geophysical and chemical (BGC) connections and feedbacks. Most importantly, ESMs incorporate the carbon cycle along with other greenhouse gas feedback processes (e.g., Flato 2011; Hurrell et al. 2013). Like ESMs, Regional System Models (RSMs) couple geophysical components with biological and chemical ones, but limit their spatial domains in favor of increased model resolution and ensemble generation for stochastic analysis. RSMs can resolve many unresolved or under-represented processes in individual components, and can better represent coupling channels between different components. RSMs can be utilized in conjunction with ESMs and GCMs in a hierarchical approach to complement each other and to reduce uncertainty (Maslowski et al. 2012).

C. THE ROLE ARCTIC OCEAN HEAT CONTENT IN THE GLOBAL CLIMATE SYSTEM

To better understand the Arctic's role in the Earth's climate system and the particular changes within the Arctic, one must thoroughly investigate the processes that control or contribute to those changes. While much research has been done in understanding atmospheric and surface thermodynamic processes, often overlooked is the fact that over 90% of the recent change in global heat has taken place in the oceans (IPCC 2013). In particular, the Arctic Ocean possesses a unique distribution of water mass properties that determine how heat energy is stored and exchanged with the sea ice, atmosphere, and the rest of the global ocean. Understanding where in the ocean this heat is stored and how it is changing at seasonal and longer time scales is essential to establishing the Arctic's global influence.

The Arctic Ocean exhibits strong stratification at various depths due to layered water masses of differing origins and properties. The deepest water masses in the Arctic are the deep and bottom waters, which are generally deeper than 1000 m. Because of the strong stability in the upper part of the Arctic Ocean, these deep waters have little effect

on the heat content near the surface (Rudels 2012). Above these deep waters are several water masses of varying properties. For the purposes of this thesis, these water masses will be grouped into one of three layers: surface mixed layer, the Atlantic Layer, and a layer that this study will call the "halocline complex" layer. Each of these layers will be described below.

The shallowest layer in the Arctic Ocean is the surface mixed layer. The properties of this layer vary throughout the season, and are dominated by the annual freeze-melt and river runoff cycle. In addition, wind mixing is another important factor, especially during summer when sea ice decreases in concentration and allows more momentum transfer from the atmosphere into the ocean. After the melt season, the below freezing atmospheric temperatures induce upward heat flux from the ocean surface, cooling the surface water. As ice forms, salt molecules are rejected from the crystallizing water, increasing the salinity of the brine intrusions in sea ice. The hyper-saline, and much denser, water is squeezed out of the crystalline matrix into channels that allow it to drain from the sea ice structure. This process, known as brine rejection, is a source negative buoyancy at the base of sea ice, and helps to destabilize the shallow waters, as salinity controls density in the Arctic Ocean. This destabilizes the shallow waters and convection occurs. In the central Arctic the resulting convection often reaches a depth of 12 m and occasionally up to 40 m (Toole et al. 2010). Once sea ice forms, snow can accumulate, insulating the ocean from atmospheric cooling.

In addition to heat fluxes being increased during the melt season, melting snow and ice on both land and the sea contribute to a positive buoyancy flux at the surface. Additional freshwater sources include river inflow, land drainage, and low salinity inflow through the Bering Strait (Rudels 2012). This decrease in surface salinity increases the vertical density gradient, leading to a stronger stratification and reduced mixing across the base of the mixed layer. Therefore, the summer mixed layer is relatively shallow when compared to the winter mixed layer. In all seasons, however, the density gradient, or seasonal pycnocline, is strong, and commonly inhibits vertical mixing of water from below into the mixed layer (Toole et al. 2010).

Figure 2 is provided as a geographic reference for the following discussion. Steele et al. (1998) and Rudels et al. (2004) describe how water of Atlantic origin enters the Arctic basin, undergoes modifications, and gradually submerges beneath fresher and less dense surface waters. The Atlantic Layer is relatively warm (> 0 ^{o}C) and salty (~ 35 psu), and can be found throughout the central Arctic basin (Steel et al. 1998; Rudels et al. 2004; Rudels 2012). Above the Atlantic Layer, waters of various local and regional sources are less categorically defined and generally colder and fresher. A strong salinity gradient, or halocline, is ubiquitous in the Arctic, and marks the top of the Atlantic Layer. Any water that is above the halocline, but below the surface mixed layer, is being called "halocline complex" water.

This halocline varies in strength and depth throughout the Arctic. In the east, where Atlantic water enters the Arctic, the halocline is sharp and just below the surface mixed layer. In the west, however, water masses with other regional or local sources separate the Atlantic Layer from the surface mixed layer. Here, just below the surface mixed layer can be found the Near Surface Temperature Maximum (NSTM), remnants of the previous winter's mixed layer, Pacific Summer Water (PSW), and Pacific Winter Water (PWW) (Jackson et al. 2010). The properties and sources of these waters have been the focus of many studies (e.g., Okkonen et al. 2009; Jackson et al. 2010; Nguyen et al. 2011; Steele et al. 2011). Generally speaking, these waters of the western halocline complex have a relatively low temperature (near freezing temperature) and low salinity (~ 30-33 psu) (Nguyen et al. 2011). The halocline complex itself is stratified, though weakly, and heat close to the HD may not readily participate in occasional entrainment events. Figure 3 depicts the schematic general oceanic circulation in and around the Arctic Ocean, including the flow of warm Atlantic water at intermediate depths (red arrows) and colder and fresher upper ocean waters (blue arrows). Figure 4 is a schematic vertical cross section along the dotted line in Figure 2 and shows the general vertical structure of the Arctic Ocean. As the figure suggests, the boundaries of the Atlantic Layer and halocline complex are gradual and not at uniform depths. This figure depicts the mixed layer depth (MLD) at 50 meters, but as discussed previously, it varies seasonally and spatially.

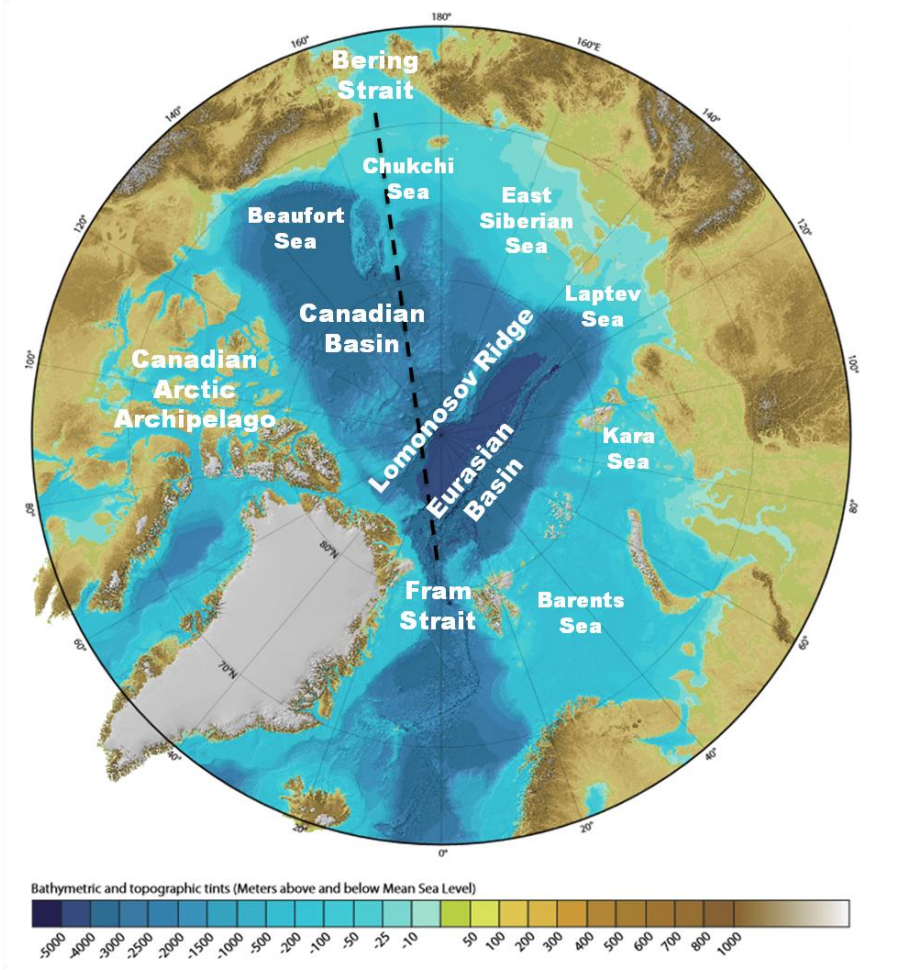

Figure 2. Annotated bathymetric/topographic map of the Arctic Region. The black dashed line is the approximate location of the cross section of Figure 4 (after Jakobsson et al. 2012).

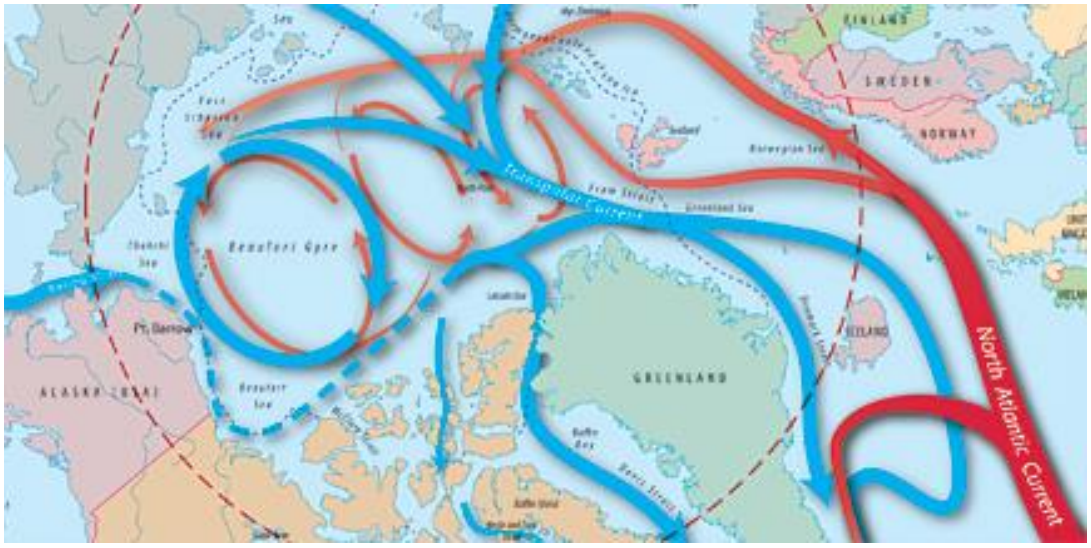

Figure 3. Schematic diagram indicating the general oceanic circulation in and around the Arctic Ocean (from WHOI 2014).

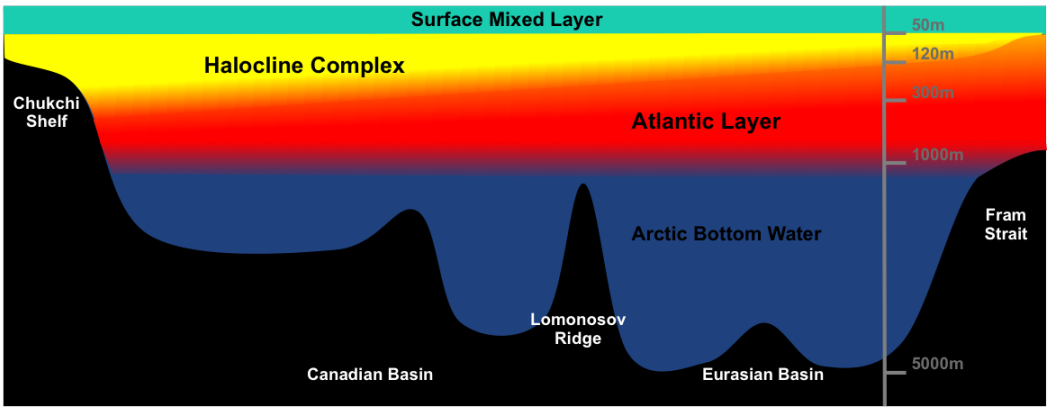

Figure 4. Schematic representation of the general layers in the Arctic Ocean in cross section from the Bering Strait to the Fram Strait. Features are not drawn to scale; the near-surface depths are exaggerated. The Lomonosov Ridge divides the Arctic into two basins, the Canadian Basin in the west, and the Eurasian Basin in the east. The shallowest layer is the Surface Mixed Layer which extends from the surface to approximately 50m. The second layer, which is defined in this thesis as the Halocline Complex Layer, extends from the Surface Mixed Layer down to the top of the Atlantic Layer. The Atlantic Layer reaches to a shallower depth in the east, where it enters the Arctic via the Fram Strait (author's own work).

D. INTENT OF STUDY

Ocean heat storage is a field of active oceanographic and climate research, and it has been increasing in the Aortic Ocean since the 1990s (Shimada et al. 2006; Jackson et al. 2011). Lique et al. (2012) used a high resolution (~10 km in the Arctic) model to identify spatial and temporal trends in heat content stored in the full ocean column. Toole et al. (2010) using ice tethered profilers (ITPs) showed that heat from below the mixed layer is unlikely to affect the surface, and therefore sea-ice. However, their study focused on the central Canada Basin far from major circulations or bathymetry features, which would result in a quiescent bias. Theses by NPS students Haynes (2010) and Mills (2011) using selected ITP data and output from the Naval Postgraduate School (NPS) GCMs and from the Regional Arctic System Model (RASM) showed that transient processes like ice deformation and eddies can potentially cause warmer water from below to be entrained into the mixed layer. Maslowski et al. (2014) also showed a positive lagged correlation between increasing modeled upper ocean heat content and decreasing ice thickness.

Previous studies of Arctic Ocean heat content have used arbitrary depth bands to analyze heat content, ignoring the fact that dynamical barriers commonly impede, if not completely prevent, ocean heat below the mixed layer from affecting sea-ice. The study by Lique et al. (2013) considered heat at all depths in the Arctic, while Maslowski et al. (2014) chose an arbitrary depth of 120 meters to be the lower bound for defining the upper ocean. The challenge is to choose depth limitations that are based on in-situ and/or modeled physical properties of the water. Any heat content calculation that includes the Atlantic layer within its depth limits will be dominated by the Atlantic layer heat and will not reflect the true amount of heat available to affect the surface waters and sea ice. Conversely, setting the depth limits too shallow will ignore some heat that should be considered.

In this study, as with Maslowski et al. (2014), only the heat from the subsurface upper ocean will be examined. For the purpose of this study, we define the upper ocean as the ocean layer below the surface mixed layer and above the halocline. The surface mixed layer will be excluded from heat content calculations to eliminate the seasonal heat signature that is determined by atmospheric radiative forcing. The lower limit of heat

content calculation will be set by the depth of the halocline, as opposed to an arbitrary depth, such as 120 m. In this way, only the heat that remains throughout the year and potentially available for melting ice will be analyzed.

The hypothesis being tested in this study is that heat content in the Arctic Ocean has been increasing and is contributing to the rapid and non-uniform sea ice retreat. To test this, subsurface ocean heat content available for entrainment into the surface mixed layer, will be analyzed on seasonal to inter-annual and multi-decadal time scales. Model results from a subset of RASM, consisting of an ice and ocean coupled components forced with realistic atmospheric forcing, along with available observational data will be examined to understand the temporal and spatial characteristics and evolution of heat content in this subsurface layer.

This thesis is organized into the following chapters: Chapter II discusses the relevance of climate modeling research in the pan-Arctic to the U.S. Navy, with an emphasis on the rate of ocean warming and sea-ice retreat; Chapter III describes the model and the data analysis methodology used to conduct this research; Chapter IV presents results from the analysis, and Chapter V synthesizes and discusses those results. Chapter V contains conclusions and makes recommendations for future research.

II. NAVY RELEVANCE

A. CHANGE AND UNCERTAINTY IN THE ARCTIC REGION

As climate of the Arctic region changes, so, too, changes the accessibility of the region. Civilian and military activities in the region are increasing, and many governments have a high stake in the Arctic, including those that border it, those looking to trade across it, and those hoping to exploit its natural resources. There are three sets of human activities that are transforming with great significance. These are: (i) maritime transit within and across the Arctic, (ii) the extraction of natural resources, and (iii) the unique culture of the indigenous peoples of the Arctic. Any alteration of those three activities could have global political and military consequences.

1. Maritime Transport

The World Meteorological Organization defines the "open sea" as ocean area with less than 10% sea ice concentration that is also free of ice of land origin (e.g., icebergs) (JCOMM 2014). As the Northern Hemisphere sea ice edge retreats north, greater expanses of open water exist. The sea ice in winter still extends across the Arctic Ocean and into the sub-polar North Pacific and North Atlantic, but the minimum sea ice extent in the summer allows for increased maritime transit in and across the Arctic Ocean. These additional sea routes could become important highways connecting the populations and industrial production centers, the majority of which are in the Northern Hemisphere (Ostreng 2012). Like the Mediterranean Sea was to the classical civilizations, the Arctic Ocean has the potential to become an intercontinental highway connecting East and West.

There are three potential routes for trans-Arctic maritime travel: the Northwest Passage (NWP), the Northern Sea Route (NSR), and the Trans-Polar Route (TPR) (TFCC 2014). Figure 5 depicts these three routes along with projections of future sea ice extent. All three of these routes include the Bering Strait between Alaska and Russia. Historically, these routes were covered in sufficiently thick and concentrated ice to deter commercial shipping throughout the year. Yet, in the five years from 2008 to 2013, there

was a 118 percent increase in maritime transit through the Bering Strait with over one million tons of cargo transported (U.S. Coast Guard [USCG] 2013). In 2012, ice conditions permitted 46 ships to transit the NSR from June to November, and in 2013, 71 ships transited the NSR during the same period, 10 of which were rated only for moderate to light ice conditions (NSRIO 2014), even though the arctic sea ice extent in 2013 was greater than in 2012. By 2025, it is projected that the NSR will be ice free for more than six weeks, allowing an estimated 450 transits (TFCC 2014). This route stays relatively close to the northern coast of Russia, and requires the passage through several straits, including the Kara Strait and Vilkitsky Strait, through Russian territorial waters. Therefore, Russia has claimed that navigation lanes used in the NSR are under full Russian control and jurisdiction (Ostreng 2012).

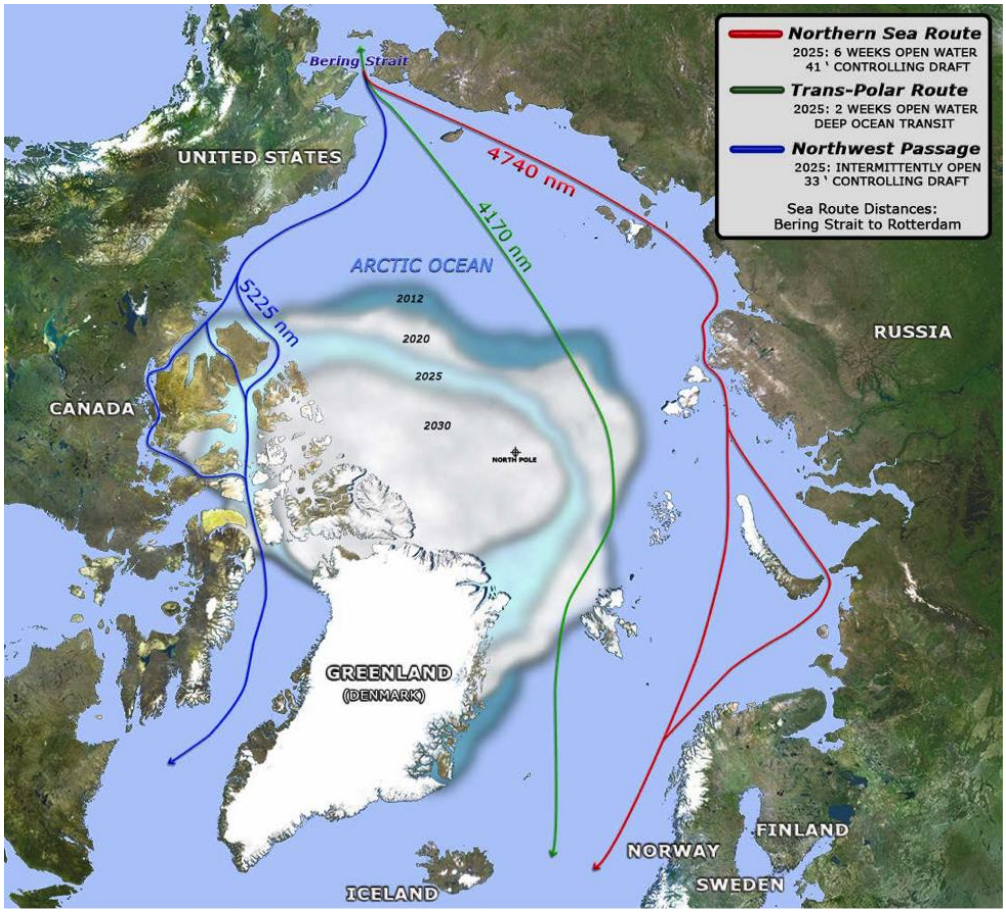

Figure 5. Anticipated Arctic transit routes with consensus projected sea ice extent minima (from Task Force Climate Change 2014).

The NWP, through the Canadian Arctic Archipelago (CAA), seems like an attractive alternative to the NSR. However, it still remains largely impassable to commercial traffic (Arctic Council 2009). The prevailing winds are directed such that drifting ice from the open sea is piled up along the northern extent of the CAA. The narrow channels between the islands trap sea ice, rather than continuing to circulate around the Arctic. Because of its high latitude, ice caught in the CAA will remain frozen throughout the year, becoming thicker and stronger multi-year ice (Howell et al. 2009). Another unique hazard of the NWP is the presence of pingos, ancient ice that is affixed to the bottom of shallow regions by frozen mud and clay (Ostreng 2012). Combined with the incomplete charting of the NWP, these ice hazards make the NWP a treacherous route for the next few decades (TFCC 2014). Despite the fact that Canada and the United States are close allies , a dispute exists between the two regarding the classification of the NWP. Canada sees the NWP as an internal waterway, while the U.S. would rather it be classified as an international strait of passage, similar to the Strait of Gibraltar or the Strait of Malacca (Ostreng 2012). Canada's primary concern for relinquishing jurisdiction to the international community stems from the *Arctic Waters Pollution Prevention Act* (AWPPA). This Canadian law establishes a 100 nautical mile environmental zone as a precaution against ship-based pollution (Ostreng 2012). This region is so far from existing emergency response infrastructure, a pollution event similar to the Exxon Valdez oil spill in the pristine ecosystem would be devastating.

The third route is the Trans-Polar Route (TPR). This route avoids current political boundaries by crossing through the seasonally open sea (see Figure 5). Although currently not open, it is projected that the ice will have retreated far enough for the TPR to be navigable for two to twelve weeks each summer by 2025 (TFCC 2014). This route is also the shortest and possibly the most economically sound (Humpert and Raspotnik 2012).

These routes are particularly attractive to commercial shippers currently vying routes between East Asia and Europe. The TPR offers a distance savings of up to 41% over the traditional routes via the Straits of Malacca and the Suez Canal, while the NWP and NSR offer a slightly less but still significant savings of 32% and 36%, respectively

(Humpert and Raspotnik 2012). Besides being shorter and cheaper, the Arctic routes bypass the highly congested and often dangerous regions of the South China Sea and the Arabian Sea. Threats of piracy, terrorism, and even collision exist in these regions, so it is no surprise that investors are looking for alternative routes (Humpert and Raspotnik 2012).

The Arctic routes are not without hazards. The tilt of the Earth's axis of rotation, relative to the elliptic, results in a reduction of solar energy reaching the Arctic for much of the year, and leaves it completely dark for weeks to months at a time. This lack of shortwave radiation input means that sea ice will always return in winter, closing the Arctic sea routes. The timing of route closure and poorly forecast sea ice drift will remain a serious threat to shipping during these so-called shoulder seasons (TFCC 2014). As long as some sea ice survives the summer, the possibility will remain of thick and hard multi-year ice floes being a hazard to even the most ice-strengthened ships. Polar lows, extremely violent storms found in high latitudes, can form in less than 48 hours and pose a serious challenge to operational weather forecasters (Turner et al. 2003). Cold atmospheric temperatures any time of year can cause sea spray to freeze on the superstructures of ships, leading to material damage and even capsizing. Therefore, before the Arctic can become a reliable route of commercial transit, significant advances must be made in weather forecasting and climate prediction, not to mention government cooperation.

2. Natural Resources

Interest in the Arctic region includes more than just maritime transportation. A recent United States Geological Survey estimates that there are 90 billion barrels of oil, 1669 trillion cubic feet of natural gas, and 44 billion barrels of liquid natural gas in the Arctic, with over 80% of these resources off shore (USGS 2008). The same study found that the already explored oil and gas fields off the shores of Alaska, Canada, and Russia comprise roughly 10% of the world's known petroleum resources (USGS 2008). This has caught the attention of oil companies, which have so far invested over $3.7 billion for offshore drilling leases (USCG 2013).

There are other significant resources that are becoming more available as perennial sea ice extent is reduced. There are major sources of nickel, iron, and other valuable metals and minerals in the Arctic (Ostreng 2012). Perhaps the natural resource that has the greatest potential for disrupting the global economy is fishing. According to Food and Agriculture Organization of the United Nations (FAO 2014), the world consumes more than 156 million tons of fish every year. This amounts to a $130 billion industry (FAO 2014). The Bering Sea alone supports a $4 billion a year fishing industry (Hufford 2009). Sigler (2009) found that cold water species of fish are moving north, and at least six species have moved from the Bering Sea past the Bering Strait into the Beaufort Sea (Logerwell 2008). However, besides the risks of ocean acidification and unsustainable fishing practices, fish stocks are at risk due to warming oceans and retreating sea ice.

3. Arctic Indigenous Peoples

Indigenous peoples, whose culture and very survival depend on a balanced Arctic ecosystem, are being threatened. Their livelihood is based largely on the hunting of marine mammals and relies on the pre-industrial seasonality of sea ice. The cities themselves are at risk of crumbling as the permafrost below their foundations melt and become unstable. These communities are becoming more reliant on external supply, increasing the demand for maritime transport in the region. The indigenous cultures are also threatened by dilution and displacement by encroachment of external interests. Despite these pressures, the Arctic peoples often describe themselves as resilient and adaptable (Arctic Centre 2014).

B. POLITICAL DISCORD

With changes to the economic and industrial status come disagreements, especially over jurisdiction and economic exclusivity. Contested jurisdiction of the maritime transit lanes described previously is not the only source of conflict in the Arctic. Currently, there exists a number of agreements, treaties, and other sources of authority in the region between various groups of nations and non-state entities, some of which overlap or conflict (Berkman and Young 2009; Koivurova and Molenaar 2009). Two of

the strongest sources of authority are the United Nations Convention on the Law of the Sea (UNCLOS) and the Arctic Council (AC). Signers of the UNCLOS treaty agree to respect each other's exclusive economic use of the waters out to 200 nautical miles from shore. However, a country may extend its economic exclusivity of sea-bed activities to the entire adjacent continental shelf, if proven to be contiguous to their territory (United Nations 2014). Such extended continental shelf claims have been made in the Arctic by Russia and Norway, while other countries are expected to follow suit (Berkman and Young 2009). Figure 6 shows a depiction of the current and anticipated claims to sea-floor exclusivity as an illustration of the sources of potential dispute.

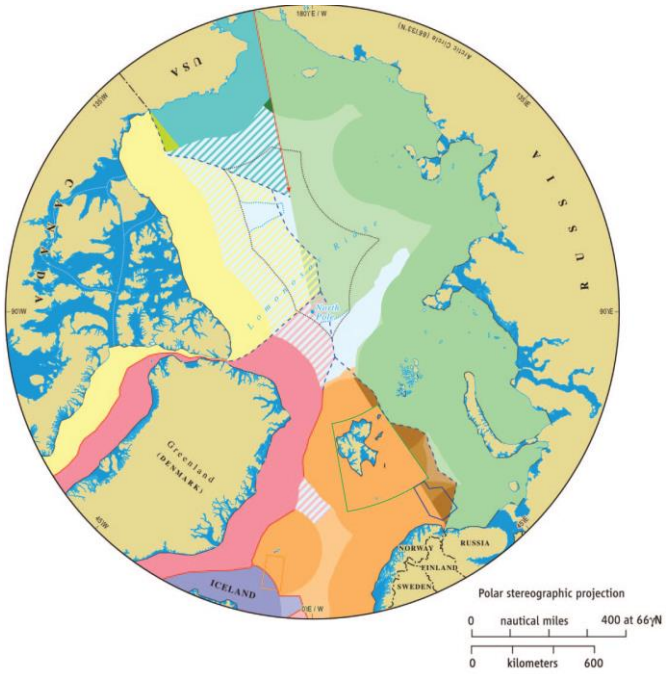

Figure 6. Representation of the current and potential claims to sea floor exclusivity colored by country. Solid colors are EEZ, light colors are potential extended continental shelf claims, and hatched areas are contested or potentially contested claims (from Berkman and Young 2009).

The United States is directly involved in several of these regional disagreements. As previously mentioned, a border dispute exists between the U.S. and Canada over use of the seafloor between Alaska and Yukon (Berkman and Young 2009). The U.S. is one

of a very few coastal nations that has not signed the UNCLOS treaty, placing Americans on the sidelines of any discussions or agreements. The U.S. is, however, a member of the Arctic Council. This council was founded in 1996 "as a high level intergovernmental forum to provide a means for promoting cooperation, coordination and interaction among the Arctic States, with the involvement of the Arctic Indigenous communities and other Arctic inhabitants" (Ottawa Declaration 1996). This council has been successful in negotiating a number of agreements from protecting indigenous culture to proper nuclear waste disposal; however, its effectiveness is limited by a clause in its charter explicitly forbidding matters of military security from being addressed (Berkman and Young 2009).

C. U.S. ARCTIC STRATEGY

Due to the harsh physical environment, increased human presence in the Arctic increases the risk of environmental and humanitarian disasters. Necessarily, the U.S. must consider its interests and responsibilities with respect to the Arctic. The *National Security Strategy* is the fundamental document upon which strategic planning is derived, and it states that the "United States is an Arctic Nation with broad and fundamental interests in the Arctic region" (White House 2010). In order to more directly address the roles and responsibilities of America in the Arctic, the *National Strategy for the Arctic Region* was released (White House 2013) with the Implementation Plan for the National Strategy for the Arctic Region following earlier this year (White House 2014).

In the *National Strategy for the Arctic Region*, three lines of effort are outlined:

- Advance United States Security Interests
- Pursue Responsible Arctic Region Stewardship
- Strengthen International Cooperation

with the following guiding principles:

- Safeguard Peace and Stability
- Make Decisions Using the Best Available Information
- Pursue Innovative Arrangements
- Consult and Coordinate with Alaska Natives

While the *National Strategy for the Arctic Region* addresses broad national goals, the Department of Defense issued a new policy for defense-specific guidance. The *Department of Defense (DOD) Arctic Strategy* identifies the desired end-state for the Arctic as "a secure and stable region where U.S. national interests are safeguarded, the U.S. homeland is protected, and nations work cooperatively to address challenges" (Office of the Secretary of Defense [OSD] 2013). The two main supporting objectives of the *DOD Arctic Strategy* are to "ensure security, support safety, and promote defense cooperation" and "prepare to respond to a wide range of challenges and contingencies" (OSD 2013). Secretary of Defense Chuck Hagel spoke about this new policy saying,

> The effects of climate change and new energy resources are far-reaching and unpredictable, demanding our attention and strategic thinking. While the opening of the Arctic will create unprecedented changes, it will also create historic opportunities. It could open up new avenues for commerce and establish new areas for cooperation between nations in the interests of all people. (Showstack 2013)

This comprehensive approach to our nation's responsibilities in the Arctic specifically identifies a need for better information regarding the current status and predictions about the future state of the Arctic (White House 2013). The *DOD Arctic Strategy* addresses this by saying that the DOD, "will leverage work done by the scientific and academic communities and seek opportunities to contribute to the observation and modeling of the atmosphere, ocean, and sea ice conditions ... to enhance military environmental forecasting capabilities" (OSD 2013). These policy documents are broadly applied to all U.S. defense activities. Since the Arctic region is primarily a maritime one, the U.S. Navy has issued follow-on guidance.

D. THE ROLE OF THE U.S. NAVY IN THE ARCTIC: CAPABILITIES, LIMITATIONS, AND OPPORTUNITIES

In 2009, four years before the release of the *National Strategy for the Arctic Region*, the Navy proactively established a working group to address how the Navy should respond to potential operations in the Arctic. This group, called Task Force Climate Change (TFCC), was tasked with "recommending policy, strategy, roadmaps, force structure, and investments for the Navy regarding the Arctic and Climate Change"

(Department of the Navy 2009). TFCC's initial report, the *U.S. Navy Arctic Roadmap* was published in 2009 and it was updated in 2014. This report states that although the Arctic region is currently an area of low threat and is expected to remain as such, the United States does have substantial security responsibilities. These include "threat early warning systems, freedom of navigation and overflight through the region, preventing terrorist attacks against the homeland, combined security obligations with Canada, and deployment of sea and are forces as required for deterrence, maritime presence, and maritime security operations" (TFCC 2014). In addition to the objectives defined by the DOD Arctic Strategy, the *Arctic Roadmap* identifies supporting objectives. In particular, the *Arctic Roadmap* states the objective: "engage public and private sector partners to improve domain awareness in the Arctic Region" (TFCC 2014).

The Arctic Roadmap Implementation Plan, included in the TFCC *U.S. Navy Arctic Roadmap 2014-2030*, specifies the ways in which the Navy will prepare to meet future requirements in the Arctic. Among the many action items listed, the following actions are pertinent to the present study:

- Provide science and technology plans for Arctic Assessment and Prediction to include Arctic Ocean circulation and stratification
- Increase the Office of Naval Research's Arctic Research Efforts...and predict the Arctic physical environment at a variety of time and space scales.
    - Sea ice extent forecasting and prediction
    - Ice and snow thickness prediction
    - Ice, sea, air interaction physics
    - Improve understanding of the physical environment and processes in the Arctic Ocean
- Encourage research into and development of comprehensive Arctic System Models (TFCC 2014)

As Defense Secretary Hagel pointed out, "But this won't happen on its own. We must wisely manage these 21st century possibilities" (Showstack 2013). The *DOD Arctic Strategy* also indicates that sufficient understanding must be gained of the changing Arctic conditions, "to balance the risk of having inadequate capabilities or insufficient capacity when required to operate in the region with the opportunity cost of making

premature and/or unnecessary investments" (OSD 2013). To this end, TFCC's Arctic Roadmap lists three phases of investment, investigation, and operation as "near-term," "mid-term," and "far-term" (TFCC 2014). The goals of the Navy in the near-term, which includes the present to 2020, are to maintain primary capability and presence via the undersea and air domains and to potentially incorporate the use of ice strengthened Military Sealift Command vessels. The near-term will also see an increased level of training, exercises, scientific missions, and personnel exchanges within the Arctic community. Much of the innovative efforts of the near-term will be along the lines of developing strategies, policies, plans, requirements, and investments into future Arctic operations. The mid-term, 2020–2030, will see an increased presence of surface vessels in the newly opened waters of the Arctic along with an increased complexity of exercises and training. In the far-term, 2030 and beyond, the Navy expects to supply the relevant Combatant Commanders with whatever maritime forces required for sustained Arctic operations. These operations are likely to include search and rescue, support to the international Defense Security Cooperation Agency, maritime security, and freedom of navigation (TFCC 2014).

E. THE ROLE OF NAVAL POSTGRADUATE SCHOOL

A common theme of the aforementioned guiding policies is the desire to reduce uncertainty about the future Arctic, especially its sea ice. Numerous Navy efforts, including those at the Naval Postgraduate School (NPS), are well underway at reducing that uncertainty. Models are of increasing importance for guiding the U.S. Department of Defense for both long term force strength planning, and to establish and operations capability in the Arctic based around being able to predict Arctic sea ice cover on daily to seasonal timescales. A collaborative effort is being led at NPS to advance understanding of past and present states of Arctic climate, in order to improve seasonal to decadal predictions of future Arctic conditions. The primary tool for this analysis is the NPS Arctic Modeling Effort (NAME) which uses a variety of coupled as well as stand-alone regional models to "resolve small-scale processes and feedbacks as well as to realistically represent large-scale climate variability and trends" (Maslowski 2013). Within this

context, this thesis focused on studying heat content in the Arctic serves several strategic roles. These are:

- Evaluating models and their ability to replicate observed changes
- Understanding climatological changes in the Arctic and how the ocean is contributing to them
- Understanding processes and feedbacks among them of relevance to arctic climate change

This thesis is also contributing to a broader understanding of important processes that models should include to improve predictions of sea ice loss. This will help reduce uncertainty of model projections, thereby reducing risk, and it will aid the U.S. Navy in making smarter decisions about investments and policy.

THIS PAGE INTENTIONALLY LEFT BLANK

III. OBSERVATIONS, MODEL DESCRIPTION, AND METHODS

A. OVERVIEW

This chapter discusses the data sets and methods used to determine the necessary quantities for calculations and analyses of ocean heat content. The variables that are analyzed include temperature, salinity, density, mixed layer depth (MLD), halocline depth (HD) and ocean heat content. For this study, we use data from both in-situ observations and numerical model hindcast. The observational data set is derived from the Woods Hole Oceanographic Institution (WHOI) Ice-Tethered Profiler (ITP) program. Model output is derived from the ice-ocean component of the Regional Arctic System Model (RASM), which is part of the larger NPS Arctic Modeling Effort (NAME). These two data sets are discussed in more detail below.

B. OBSERVATIONAL DATA SET: ICE-TETHERED PROFILERS

The Arctic Ocean is a difficult place to conduct observations. Harsh environmental conditions, remoteness, and lack of supporting infrastructure cause expeditions to be relatively expensive. Therefore, in-situ observational data sets have traditionally been sparse. Autonomous sensing systems, such as the Argo program, have been developed to overcome this data gap and provide continuous monitoring of parameters such as temperature, salinity, and velocity (Argo 2014). The ITP (Figure 7) was developed to withstand the unique conditions of the polar regions and is capable of returning in real time, with better than 1 m vertical resolution, profiles of temperature and salinity. The ITP is a Lagrangian platform that is tethered to, and drifts with, an ice floe, and consists of three components: a surface instrument package that houses an Iridium satellite phone and a GPS antenna, and processes and transmits the data, a wire-rope tether of arbitrary length (up to 800 m), and an instrumented profiler that travels up and down the tether. The profiler houses a conductivity, temperature, and depth (CTD) sensor along with other instruments. Measurements are usually made between depths of 5 m (to keep CTD from colliding with ice floe) and 750 m, and typically two to four times a day (Krishfield et al. 2008).

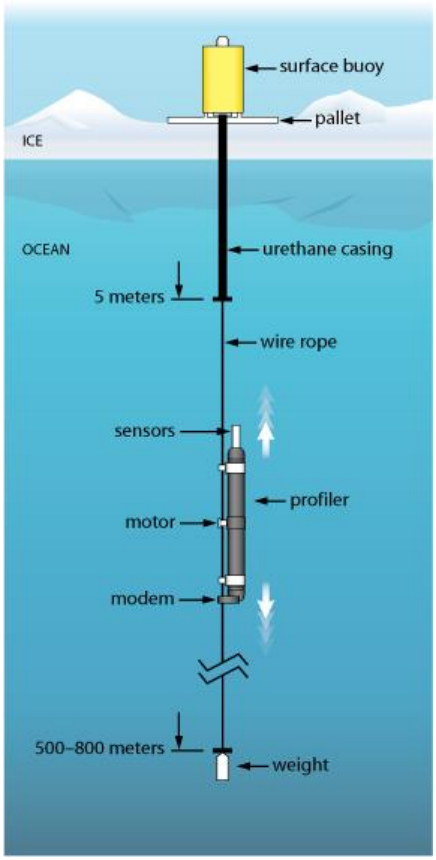

Figure 7. Diagram of an Ice Tethered Profiler. From top to bottom: a surface buoy contains data processors and antennae; a pallet provides stability to the surface buoy; a wire rope extends from the surface buoy down to 500 - 800 m; a urethane casing protects the wire rope through the ice down to 5 meters; a motorized profiler contains environmental sensors and an acoustic modem for communication with the surface buoy (from WHOI 2014).

The ITP data analyzed in this study were made available by the ITP Program hosted at the Woods Hole Oceanographic Institution (WHOI) (WHOI 2014). Since 2004, ITPs have been deployed in the Arctic Ocean, the Southern Ocean, and various other ice-covered bodies of water. WHOI makes available ITP data at various levels of review and quality control. The highest quality data, referred to as Level 3 and is considered archive-quality, was used in the present study (WHOI 2014). Eleven ITPs were chosen: 1, 6, 8, 9, 18, 23, 33, and 41 from the Beaufort Sea region, and ITPs 7 and 19 from the Eurasian Basin region, and ITP 36 from the East Siberian Sea region (Figure 8). These ITPs were chosen for their coverage of different regions as well as for their duration and quality.

The western and eastern Arctic have different water mass properties described previously, so sampling multiple regions is important for characterizing the spatial variations in the parameters of interest. The selected group of ITPs spans the period from August 2005 to December 2010, allowing for multi-year analysis and comparison with model output. Table 1 provides a more detailed description of the selected ITPs.

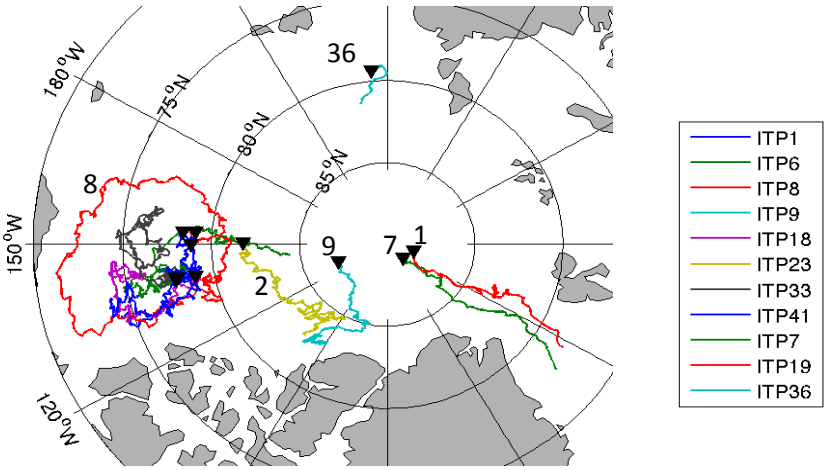

Figure 8. Drift tracks of selected ITPs. Triangles indicate start positions. For clarity, several ITPs are labeled. ITPs 7, 19, and 36 are considered to be in the eastern Arctic; the remaining ITPs are considered to be in the western Arctic. Some of the tracks have been numbered for clarity.

ITP Name	Region	Date of First Profile of Interest	Date of Last Profile of Interest	Shallowest Depth (m)	Deepest Depth (m)	Number of Profiles
ITP1	Beaufort Sea	15-Aug-2005	7-Jan-2007	10	750	2043
ITP6	Beaufort Sea	4-Sep-2006	2-Jul-2008	9	760	1335
ITP7	Eurasian Basin	28-Mar-2007	31-Oct-2007	7	760	746
ITP8	Beaufort Sea	11-Aug-2007	3-Oct-2009	7	760	1569
ITP9	Beaufort Sea	11-Sep-2007	7-Sep-2010	7	760	1480
ITP18	Beaufort Sea	16-Aug-2007	15-Nov-2009	7	750	914
ITP19	Eurasian Basin	7-Mar-2008	21-Nov-2008	7	760	912
ITP23	Beaufort Sea	5-Aug-2008	11-Jul-2010	7	750	1410
ITP33	Beaufort Sea	10-Jul-2009	26-Jan-2011	7	760	952
ITP36	Laptev Sea	29-Aug-2009	13-Oct-2009	7	760	90
ITP41	Beaufort Sea	3-Oct-2010	12-Oct-2012	7	760	1480

Table 1. Details of selected ITPs.

1. Identifying the Mixed Layer Depth in ITP Data

The Arctic Ocean surface mixed layer stores heat during summer and releases it all back to the atmosphere, before sea ice can freeze at the surface. To separate the contributions of heat content from below the mixed layer from those within it, its thickness (or depth, i.e., MLD) must first be determined. The thickness of the mixed layer is dependent upon the effects of turbulent mixing, and there are many different methods that can be used to identify MLD (e.g., Thomson and Fine 2003; Holte and Talley 2009). Often in the subtropical seas, MLD can be determined by the depth of the surface isothermal layer because salinity is a minor contributor of density variation at these temperatures (Holte and Talley 2009). However, in the Arctic where surface temperatures are near freezing, changes in salinity will have much larger affects and cannot be neglected. There are two commonly used types of methods for finding the MLD. These are threshold methods, and gradient methods. The threshold methods pick a variable, usually either temperature or density, and set a threshold for magnitude of change from some reference depth, usually the surface, or just below it (Thomson and Fine 2003). For example, a commonly used threshold method defines the MLD as the depth at which density has increased by 0.01 kg/m^3 from a reference depth (e.g., Scheider and Muller 1990; Toole et al. 2010). Other density thresholds that have been used are a density increase of 0.25 kg/m^3 from the surface (e.g., Timmermans et al. 2012) or an increase of 20% of the density change between the surface and 100 m (Haynes 2010). Alternatively, the MLD could be defined as a depth with maximum density gradient (Timmermans et al. 2012). For this study, these four methods will be called MLD-1, MLD-2, MLD-3, and MLD-4. Table 2 contains a brief summary of these methods.

Method Name	Identifies MLD as depth of:
MLD-1	Density 0.01 kg/m3 greater than reference density
MLD-2	Density 0.25 kg/m3 greater than reference density
MLD-3	20% of density change in shallowest 100 m
MLD-4	Maximum dρ/dz

Table 2. Summary of methods to identify the mixed layer depth. The first column lists the method names; the second column briefly describes the method.

To compare these four methods, density profiles were calculated from the temperature, salinity, and depth measurements from each ITP using the equation of state defined in Jackett et al., (2006). ITPs 7 and 41 were chosen to test the four methods of MLD calculation as representatives of the western and eastern Arctic conditions. Time series of temperature, salinity, and density with the MLD variations are plotted in Figures 9 and 10. Similar to what was found in Timmermans et al. (2012), Method MLD-1 produced an MLD that was generally too shallow (> 10 m throughout all seasons) and was very sensitive to the slightest change in density gradient. The MLD generated by this method varied wildly (~ 20 m) between time steps and was considered an inappropriate method. The three remaining methods produced much more consistent results.

To further compare these methods, a selection of temperature, salinity, and density profiles are shown in Figures 11 and 12. All three methods do well in finding the MLD during the summer and winter when stratification is the strongest, but the time series demonstrate the sensitivity of the gradient method to minute fluctuations in density (Figures 9 and 10). The near-surface waters of the Eurasian Basin undergo significant changes in density through the transition seasons and the density profile changes subtly (see Figure 12). Therefore, the maximum density gradient jumps between what should be the surface mixed layer, and a much deeper pycnocline associated with the top of the Atlantic Layer. The high variance of this result, and its misidentification of the MLD during certain seasons necessitates the elimination of method MLD-4 as a not suitable method.

Although the MLD-3 method produces a MLD that is similar to the MLD-2 method, it often places the MLD too deep. Therefore, for the purposes of this study, MLD-2 will be used to define the mixed layer depth. Explicitly, this is a depth at which the density has increased by 0.25 kg/m^3 from the shallowest measurement. This is similar to what was found by Timmermans et al. (2012), who also showed that strength of the density gradient at the base of the mixed layer was strong enough in most cases that slight changes to the threshold of 0.25 kg/m^3 or reference depth will have an insignificant effect on the resulting MLD.

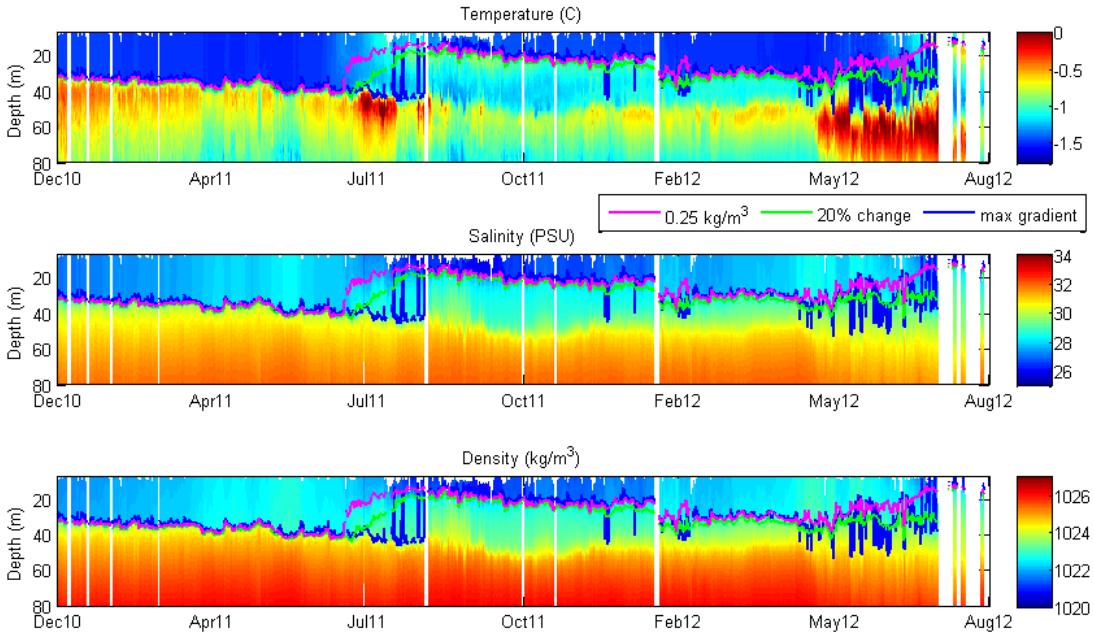

Figure 9. ITP 41 (Beaufort Sea) temperature, salinity, and density profiles for the duration of the sampling period with different methods of calculating MLD overlaid. The 0.25 kg/m^3 criterion is in red, the 20% change criterion is in green, and the maximum density gradient criterion is in blue.

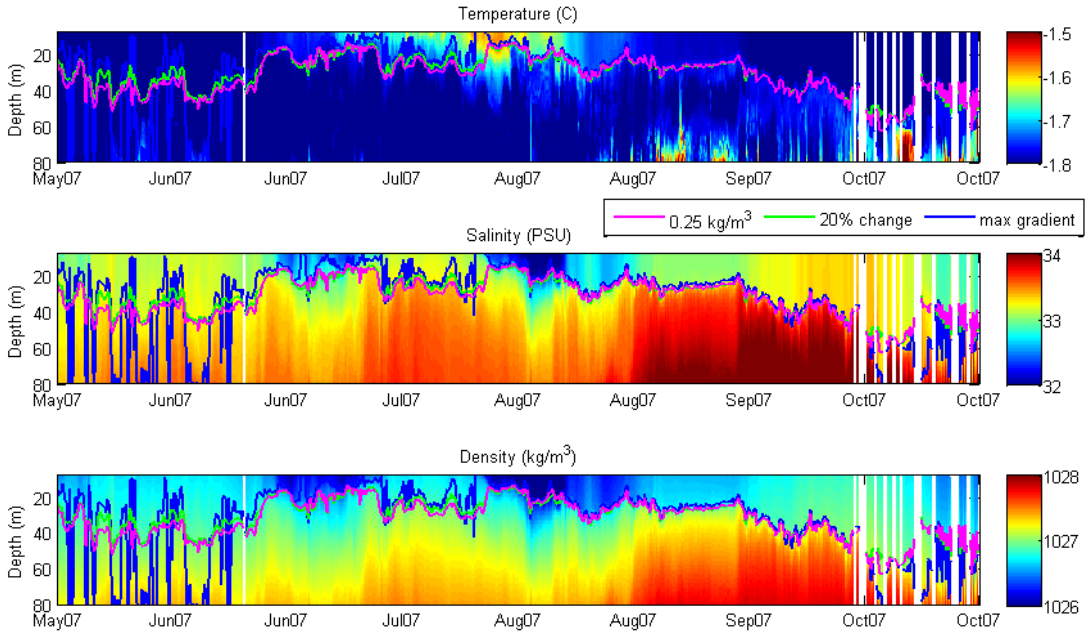

Figure 10. ITP 7 (Eurasian Basin) temperature, salinity, and density profiles for the duration of the sampling period with different methods of calculating MLD overlaid. The 0.25 kg/m^3 criterion is in red, the 20% change criterion is in green, and the maximum density gradient criterion is in blue. The Atlantic Layer can be seen below 100 m, and the maximum density gradient criterion often misidentifies this pycnocline as the MLD.

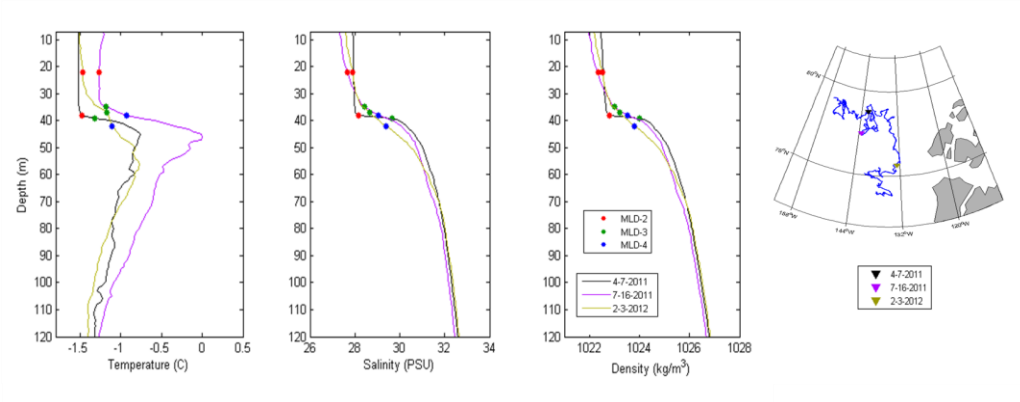

Figure 11. Temperature, salinity, and density profiles for ITP 41 (Beaufort Sea) on April 7, 2011 (black line), July 16, 2011 (magenta line), and February 3, 2012 (yellow line). MLDs determined by methods MLD-2 (red dot), MLD-3 (green dot), and MLD-4 (blue dot) are overlaid. In all three profiles, MLD-2 produces the most realistic value of MLD. Locations of each profile are plotted on the conformal conic projection to the right.

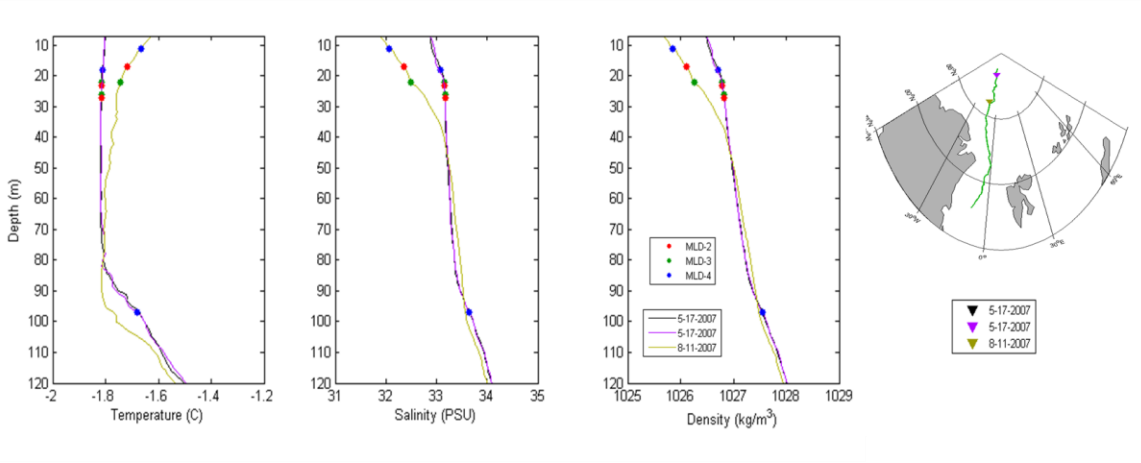

Figure 12. Same as Figure 7, but for ITP 7. The profiles are from the morning (black) and afternoon (magenta) of May 17, 2007, and August 11, 2007. On two successive observations on May 17, 2007, MLD-4 changes by almost 100 m and is considered unrealistic.

2. Identifying the Halocline Depth in ITP Data

The Atlantic layer typically has a temperature consistently more than 1.5 ^{o}C above freezing (Rudels 2012), which is warm enough to cause any heat content calculation for the Arctic to be dominated by this layer (see Figure 4). Therefore, this study will attempt to remove the Atlantic layer heat signature, by only calculating the heat content down to the top of the Atlantic layer, which will be called the halocline depth (HD). The description provided in this section details methods used to adapt observational methods used to identify central Arctic water masses to a high resolution model. It is important to note that while the Atlantic layer is present in both the Eurasian and Canadian Basins, its properties are not uniform. Previous attempts at identifying the halocline depth have been restricted to sub-regions of the Arctic Ocean in which the water mass properties are relatively consistent. As previously discussed, Rudels et al., (2004) and Rudels (2012) identified the Atlantic layer as water with temperatures above 0 ^{o}C. Rudels et al. (2004) also defined the halocline as the waters between the mixed layer and the Atlantic layer, typically between approximately 50 m and 250 m. They discussed properties of the halocline varying spatially around the Arctic, but no precise depth was defined (Rudels et al. 2004). In the western Arctic the intrusion of water from the Pacific, via the Bering Strait, creates a distinct layer of relatively cold (~ -1 ^{o}C) and fresh (~ 33.1

psu) water (Woodgate et al. 2005). This extra layer of water creates two significant local pycnoclines, one that separates the ambient surface layer from the Pacific layer, and another that separates the Pacific layer from the Atlantic layer. These two pycnoclines are typically called the Upper Halocline and Lower Halocline, and have different properties than the halocline in the eastern Arctic (Nguyen et al. 2012). These definitions of the halocline are only applicable to the deep basin regions within the Arctic Ocean, and are not valid on the continental shelf regions or south of the Bering and Fram Straits (see Figure 2). This study will include all of the waters between the surface mixed layer and the Atlantic layer into one large halocline complex, and various methods to determine the specific bottom of this halocline complex is the focus of this section.

Since the aim is to remove the Atlantic layer heat signature from these analyses, temperature will be the variable of focus, though salinity will also be crucial for identifying water masses. Figures 13 and 14 show the T-S characteristics of the eastern and western Arctic regions, respectively. Other ITPs showed similar structure and variability. ITP 41 from the western Arctic shows how the various water masses influence the T-S characteristics of the water column. The Atlantic layer is warm (> 0 ^{o}C) and salty (> 33.5 psu) with a sharp temperature gradient above it. Warm water (~ -1.5 to -0.5 ^{o}C) is sandwiched between the Atlantic layer and the mixed layer. This warm middle layer must be included in heat content calculations, but not the Atlantic layer below. Therefore, the halocline depth will be defined as the minimum temperature immediately above the Atlantic layer (Figure 13).

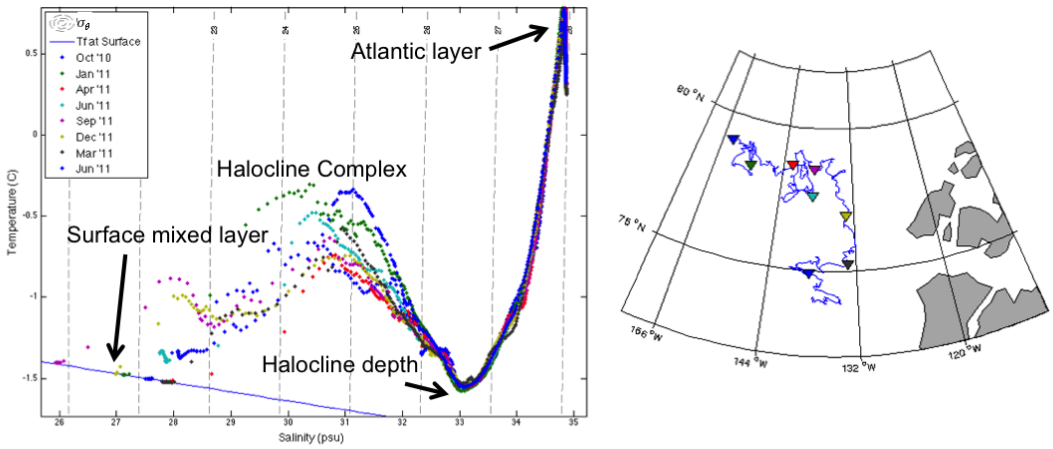

Figure 13. Temperature-Salinity diagram for selected profiles from ITP 41 with lines of constant potential density anomaly overlaid as grey dashed lines. The Atlantic layer water mass, surface mixed layer, and halocline depth are indicated with arrows. The freezing temperature at the surface is plotted as a blue line. Locations of each profile are plotted on the conformal conic projection to the right.

ITP7 shows a different situation in the eastern Arctic (Figure 14). There is no noticeably warm and fresh layer above the Atlantic layer, but a transition region can be identified where the properties of the Atlantic layer are no longer dominant. This transition point is identified by a significant change in the slope of the temperature with respect to salinity. More formally, the halocline depth for eastern Arctic ITPs is set as the depth at which the second derivative of temperature with respect to salinity is a maximum. This subtle yet significant difference in the methods of determining the halocline depth will become more important when exploring model results that cover the entire Arctic Ocean.

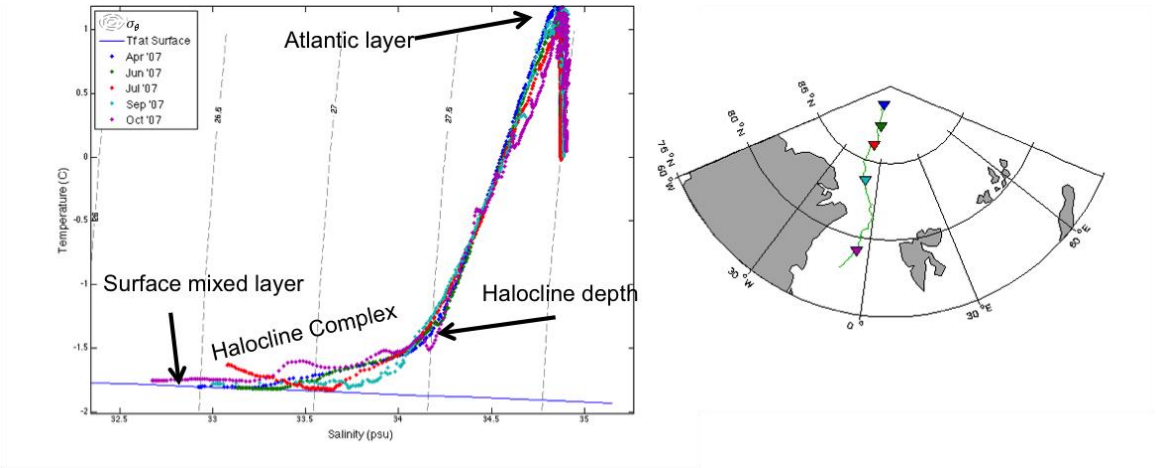

Figure 14. Same as Figure 9, but for ITP 7.

Sample temperature, salinity, and density profiles and time series from ITPs 41 and 7 are plotted in Figures 15 through 18. As a reference, the freezing temperature is plotted with actual temperature. Comparing the profiles from the two ITPs, it can be seen that the halocline is generally deeper in the Beaufort Sea than in the Eurasian Basin. Comparing the temperature and freezing temperature lines can give an idea as to how much heat is contained in that layer.

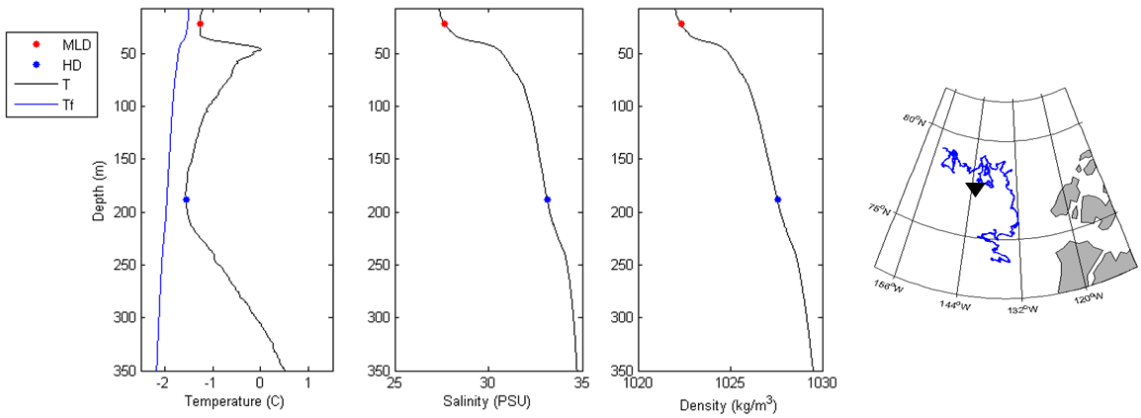

Figure 15. Temperature and freezing temperature, salinity, and density profiles for ITP 41, October 3rd, 2010. MLD is marked with a red dot, and HD is marked with a blue dot. The location of this profile is indicated on the conformal conic projection to the right with a black triangle.

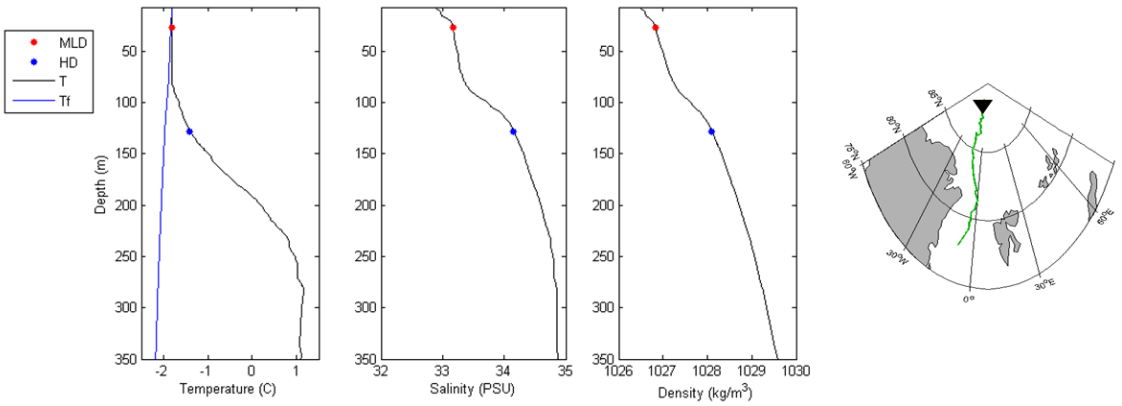

Figure 16. The same as Figure 15, but for ITP 7, April 29, 2007.

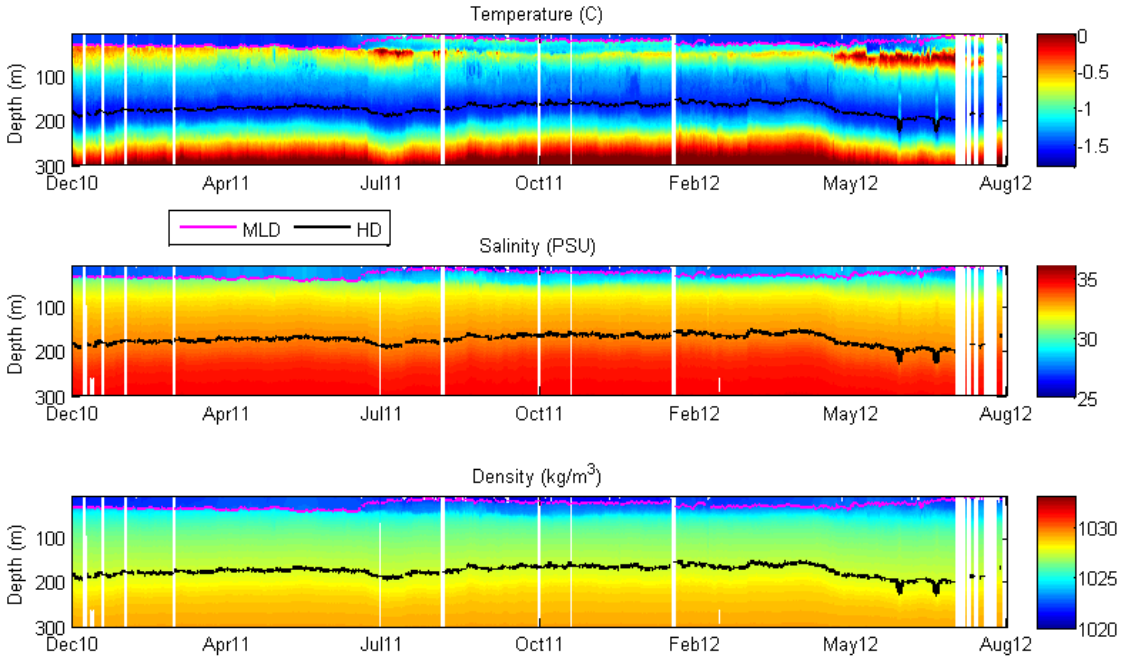

Figure 17. Temperature, salinity, and potential density anomaly time series for ITP 41. MLD is marked in magenta, and HD is marked in black.

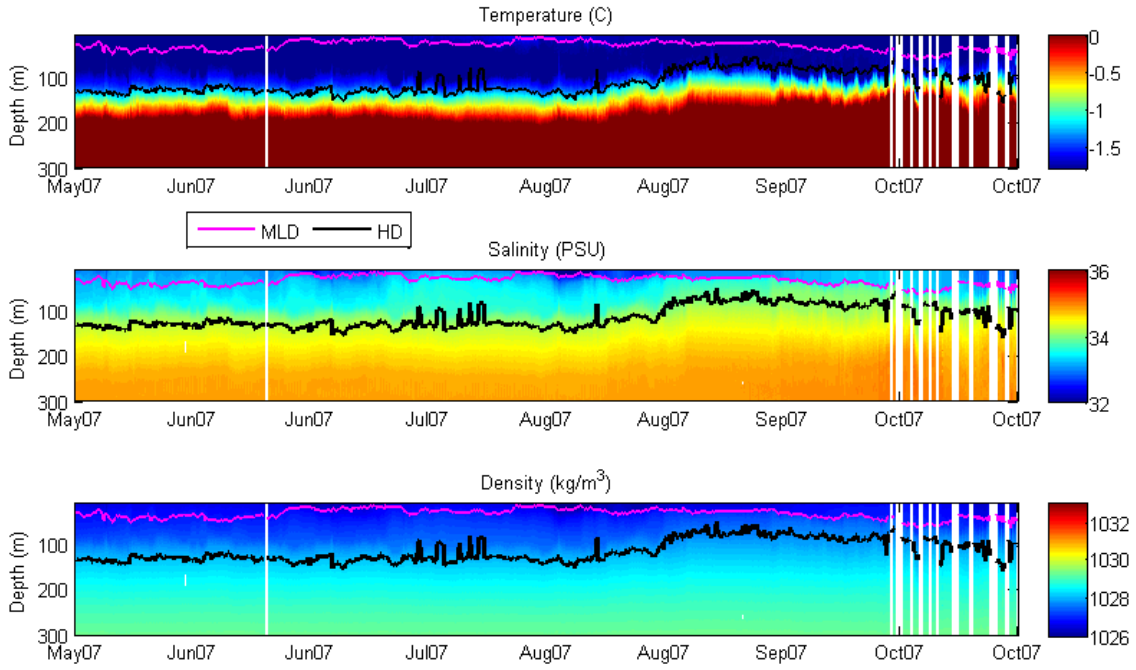

Figure 18. Same as Figure 17, but for ITP 7. MLD is marked in magenta, and HD is marked in black. Noise in HD data after October 2007 is due to the ITP drifting out of the central Arctic and into the North Atlantic where these methods are not applicable.

3. Calculating Heat Content

The layer of interest lies between the MLD and HD. The MLD and HD will be the upper and lower limits for calculating ocean heat content. Heat content (HC) is computed as follows:

$$HC(x,y,t) = \int_z \rho(t,x,y,z) C_p \left(T(t,x,y,z) - T_{ref} \right) dz$$

where T is temperature at a given point and time, T_{ref} is a reference temperature (chosen as the freezing temperature for that pressure and salinity), ρ is the density of that unit volume, and C_p is the specific heat capacity of water (4186 J/kg^{o}C). Here we integrate across a range of depths. The limits of integration can be set in a number of ways. To identify the heat contribution of the mixed layer and halocline complex layer, five sets of limits will be used: surface to 120m, 33m to 120 m, MLD to 120m, MLD to HD, and MLD to 270 m.

C. MODEL DATA SET: REGIONAL ARCTIC SYSTEM MODEL (RASM)

1. RASM Description

The case for a community based Arctic System Model (ASM) has been made by various scientific reports (e.g., Arctic Observing Network 2010; Roberts et al. 2010). Roberts et al. (2010) made the case for a holistic modeling effort that integrated the physical, chemical, biological, and social components of the Arctic System, which would be necessary for understanding and predicting change. Feedbacks between air, ocean, ice, biochemical, land, and anthropogenic processes, are not accounted for by stand-alone models, regardless of resolution, and are poorly represented in GCMs due to coarse resolution, crude parameterization of important sub-grid scale processes, and insufficient boundary conditions (Roberts et al. 2010; Maslowski et al. 2012). An ASM can bridge the gap between coarser resolution GCMs and finer-scale, stand-alone process studies (Roberts et al. 2010).

NPS models mentioned previously, such as NAME, have shown skill in representing sea ice edge, thickness, and volume fluctuations (Maslowski et al. 2007; McGeehan and Maslowski 2011) especially when compared to GCMs (Maslowski et al. 2012). NAME has also shown the significance of small scale processes such as Alaskan Stream eddies, Aleutian throughflow, Bering Shelf dynamics, and Canadian Arctic Archipelago (CAA) throughflow (Maslowski et al. 2008; Clement Kinney et al. 2008; Clement Kinney and Maslowski 2012; McGeehan and Maslowski 2012). These results, among others, have motivated the development of a fully coupled, high resolution ASM.

The Regional Arctic System Model (RASM) is a limited-domain, fully coupled, high-resolution atmosphere, ocean, ice, and land model. The primary components are the Weather Research and Forecasting (WRF), Los Alamos National Laboratory (LANL) Parallel Ocean Program (POP) and Sea Ice Model (CICE), and the Variable Infiltration Capacity (VIC) land hydrology model. These four components are coupled using the Community Earth System Model (CESM) coupler, CPL7. The domain of RASM includes the Arctic Ocean and surrounding marginal seas, such as the Laptev, Kara, and Barents Seas, as well as the sub-Arctic North Pacific, including the Bering Sea, Sea of

Okhotsk, Sea of Japan, and Gulf of Alaska, and the sub-Arctic North Atlantic, including the Nordic Seas, Labrador Sea, and Hudson Bay (Figure 19).

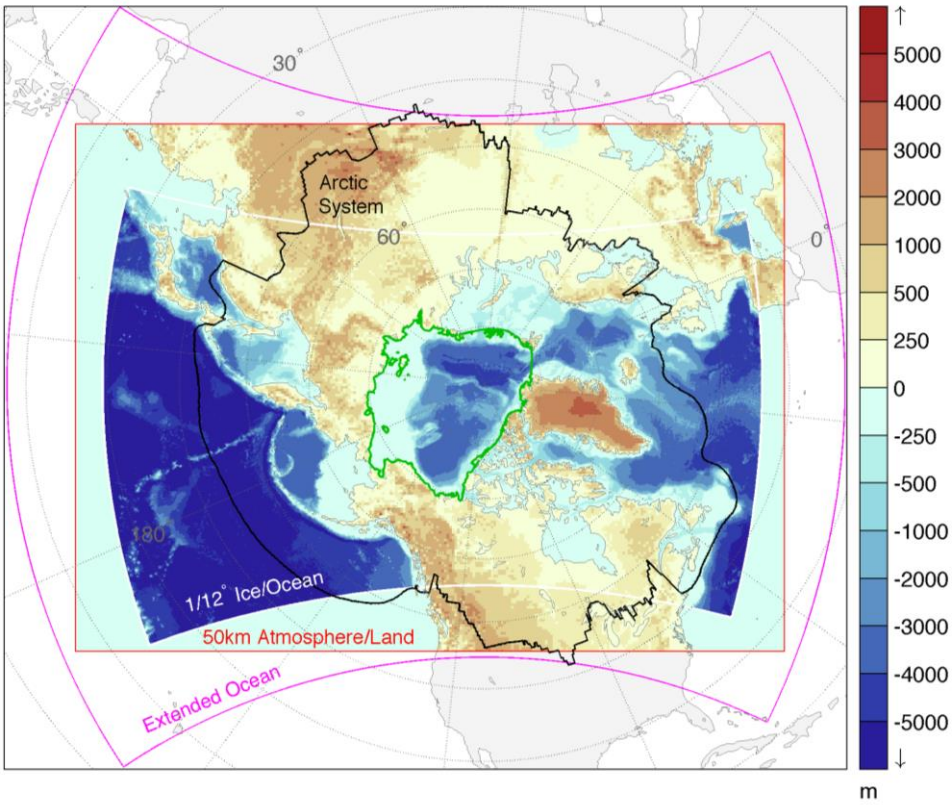

Figure 19. RASM domain. WRF and VIC model domains are outlined in red, POP and CICE domains are shaded by depth/elevation. Arctic System domain for bio-chemical and runoff is outlined in black, and the central Arctic is outlined in green (from Roberts 2014).

RASM is configurable in multiple ways to study differing processes. For the purposes of this study, the RASM "H-case" was used. In H-case as in the fully coupled RASM, POP is configured on a rotated spherical coordinate grid with horizontal resolution of $1/12^{o}$ (~ 9 km), has 45 vertical layers with 8 layers in the upper 50 m, and is fully coupled with CICE. See Table 3 for a detailed list of ocean model levels and associated depths. Freshwater input from precipitation and runoff is very important in the Arctic, especially since salinity dominates the calculation of density. In H-case, the land model exists only as a stub and the freshwater flux from river runoff is not explicitly

modeled, but parameterized by using observed monthly ocean surface salinity climatology as a reference for Newtonian relaxation. As a subset of the fully coupled RASM, H-case replaces the atmospheric component with a data model, using realistic forcing from the Common Ocean Reference Experiment version two (CORE2) reanalysis from the National Center for Atmospheric Research (NCAR). The CORE2 reanalysis spans the period from 1948 to 2009. This enables the ice-ocean model to be run in hindcast for a greater period than in previous studies. The specifics of the H-case configuration reduce computation time, and will provide a baseline for comparison to other configurations not considered in this study. For a more detailed discussion on RASM configuration, see Maslowski et al. (2012), Osinski et al. (2014), and Roberts et al. (2014).

Level	Thickness	Lower Depth	Mid-depth
1	5	5	2.5
2	5	10	7.5
3	5	15	12.5
4	5	20	17.5
5	6.03	26.03	23.015
6	7.28	33.31	29.67
7	8.78	42.08	37.69
8	10.59	52.67	47.375
9	12.77	65.44	59.055
10	15.4	80.84	73.14
11	18.58	99.43	90.14
12	22.41	121.84	110.635
13	27.04	148.888	135.36
14	32.62	181.49	165.18
15	39.34	220.84	201.17
16	47.46	268.3	244.57
17	57.25	325.54	296.915
18	69.06	394.6	360.07
19	83.3	477.9	436.25
20	100.48	578.39	528.15
21	121.61	700	639.195
22	150	850	775
23	200	1050	950
24	200	1250	1150
25	200	1450	1350
26	200	1650	1550
27	200	1850	1750
28	200	2050	1950
29	200	2250	2150
30	200	2450	2350
31	200	2650	2550
32	200	2850	2750
33	200	3050	2950
34	200	3250	3150
35	250	3500	3375
36	250	3750	3625
37	250	4000	3875
38	250	4250	4125
39	250	4500	4375
40	250	4750	4625
41	300	5050	4900
42	300	5350	5200
43	300	5650	5500
44	300	5950	5800
45	300	6250	6100

Table 3. RASM POP-2 ocean model layer depths in meters.

2. MLD in RASM output

The same methods for calculating MLD and HD using the ITP data set can be applied to RASM output, though with slight modifications. These modifications are necessary due to the different resolution of the two data sets. ITPs sample two to four times a day and at 1 meter vertical resolution. The configuration of RASM that this study uses outputs monthly means with 5 to 300 meter vertical resolution. Therefore, the ITP methods described above cannot be directly applied to the model data set.

The four methods of determining MLD, 0.01 kg/m^3, 0.25 kg/m^3, 20% change, and maximum density gradient, were applied to selected RASM locations and times. A comparison of the four methods can be seen in Figures 20 and 21. These figures show monthly mean profiles of density for four different months at selected model locations in the Beaufort Sea (Figure 20) and in the Eurasian Basin (Figure 21). Figure 22 shows the locations of those points in space. The 0.25 kg/m^3 density change criterion most consistently finds an appropriate MLD in RASM output, just as it did with the ITP data. Therefore, this method will also be used for generating RASM MLDs.

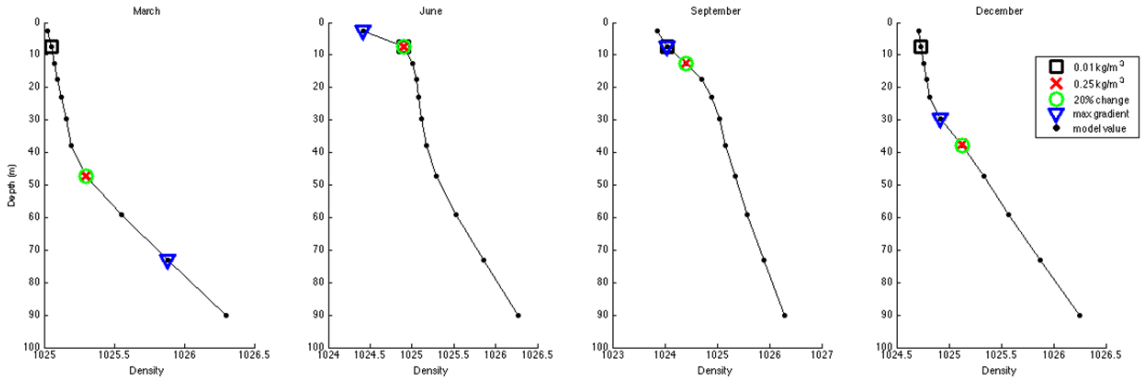

Figure 20. Model density profiles for March, June, September, and December 2007 in the Beaufort Sea. Black dots are actual model values, with linear interpolations plotted for ease of viewing. The four methods of determining MLD (indicated with colored shapes) used raw model data without interpolations. In all months, multiple methods produce the same value of MLD.

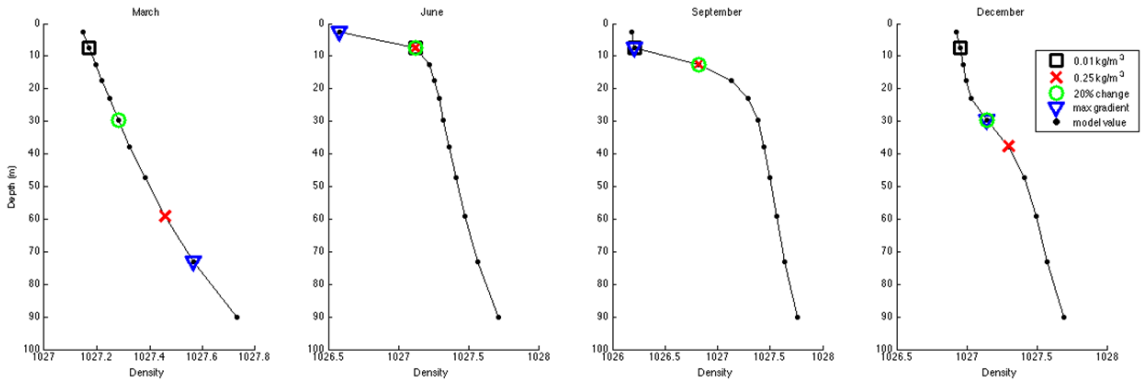

Figure 21. Same as Figure 21, but for the Eurasian Basin.

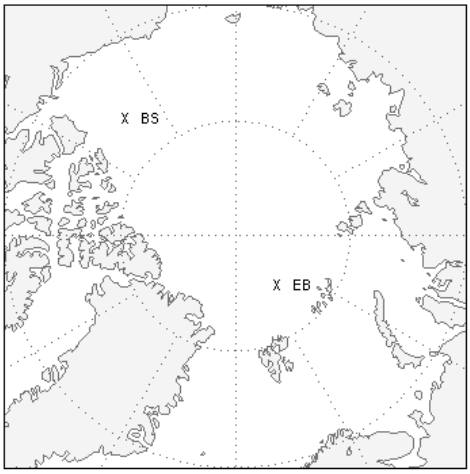

Figure 22. Locations of sample profiles from the Beaufort Sea (BS) and Eurasian Basin (EB) shown in Figures 20 and 21.

3. HD in RASM Output

The halocline depth is more difficult to identify in the model domain as compared to ITP observations. In the observational data, it is easy to adjust the algorithm for finding the halocline depth because there are only a few ITPs to analyze. The subset of the model domain being analyzed consists of over 310 million profiles when considering both space and time. It is desirable, therefore, to create a method that can be applied consistently across the entire domain. For the purposes of this study four methods, denoted as HD-1, HD-2, HD-3, and HD-4, are compared to select the optimal one. Three

of these methods are based on the temperature gradient, similar to the methods used in analyzing the ITP data. A brief summary of these methods is provided in Table 3.

Method Name	Identifies HD as depth of:	Shallow depth limit:	Deep depth limit:
HD-1	min dT/Dz	MLD	$T = 0^o$ C
HD-2	min dT/Dz	MLD	S = 34.55 psu
HD-3	min dT/Dz	MLD	Z = 360 m
HD-4	max N^2	MLD	Z = bottom

Table 4. Summary of methods used to identify model halocline depth. The first column lists the given names of the methods. The second column lists the quantity used for determining the value of HD. The third and fourth columns list the shallow and deep limits of depth of the quantity listed in column two.

Methods HD-1, HD-2, and HD-3 all look for a local minimum temperature gradient above the Atlantic layer, in addition to temperature, salinity and depth constraints. The local minimum of temperature gradient indicates where the dominating temperature influence has changed. Picking the first local minimum of temperature gradient above the Atlantic layer minimizes the contributions of heat from the Atlantic layer. It was found that the calculated halocline depth is sensitive to the thresholds used to define the Atlantic layer. Therefore, three different methods of identifying the Atlantic layer were used. Method HD-1 looks for the minimum temperature gradient above the depth at which temperature exceeds 0 ^{o}C; this temperature cutoff is similar to previous definitions of the Atlantic layer based on temperature (e.g., Rudels et al. 2004). Method HD-2 looks for the minimum temperature gradient above the depth at which salinity exceeds 34.55 psu. This threshold was chosen based on the findings of Rudels et al. (2004) and Woodgate et al. (2005) who characterized the Atlantic layer of having a salinity of ~ 35 psu and > 34 psu, respectively. The results of this method are quite sensitive to the choice of salinity threshold, and 34.55 psu produced the most consistent and realistic results. Method HD-3 looks for the minimum temperature gradient above the

arbitrary depth of 360 meters. The choice of this depth has a large effect on the results of the method, and will be discussed in more detail later.

Method HD-4 does not use temperature as the determining variable, but the density gradient, or more precisely the buoyancy frequency, instead. The buoyancy frequency for model level *i* is determined by:

$$N^2{}_i = -\frac{g}{\rho_i}\left(\frac{\rho_{i+1}-\rho_i}{z_{i+1}-z_i}\right)$$

where g is gravitational acceleration (9.8 m/s^2), ρ_i is the density of the i^{th} model level, and z_i is the middle (centroid) depth of the i^{th} model level. Since buoyancy frequency is an indicator of stability, a local maximum should indicate a barrier to vertical mixing, identifying the boundary of the Atlantic layer water mass. Method HD-4 defines the halocline depth as the depth of the local minimum of buoyancy frequency below the MLD, and will be used as a comparison to the methods based on temperature.

To compare the four methods, maps of the halocline depth produced by each method are plotted in Figure 23. The magenta, black, and green symbols indicate HDs at three different locations using the temperature based methods, and help to show significantly different results. The three locations are in the Chukchi Shelf region (labeled "CS"), the Central Arctic ("CA"), and the Eurasian Basin ("EB"). Profiles of temperature, salinity, density, and buoyancy frequency are plotted in Figures 24 -29 to compare the various methods.

The method that defines the Atlantic layer by its temperature (Figure 23 a.) produces inconsistent results. In some cases, the water temperature exceeds 0^{o}C at depths shallower than the Atlantic layer, producing either too shallow or null results. The method that defines the Atlantic layer by its salinity (Figure 23 b.) produces consistent and realistic results. This method is sensitive to the selection of a salinity threshold, but the value of 34.55 appears to produce consistent results. The method that defines the Atlantic layer by its depth (Figure 23 c.) is ineffective because no single depth threshold is appropriate in all regions. Since the Atlantic layer is deeper in the western Arctic, a deeper threshold must be set compared to the eastern Arctic. As opposed to the salinity

threshold, there is no single depth threshold that produces realistic results for all regions. The depth threshold of 360m was chosen for comparison here because of all the depths compared, this produced the most realistic results for most, but not all, regions. The maximum buoyancy frequency method generally selects depths between 0 and 100 m (Figure 23 d.), which is much shallower than those observed (e.g., Rudels et al. 2004). Additionally, the method produces null results in some regions where there exists no local maximum of N^2 (e.g., in the Beaufort Sea, Figures 24 and 25). The vertical structure of N^2 can also be dominated by the stratification at the base of the mixed layer. When the two maxima of N^2 are close together in depth, they become indistinguishable (e.g., in the Central Arctic, Figure 26). Therefore, this method was rejected.

Based on its ability to consistently produce realistic results across all regions and seasons, method HD-2 is chosen to define the halocline depth in the RASM H-case monthly mean data set. These four methods are not the only possible ways to define the halocline depth. Future work could include investigating other methods, or the possibility of a definition that varies spatially to better reflect the varying water mass properties across the basins.

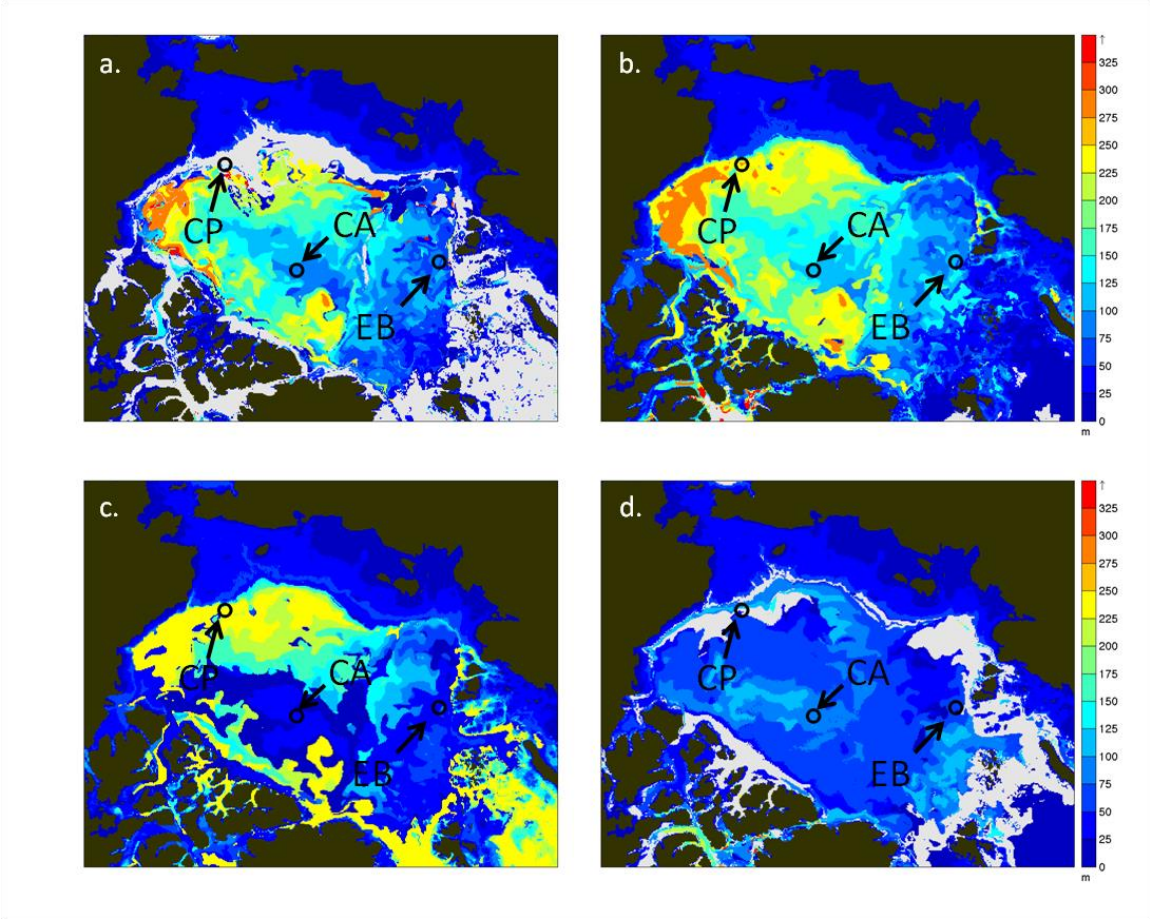

Figure 23. Maps of halocline depth produced by different methods: a) HD-1 defined as minimum temperature gradient shallower than a depth at which temperature is greater than 0^{o}C; b) HD-2 defined as minimum temperature gradient shallower than a depth at which salinity is greater than 34.55 psu; c) HD-3 defined as minimum temperature gradient shallower than 360m; d) HD-4 defined as maximum buoyancy frequency below the MLD. Grey pixels represent a model point where that method produces a null result, i.e. no local minimum in that depth range. Profiles from three locations are compared: Chukchi Plateau (CP), Central Arctic (CA), and Eurasian Basin (EB).

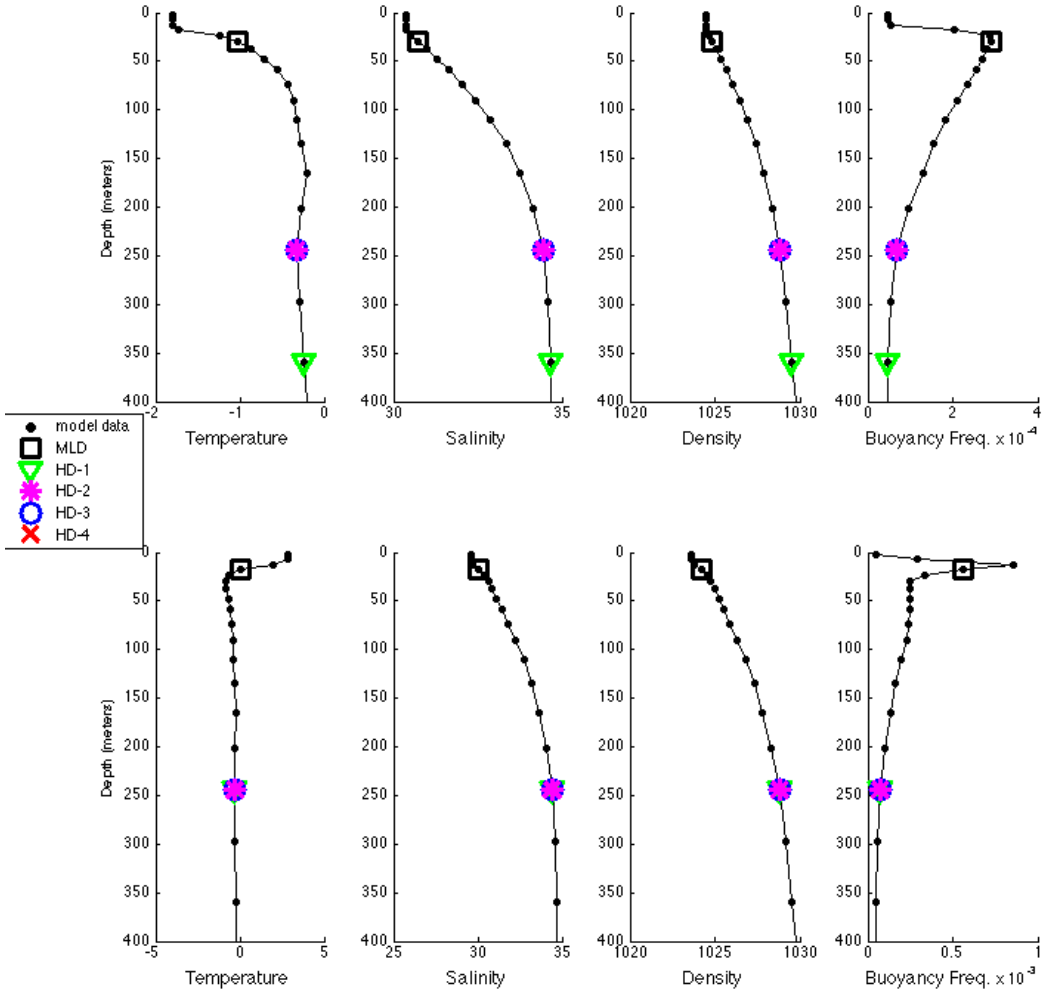

Figure 24. Model temperature, salinity, density, and buoyancy frequency for a point over the Chukchi Plateau during the month of March (top) and September (bottom), 2007. MLD is marked with a black square. The four methods for calculating the HD are listed as HD-1 (green triangle), HD-2 (magenta asterisks), HD-3 (blue circle), and HD-4 (red X). Some of the methods result in the same HD. There is no local maximum of buoyancy frequency below the MLD, so method HD-4 produces a null result.

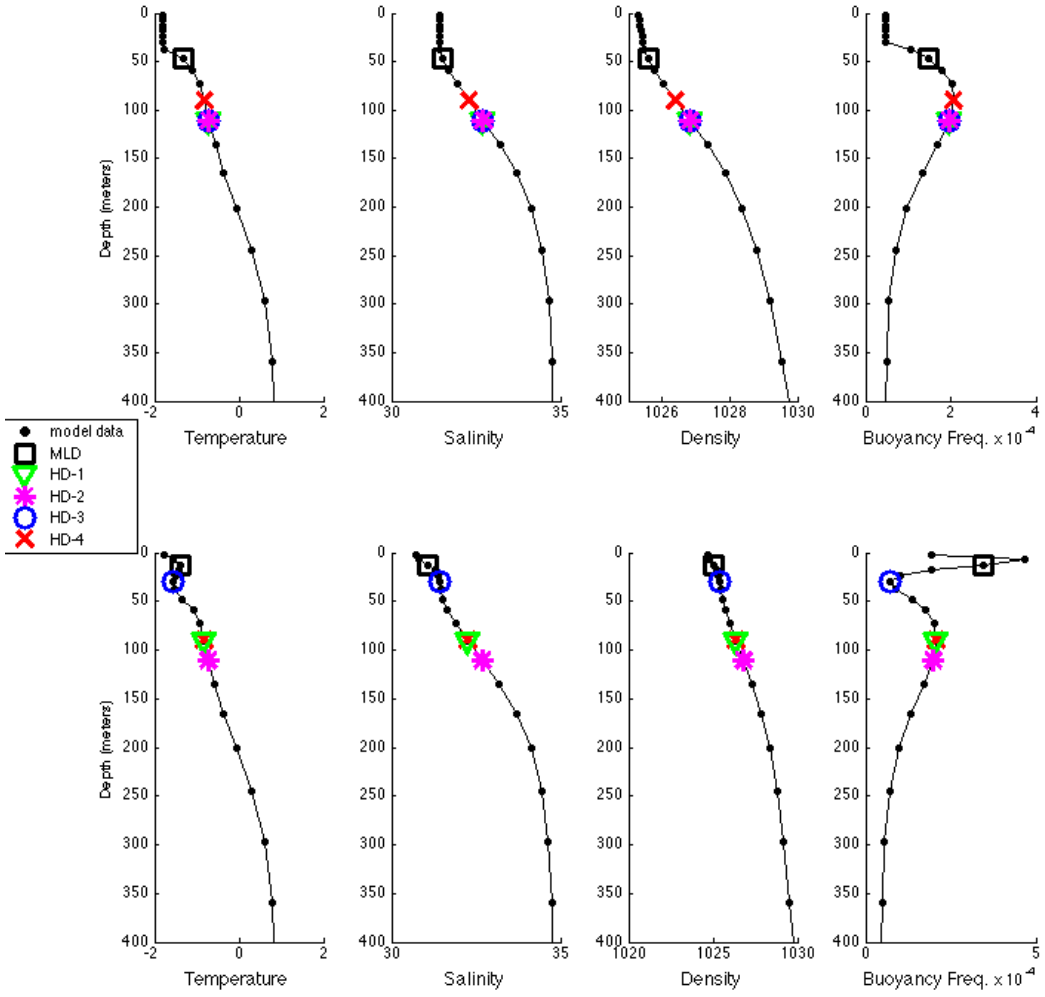

Figure 25. Same as Figure 20, but for a point in the Central Arctic.

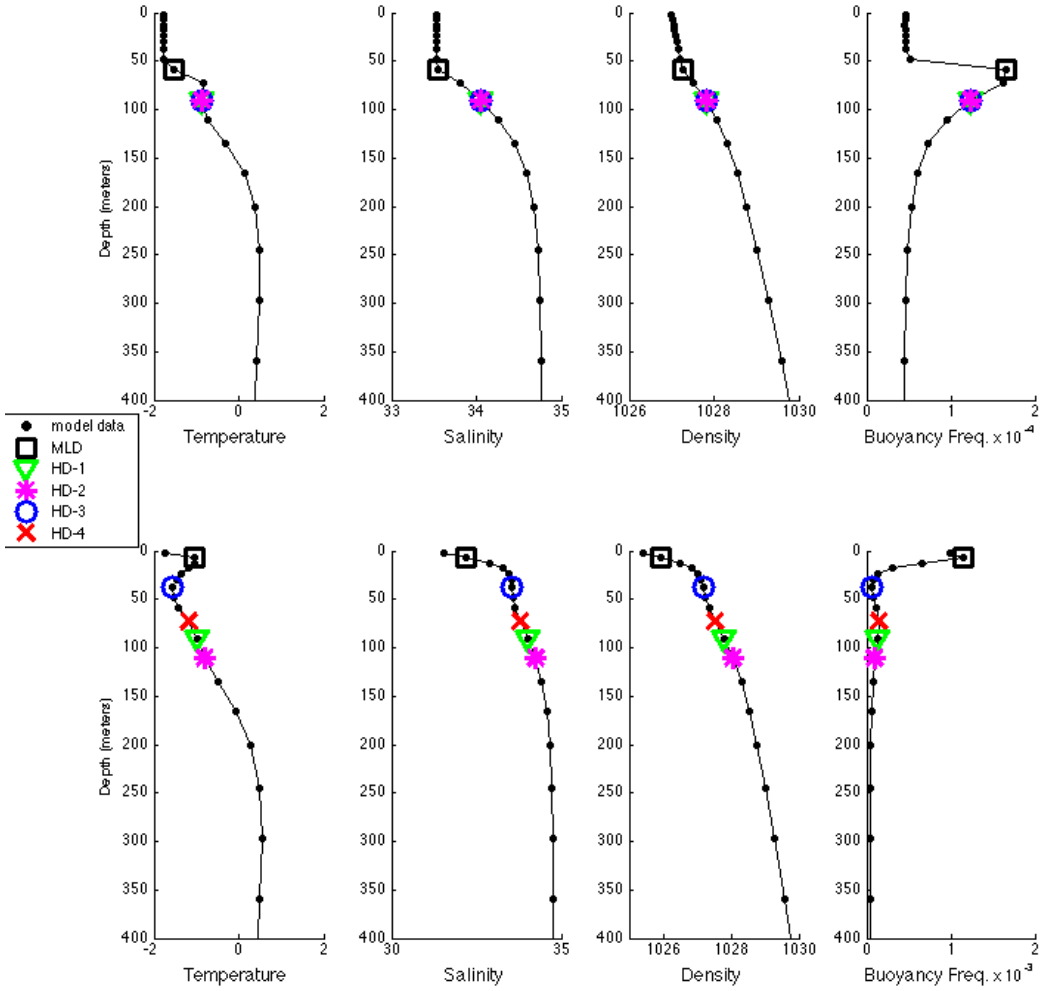

Figure 26. Same as Figure 20, but for a point in the Eurasian Basin.

4. Heat Content in RASM Output

The primary goal of this study is to investigate the heat content stored in the upper ocean to identify spatial and temporal trends as it may affect sea-ice conditions. This calculation is performed in the same way as with the ITP data. To identify the heat contribution of the mixed layer and halocline complex layer, five sets of limits will be used: surface to 120m, 33m to 120 m, MLD to 120m, MLD to HD, and MLD to 270 m.

IV. RESULTS: UPPER OCEAN HEAT CONTENT IN RASM-H AND ICE TETHERED PROFILERS

A. OVERVIEW

In the previous chapter we established the methods for understanding changes in the upper ocean heat content in the Arctic Ocean using both models and observations. Here we apply these methods using results from the Regional Arctic System Model H-case (RASM-H) and data from Ice Tethered Profilers (ITPs). Subsequently, Chapter V will discuss important findings derived from these results and their implications.

B. MODEL RESULTS: RASM-H

1. Mixed Layer Depth and Halocline Depth

The RASM-H output being analyzed in this study are the monthly mean fields from 1948 through 2009. Monthly means allow for a seasonal to inter-annual and multi-decadal analyses. Using methods described in Chapter III, the MLD and HD values were calculated for every model grid point for each of the monthly outputs during the 62-year model run. One way to visualize these results is in a 2-D map of MLD or HD values for a single month. Figures 27 and 28 are examples of MLD and HD generated from a single RASM-H monthly mean output, respectively. In order to demonstrate sensitivity in the methods, we have chosen a single year (1979), which is broadly representative of other years in our times series in terms of mixed layer depth results.

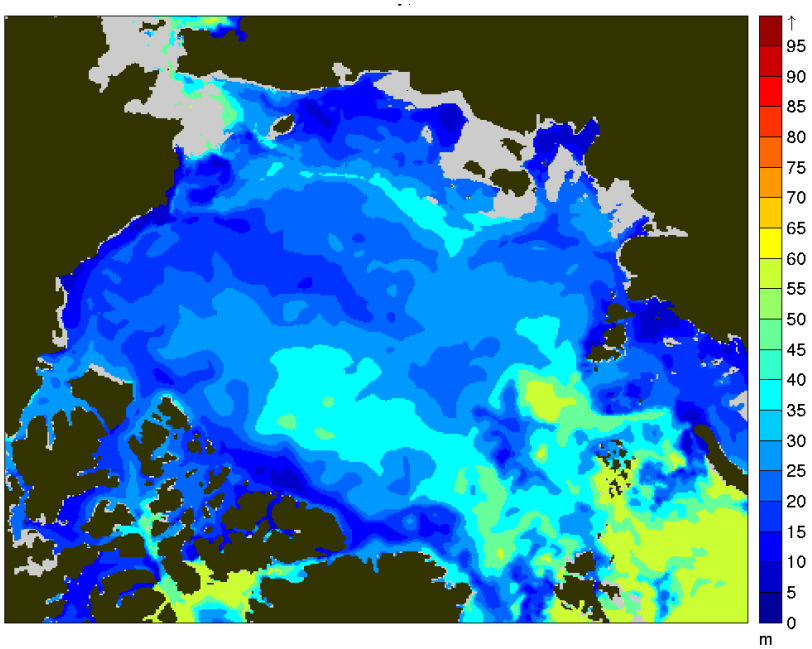

Figure 27. Mixed Layer Depth-from RASM January 1979 mean. The gray colored areas indicate where the MLD finding algorithm produces a null result. This is likely due to the water column being well-mixed down to the bottom, as in shelf regions.

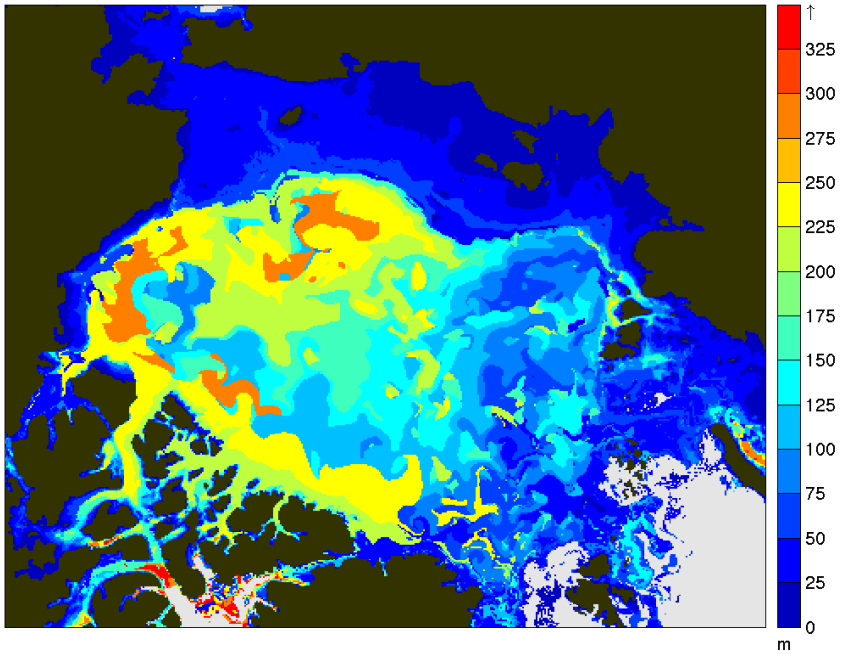

Figure 28. Same as Figure 27, but for HD. The gray colored areas indicate where the HD finding algorithm produces a null result. This is likely due to the Atlantic layer extending to the MLD or the surface.

A mean annual cycle was derived from the full time series by taking each respective month of the year for the duration of the time series. Figures 29 and 30 show the mean March, June, September, and December maps of MLD and HD. March represents the end of the northern hemisphere winter and when sea ice has reached its maximum extent. Conversely, September represents the end of the melting season and the beginning of the freezing season. June and December are transition months. Across the entire basin, MLDs deepen during the freezing period from September to March, and then shallow from March to September. Therefore, a maximum MLD is seen in March and a minimum in June and September. This deepening and shallowing, however, is not uniform across the region. In all seasons, the winds are generally cyclonic over the Arctic Ocean, which causes Ekman convergence, driving the MLD deeper. Also, the highest latitudes have the earliest freeze onset, which gives these regions a longer period of time for dynamic instability mixing to occur. On the continental shelves, the ocean depth is shallow enough that the bottom mixing and surface mixing combine to produce a full ocean column that is well mixed. There are also regions of deeper MLD on the Atlantic side of the Arctic. This is likely due to increased wind-driven mixing caused by storms, which are common in this region.

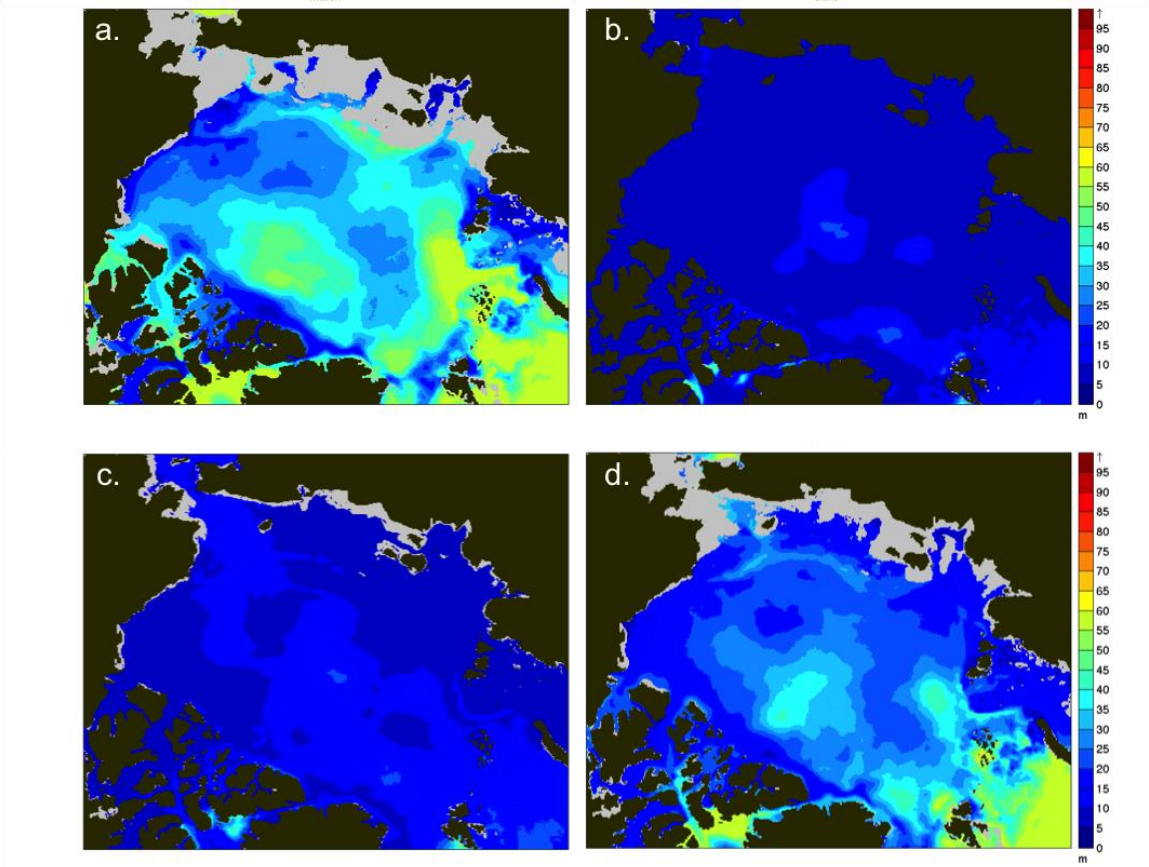

Figure 29. Long term mean of March (a.), June (b.), September (c.), and December (d.) MLD. The light grey colored areas indicate where the MLD finding algorithm produced a null result. This indicates that full ocean column is well mixed at this location.

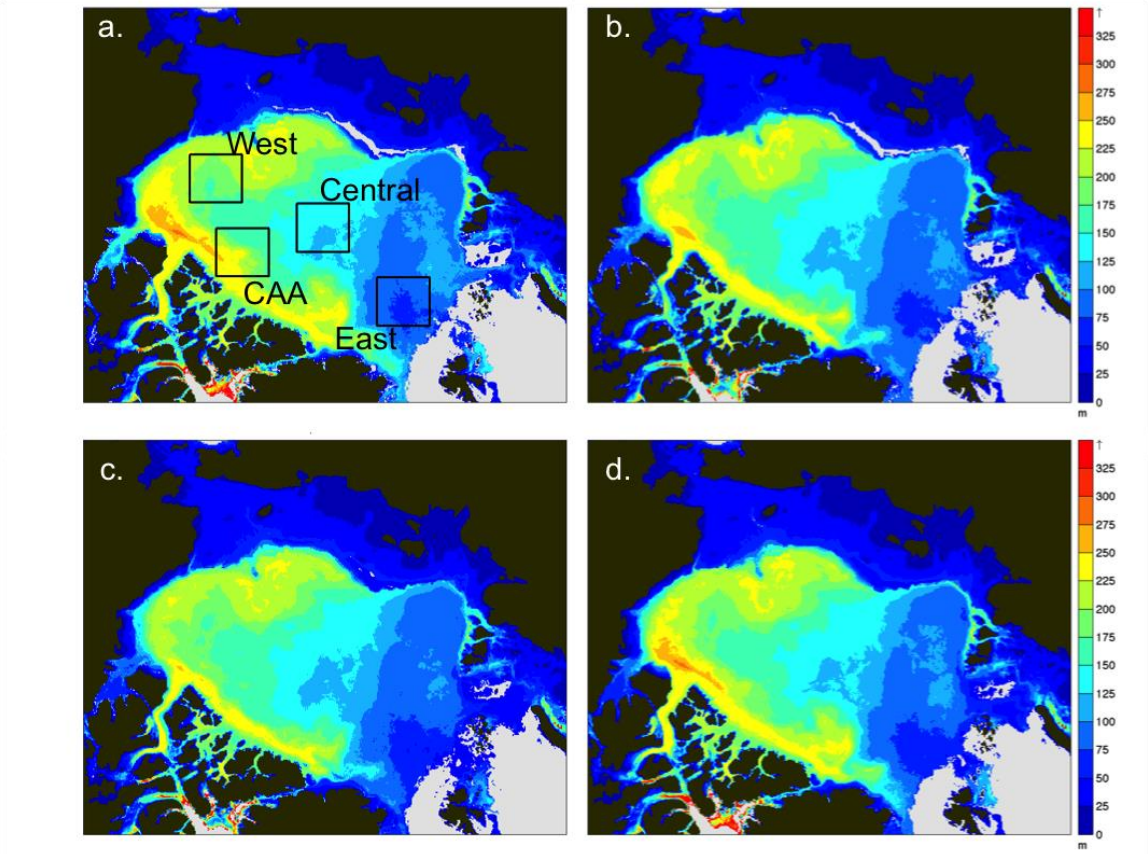

Figure 30. Same as Figure 29 but for the halocline depth. The light grey area indicates where the halocline algorithm produced a null result. This indicates that the stratification is atypical, including where the Atlantic layer extends all the way to the mixed layer or the surface. The black boxes in panel a. outline sub-regions used in the spatial analysis. The regions are square, 50 model grid cells in length and width, and represent the western, central, eastern, and Canadian Arctic Archipelago regions of the Arctic Ocean.

To better understand the temporal variations, all MLD and HD values in the spatial domain were averaged for each monthly time step. A time series of the basin-wide mean MLD and HD from 1948 to 2009 is shown in Figure 31. Because of the way MLDs are referenced to the surface layer, and the discrete level nature of RASM-H, the minimum possible MLD value is 7.5 m (see Table 3). Realistically, this corresponds to the model level that spans 5 to 10 m, making the effective minimum MLD for heat content calculations 5 m. Similarly, the model levels near the depth of the halocline are approximately 20 to 50 m thick. Therefore, any subtle change in temperature gradients

may cause the HD to jump up to 50 m shallower or deeper. By using basin-wide means, the impact of discrete model layer jumps are minimized.

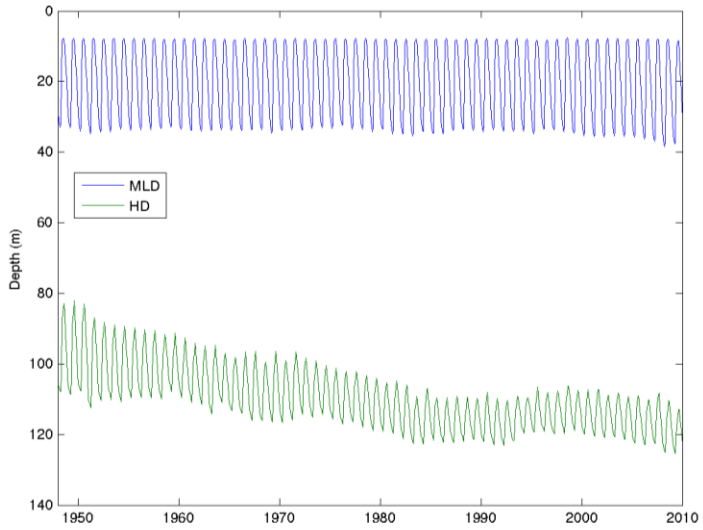

Figure 31. Time series of the basin-wide average of MLD (blue) and HD (green). The ocean surface is at the top.

Figure 38 shows the mean annual cycle of the basin-wide mean MLD and HD. A minimum value of MLD of 7.5 m is reached on the basin-wide average every August, and a maximum mean MLD of approximately 35 m is reached in April. The HD follows a similar pattern of shallowing during the spring to ~ 105 m and deepening down to ~115 M throughout the winter. The average seasonal swing of HD is around 20 m.

This mean annual cycle is then removed from the full time series to produce time series of MLD and HD anomalies in Figure 32. There still remains an annual signal in this time series because some years have a greater than mean seasonal variability. For example, in the last five years of the time series, the winter MLD is deeper than the average winter MLD, though the summer MLD remains close to the mean. This indicates that the summertime minimum MLD has remained unchanged, while the wintertime maximum MLD has deepened. To examine how the mean annual cycle has changed over the years, the mean annual cycles of MLD and HD were calculated for different time periods. Recall that RASM-H is the ice-ocean component which is driven by atmospheric

forcing from a reanalysis. Since the period from 1948 to 1979 does not include satellite data, it is worthwhile to calculate the mean annual cycles from this period. Also, the period 1948 to 1959 appears to have the largest seasonal variations, so that mean annual cycle is calculated as well. These are plotted along with the full 1948 to 2009 mean annual cycle in Figure 32. The MLD mean annual cycles are almost identical, while the HD mean annual cycles are deepening over time. Additionally, the range of depth variation is greater in earlier years. However, the timing of the maximum and minimum depths is uniform, so there is no reason to exclude the pre-1979 data from further analysis.

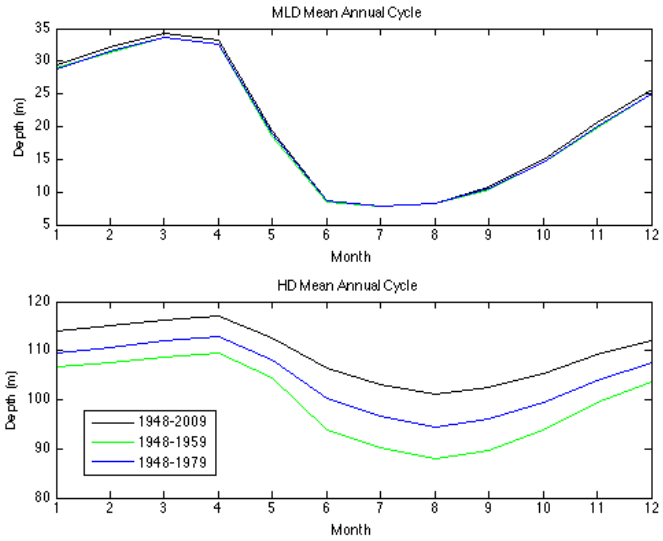

Figure 32. The mean annual cycle of the basin-wide average of MLD (top panel) and HD (bottom panel). The full time series mean annual cycle is black. The periods from 1948 to 1959 and 1948 to 1979 are overlaid in blue and green, respectively.

Figure 33 shows that both the MLD and HD have deepened since 1948, though the change in HD has been much more dramatic. Halocline depth increased by about 25 m during the course of the model run, with most of this increase coming during the period 1948 to about 1982. There is another deepening trend in the HD during the 2000s, similar to the deepening seen in the MLD. The greatest year-to-year changes in HD occur in the first few years of the time series.

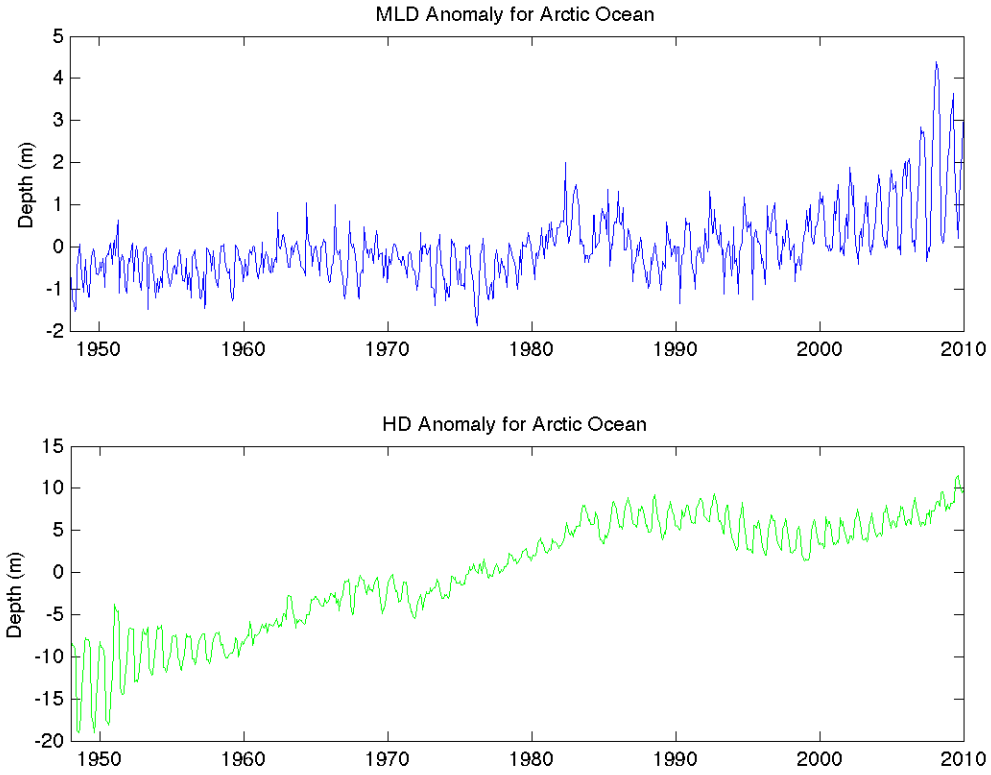

Figure 33. Time series of the basin-wide average of MLD (top panel) and HD (bottom panel) anomalies (monthly means minus mean annual cycle). An apparent 12 month cycle remains for years with anomalously wide or narrow annual variability.

To better quantify the regional variations in MLD and HD, four sub-regions are defined and compared. The four regions are outlined in Figure 30a, and are squares, each 50 model grid cells in length and width. Figure 34 shows the mean annual cycles of MLD (top) and HD (bottom) for each of the four sub-regions as well as for the full basin. All regions reach the same minimum MLD of 7.5 m at about the same time, but they have a various maximum MLD. The maximum MLD is deepest in the east with a value of just under 50 m; the central region shows a similar range of depths. The Canadian Arctic Archipelago region reaches a maximum MLD of about 40 m. The western region has the

shallowest MLD during the winter, reaching only 28 m at a maximum. In general, the MLD varies 20 to 50 m during the course of the year.

There is a much greater variation from region to region with respect to halocline depth. In general, all regions have the deepest HD in the winter and spring months, and the shallowest HD in the summer and fall. The eastern region has the shallowest HD, ranging from 95 to 105 m. The central region has the next deepest HD, ranging from 135 to 150 m. The CAA region has the widest annual variability, ranging from 165 to 190 m. Although the HD is deepest in the west, it has almost zero variation in its annual cycle. It is continuously around 200 m. These annual variations are discussed further in Chapter V.

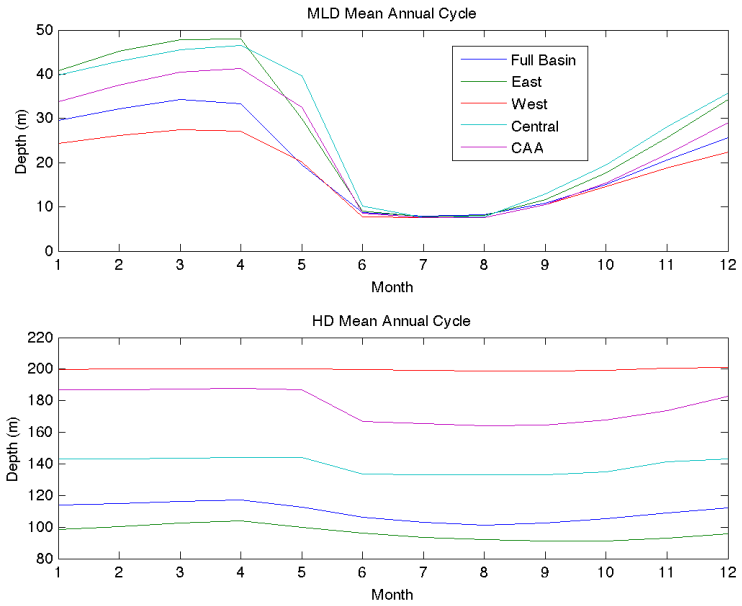

Figure 34. Mean annual cycles of MLD (top) and HD (bottom) for the full basin and the four sub-regions.

In addition to having differing mean annual cycles, the long-term inter-annual variability is different for each region. Figure 35 shows the MLD and HD anomaly time series for each region compared against the full-basin. With respect to MLD, the eastern region has seen the biggest long-term change, increasing by over 35 m between 1960 and 2010. Conversely, the mixed layer has become more shallow during the same period in the CAA region. The long-term deepening of the halocline appears to be driven by

changes in the west and CAA. The halocline depth in these regions deepened by over 100 m since 1948, with a large maximum anomaly in the late 1990s. Given more research time, it would be useful to see if this variation is correlated to climactic signals such as the Arctic Oscillation.

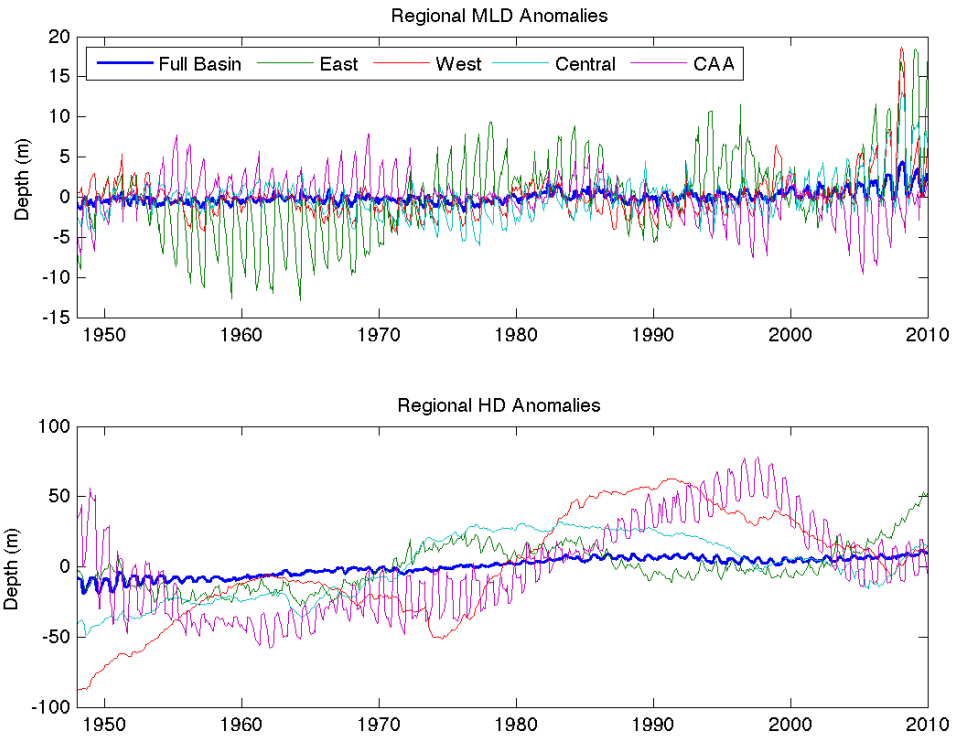

Figure 35. Anomalies, calculated as deviation from the mean annual cycle, of MLD and HD from 1948 to the end of 2009. Five regions are depicted: full-basin mean (blue), east (green), west (red), central (cyan), and CAA (magenta).

The important findings with respect to the Mixed Layer Depth and Halocline Depth are the spatial and temporal variations. The MLD does not vary significantly with region or over the long-term, but shorter time-scale variations are not negligible. The HD, however, shows significant changes. Excluding continental shelf regions, the halocline is much deeper in the western Arctic, and the western regions show much larger amplitude variations in time. The next section of this chapter will discuss heat content, and the impacts of a varying halocline depth.

2. Heat Content

As discussed in Chapter III, five methods for calculating heat content were examined; refer to Table 5 for a summary of the methods. These five methods are compared in order to identify which method best describes the ocean heat content contained in the less-stratified layer above the Atlantic layer, but below the mixed layer. Heat in this subsurface layer has the best chance of being mixed up into the surface layer and melting or reducing growth of sea ice, yet it is deep enough to be insulated from the atmosphere during the winter.

Methods HC-1 and HC-2 were used by Maslowski et al. (2014) to identify and remove the seasonal heat content signal generated by the mixed layer. Heat in the mixed layer is easily removed to the atmosphere before the winter freezeup, hence it does not contribute to the long term heat storage. In that study, 33m was chosen as the mean MLD, assuming the variations from the mean would cancel out in the long run. In the present study, method HC-3 precisely removes the mixed layer heat signature.

These three methods use a lower depth limit of 120m. This depth was chosen by Maslowski et al. (2014) as the model level closest to an approximation for the halocline depth in the eastern Arctic. The western Arctic, however, has a much deeper halocline, observed to be between 250 and 350 m by Polyakov et al. (2010). Method HC-5 uses 270 m as a lower depth limit, as this depth corresponds to the closest model level (refer to Table 3). Method HC-4 uses the calculated halocline depth at each point as a lower limit to the heat content integral.

Using each method, heat content per model grid cell was calculated for each RASM-H monthly output. A representative snapshot of March, 1979, is plotted in Figure 36. The color scale is in TJ, and the same scale is used for all five methods. As will be discussed further in Chapter V, methods HC-1, HC-2, and HC-3 produce similar results. These three methods produce much higher heat content in the eastern Arctic, especially near Fram Strait. Method HC-4 identifies more heat in the western Arctic, while method HC-5 identifies much more heat than the other methods throughout the basin, but especially in the eastern Arctic.

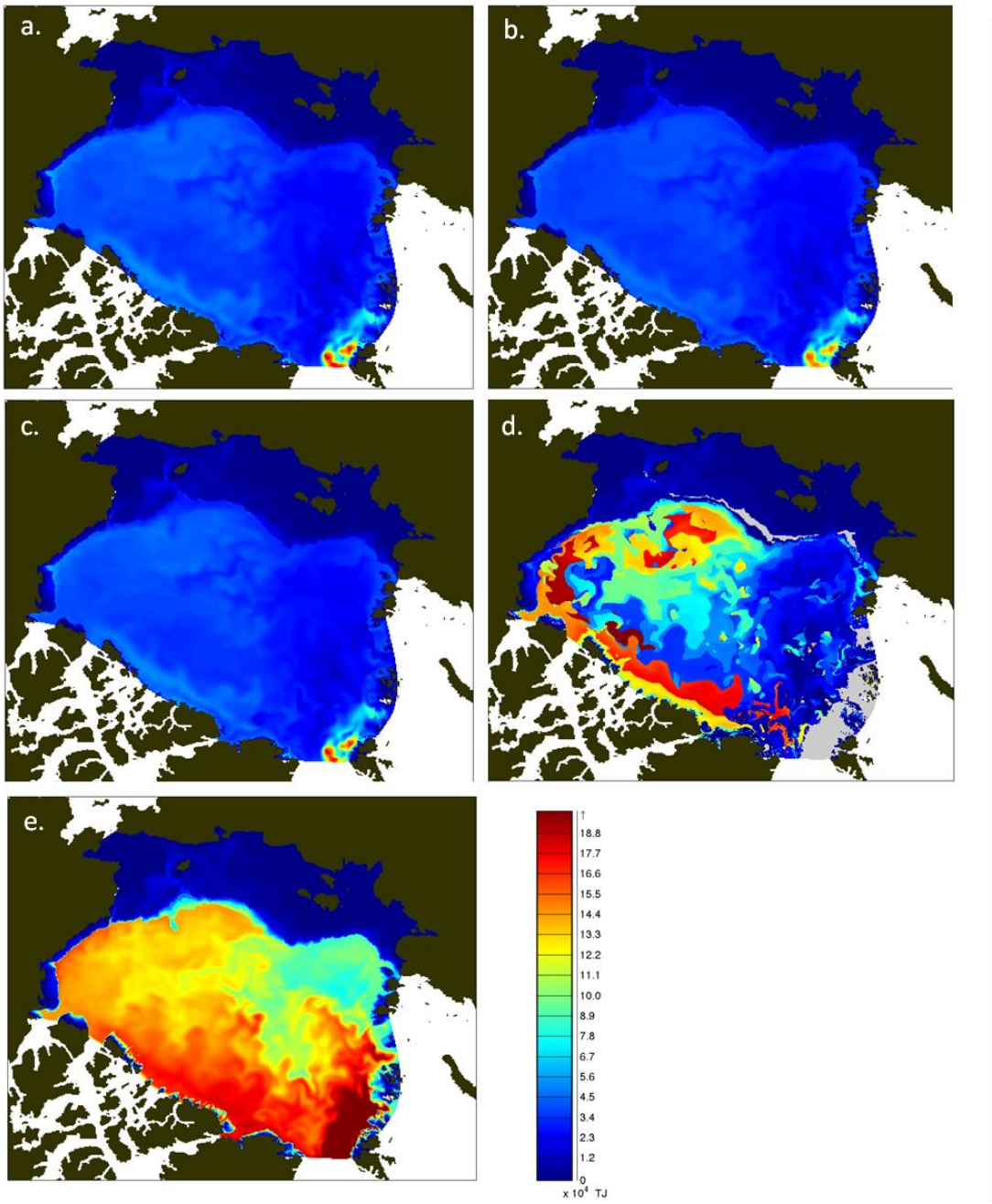

Figure 36. Heat content per model grid cell calculated using each of the five methods: a. HC-1; b. HC-2; c. HC-3; d. HC-4; e. HC-5. This uses the same projection as previous figures (e.g., Figures 29 and 30). Since the present study is focused on the central Arctic Ocean, data from outside the region of interest is masked out in white using the same mask as in IceSAT studies of Kwok et al (2007). Panel d, (HC-4, mixed layer depth to halocline depth) uses a grey mask where there is no halocline depth.

A brief review of these results indicates a few areas worth investigating further. There are large differences in the results of the five different sets of depth limits in the heat content calculations. There are also significant spatial variations even within each method. When a fixed depth is used for the lower limit, heat content from the Atlantic layer is included. These methods do not accurately represent the upper ocean heat content, because they count heat from below the halocline, hence it cannot reach the surface. Overall, the method HC-4 achieves the desired effect of removing the Atlantic Layer heat signature, while still including the heat content of the less stratified waters above.

As with the MLD and HD analysis, a mean annual cycle was calculated for each heat content estimation method. Figures 37 through 41 show the mean March, June, September, and December heat content maps for the five different methods. The general differences between the five methods were previously discussed and will be elaborated on in Chapter V.

For method HC-1 (Figure 37), the only significant spatial variations identifiable in the annual cycle are found along the continental shelves. The Chukchi Shelf shows warming in September, as does the Beaufort Slope just north of Alaska and western Canada. A similar spatial variation is found in methods HC-2 and HC-3 (Figures 38 and 39); however, these two methods show a smaller magnitude of variation. The two remaining methods, HC-4 and HC-5, also show an increased amount of heat content in the Chukchi Sea and Beaufort Slope regions in the summer, but those magnitudes of heat content are dwarfed by changes in other regions. There is little seasonal variation in the spatial patterns of HC-5, but that is not the case for HC-4. HC-4 (Figure 40) produces a greater value of heat content in the winter months (December and March) in the extreme western and southern parts of the basin adjacent to the CAA.

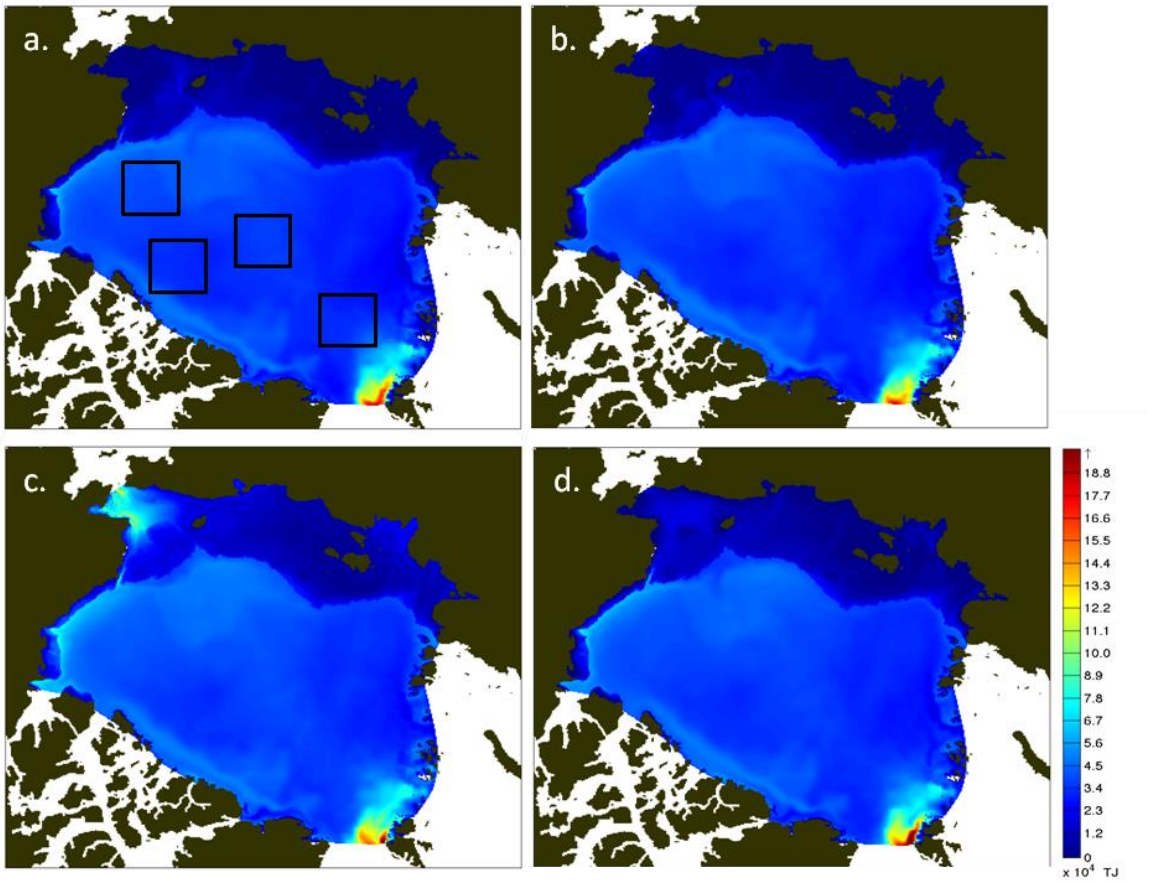

Figure 37. Mean monthly heat content per grid cell (TJ) between the surface and 120 m (method HC-1) for (a) March with outlines of sub-regions, (b) June, (c) September, (d) December. The same projection and mask are used as in Figure 36.

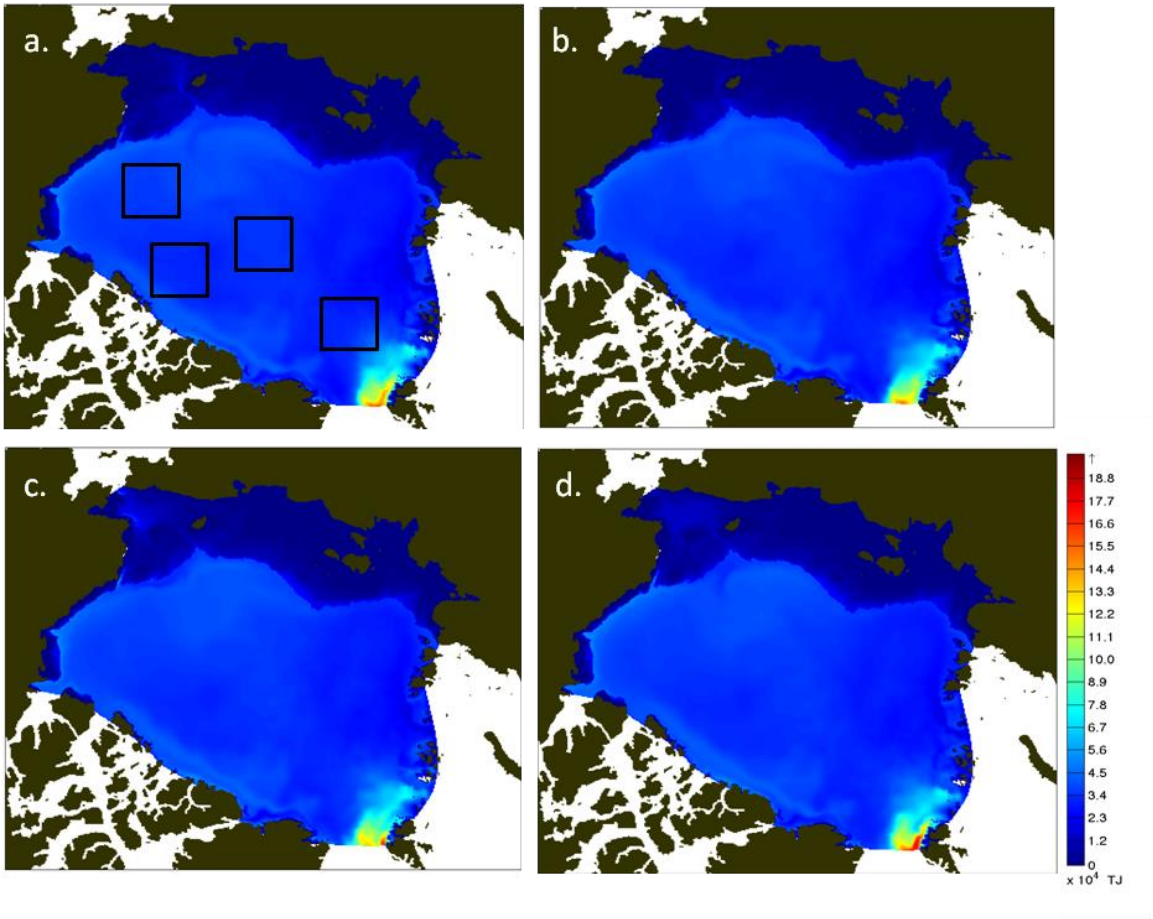

Figure 38. Same as Figure 37, but for 33 m to 120 m (method HC-2).

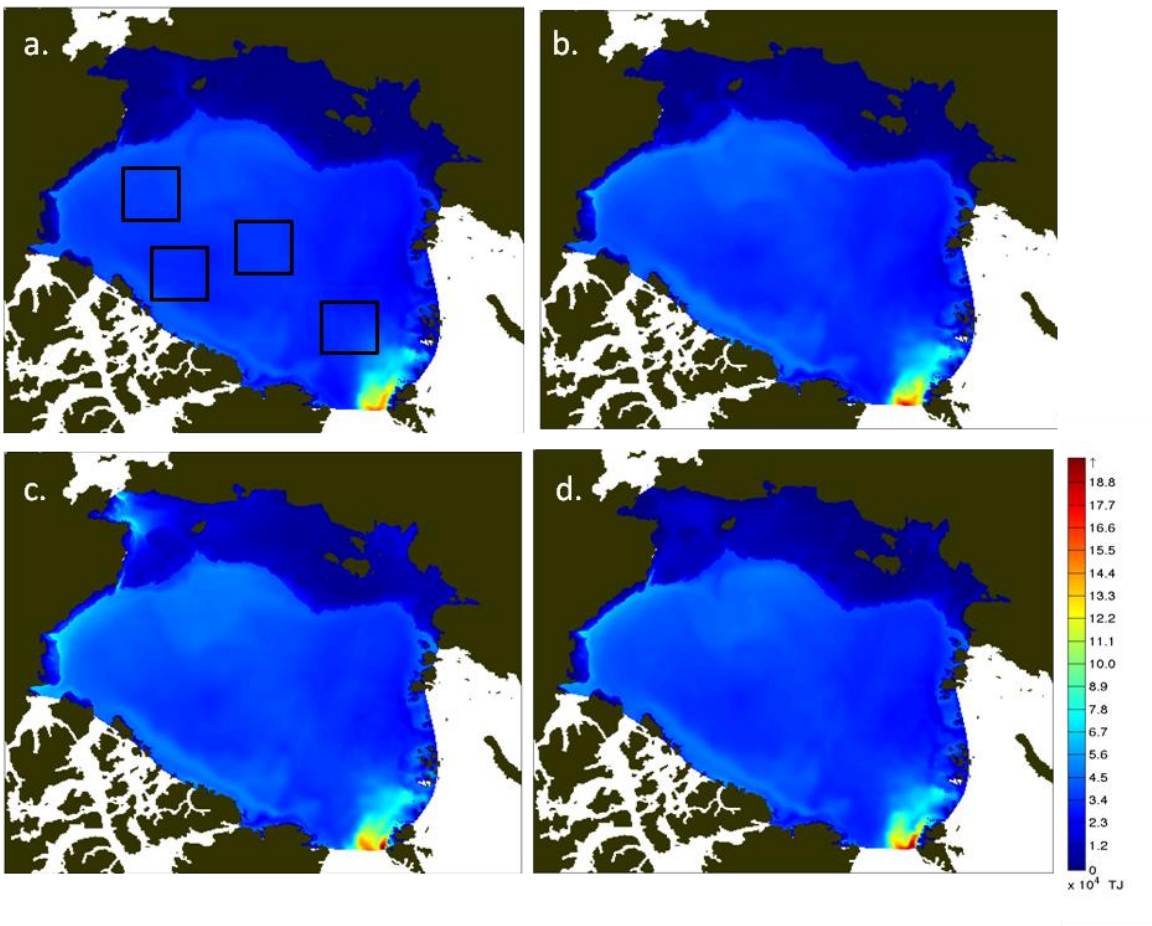

Figure 39. Same as Figure 37, but for MLD to 120 m (method HC-3).

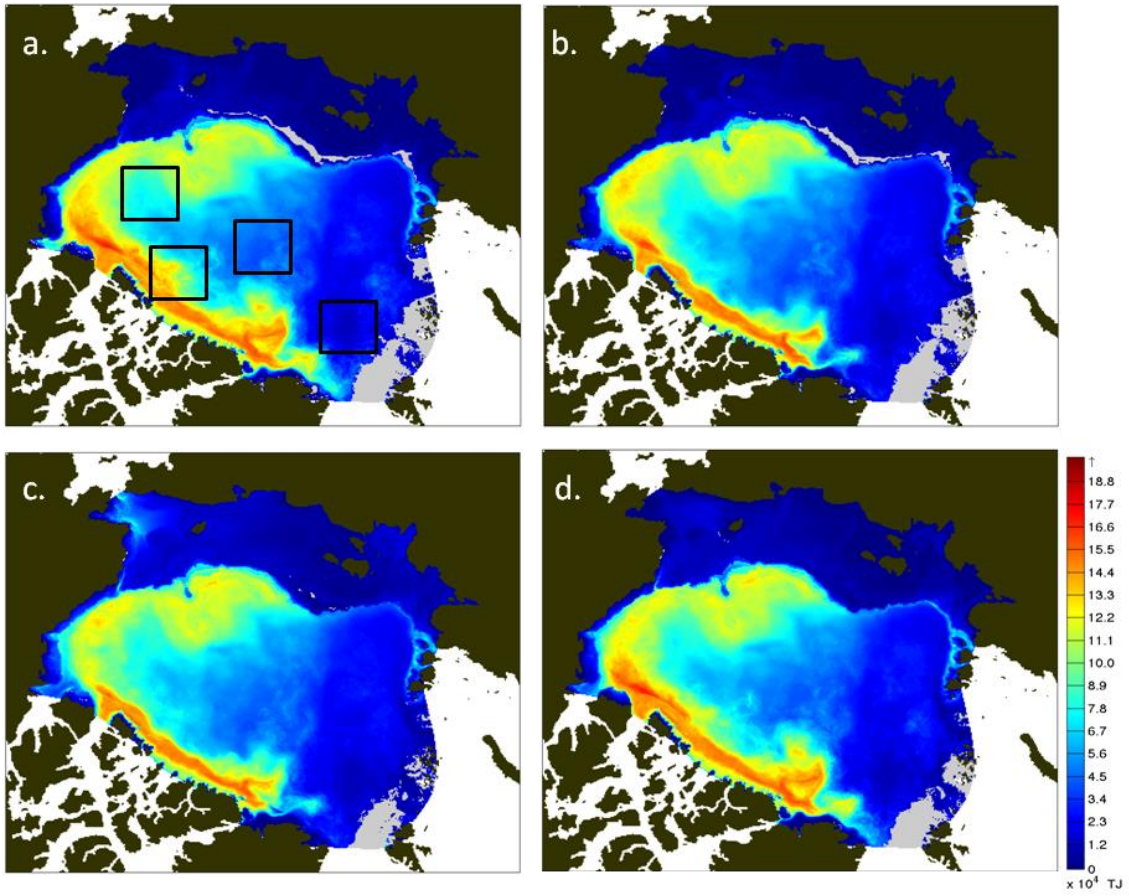

Figure 40. Same as Figure 37, but for MLD to HD (method HC-4). The light grey areas indicate where the HD finding algorithm produces a null result.

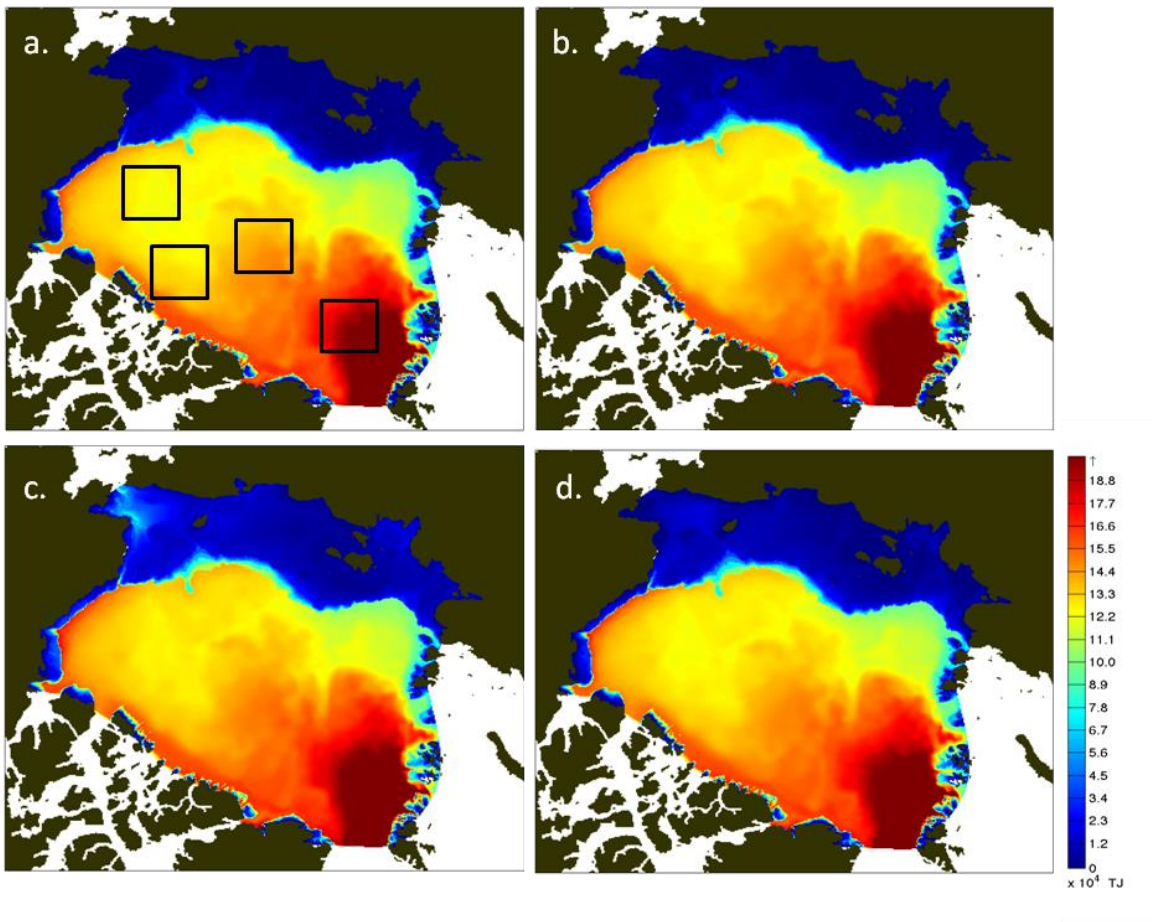

Figure 41. Same as Figure 37, but for MLD to 270 m (method HC-5).

By comparing months from the annual cycle, you can see that the spatial patterns of heat content do not vary much during the year. There are, however, are small variations which are better analyzed using time series. This will be the subject of the next section.

a. Full Arctic Ocean Temporal Variations

Time series of heat content for the full Arctic Ocean are shown in Figures 48 and 49. Figure 42 compares all five methods plotted on the same axes for a direct comparison, while Figure 43 breaks them into separate panes for a more detailed look at the individual methods. The mean annual cycle for each method was also calculated and is displayed in Figure 44. Four of the five methods produce annual cycles with the

warmest months coming late in the summer and the coolest months in late winter. The MLD to HD method goes against this trend and will be discussed further in Chapter V.

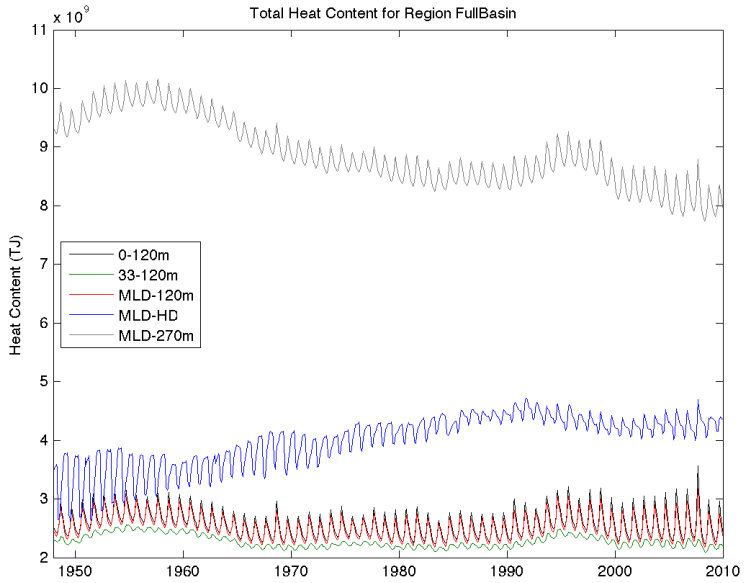

Figure 42. Total heat content time series for the full Arctic Ocean for all five sets of depth limits.

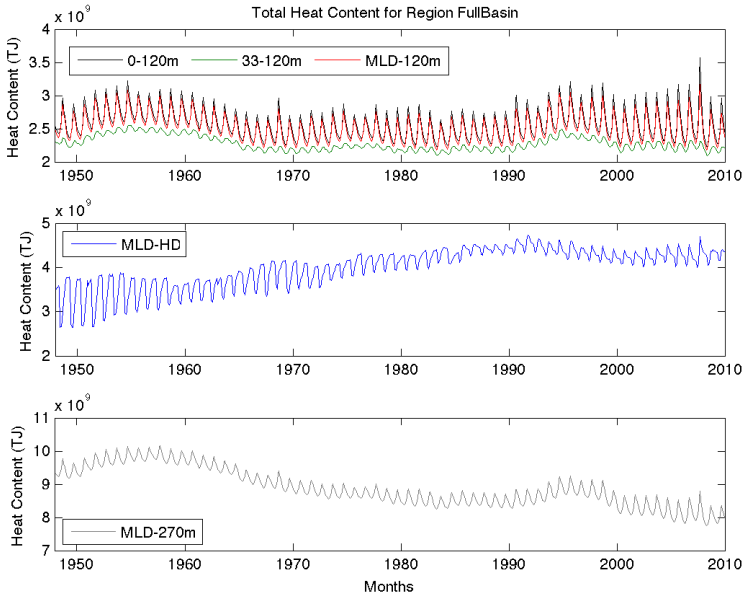

Figure 43. Same as Figure 42, but the MLD to HD (middle panel) and MLD to 270 m (bottom panel) methods are plotted on their own axes for ease of viewing. Vertical scales differ from panel to panel.

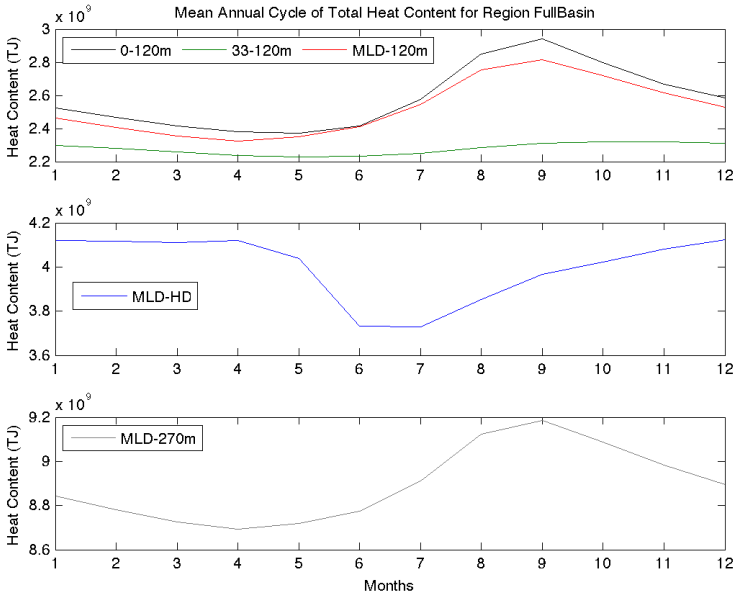

Figure 44. Mean annual cycles for the five ways of calculating heat content for the full Arctic Ocean. The MLD to HD (middle panel) and MLD to 270 m (bottom panel) methods are plotted on their own axes for ease of viewing. Vertical scales differ from panel to panel.

The mean annual cycles are subtracted from the absolute heat content values to obtain time series of heat content anomalies, which are plotted in Figure 45. This allows for an easier identification of long term trends. No long term trend appears to exist in the shallower three methods (HC-1, HC-2, and HC-3), but an amplified seasonal signal can be seen in the mid-2000s. Method HC-2 (which uses a fixed upper depth of 33m) has the weakest seasonal variability.

Large long-term trends are found in the HC-4 and HC-5 methods. Heat content between the mixed layer and the Atlantic layer (HC-4) increases significantly from 1948 to 1990, but then decreases slightly during the 1990s. The heat content in this layer increases again slightly from 2000 onward. Heat content found by method HC-5 shows a long-term decrease, but with local maxima in the late 1950s and late 1990s.

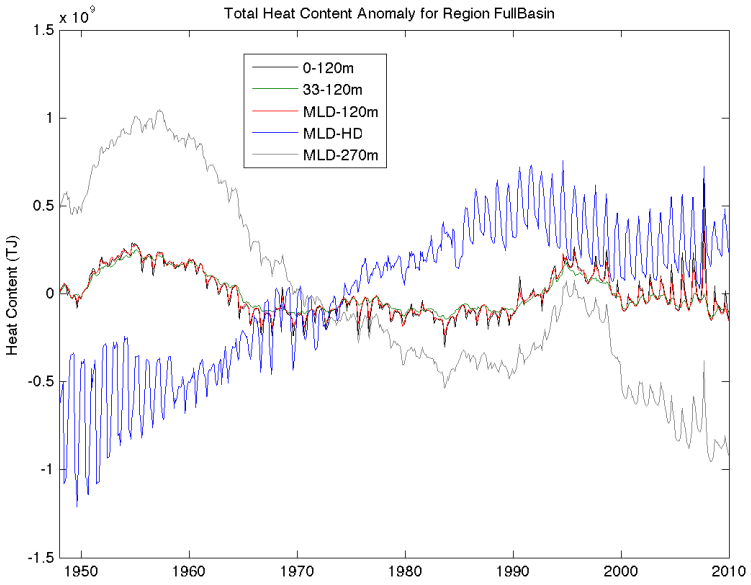

Figure 45. Heat content anomalies, calculated by subtracting the mean annual cycle of heat content from the absolute values, for all five methods in the Arctic Ocean.

b. Regional Variations

The 2-D plots of heat content in Figures 42 through 45 illustrate the regional variations in heat content within each method, as well as between methods. To better quantify these differences, time series of heat content from the regional sub-sets defined above (see Figure 30 a.) are analyzed next. The regions are 50 by 50 grid cells, so their approximate spatial extent is each about 200,000 km^2. Figure 46 shows the mean annual cycle of the five different methods of calculating heat content for each region. This mean annual cycle for each method is removed from the absolute total heat content time series to produce the anomalies for each region in Figure 47.

For all regions, methods HC-1, HC-2, and HC-3 have similar mean annual cycles. As with the full basin annual cycle, HC-2 (33 m to 120 m) has the narrowest range of seasonal variability and has the least amount of heat in most months. The HC-3 method, which uses a dynamically varying MLD as the upper depth limit, generally produces the same amount of heat as HC-1 from May to September and close to the same as HC-2 from February to April. This correlates with the mean annual signal of monthly MLDs,

where the MLD is shallowest in May through September and deepest from February to April (see Figure 34.)

There is a large difference in mean annual cycles for HC-4 (MLD to HD, middle panels) across all regions. Regions East, West, and Central have similar magnitudes of variation, but region CAA has almost an order of magnitude larger seasonal variation. The seasonal variation of the eastern, western, and central regions is approximately 0.15 x 10^8TJ, but is 0.8 x 10^8TJ in the CAA. Additionally, the total amount of heat content is different from region to region. Region East has the smallest amount of heat content in this layer, approximately 0.41 to 0.52 x 10^8TJ. The central region has almost twice this heat content, ranging from about 1.16 to 1.23 x 10^8TJ. The western and CAA regions have the most amount of heat in the MLD to HD layer, at around 2.2 x 10^8TJ. The reasons for these variations, and implications for affecting the patterns of sea ice melting, are discussed in the next chapter.

The bottom panels in Figure 46 show the mean annual cycle of heat content calculated by method HC-5, which uses a fixed lower depth of 270 m. This method produces the most heat of all the methods. The magnitude of seasonal variability is similar in all regions, though the total amount of heat is greatest in the east.

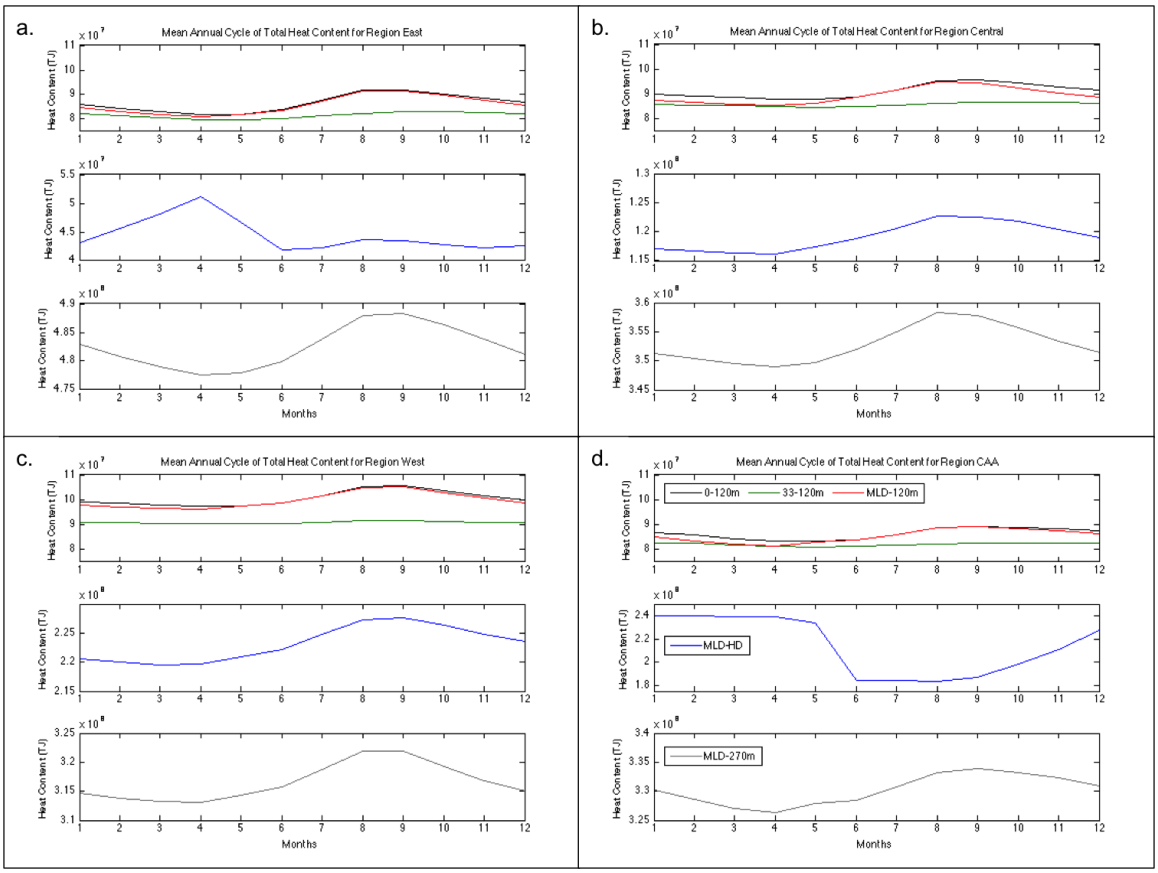

Figure 46. Mean annual cycles of total heat content in each sub-region, as calculated with five different methods. a) East, b) Central, c) West, d) CAA. Methods HC-1, HC-2, and HC-3 are the top panel of each figure; the vertical scales are the same. Method HC-4 is the middle panel; for figures a), b), and c), the scales are the same, but the maxima and minima are different. For figure d), a different scale is used. Method HC-5 is the bottom panel of each figure; the same scales are used, but the maxima and minima are different.

As before, these mean annual cycles are subtracted from the full 1948 to 2009 time series of heat content to obtain anomalies that are plotted in Figure 47. This way, inter-annual to multi-decadal trends can be identified. In all four regions, the three methods using 120 m as a lower depth (HC-1, HC-2, and HC-3) produce nearly identical results in the long term. With respect to these methods, the eastern Arctic shows the most long-term variability, with an overall declining trend during the time series. The western and CAA regions also show a decline in heat content above 120 m, but only in the time period after 2000. The central region has a slight increase in heat content above 120 m in

the late 2000s. The methods HC-4 and HC-5 generally show much more variability with time and from region to region. In the east, heat content anomalies from HC-4 are relatively small, but with a positive trend since 1990. The heat content anomalies from HC-5 show a very large negative trend from 1970 to 1980, and again from the mid-1990s through 2009, with a positive trend in the 1980s. Heat content anomalies from HC-4 and HC-5 in the eastern region follow similar trends to those in the east, but with different magnitudes. HC-4 heat content anomalies increase from 1948 to 1980, then gradually decrease to the mid-2000s, but then increase again. HC-5 heat content anomalies are opposite those of HC-4 until the mid-2000s when they both increase. In the west and CAA, method HC-5 anomalies are similar to those of HC-1, HC-2, and HC-3, but with slightly larger amplitudes, especially in recent years. However, the heat estimated by method HC-4 is very different. In the west, heat content increases by more than 2.5×10^8 TJ, which means that heat content more than doubles in value from 1948 to the mid-1990s. From the 1990s onward, this layer of heat content decreases back to the value of the long-term mean. In the CAA region, heat content from method HC-4 also doubles, but the trend lags behind that of the west by about five years. Heat content reaches a maximum in the late 1990s here. This layer in the CAA also still retains a large annual cycle, even though the mean annual cycle has been removed, what will be discussed further in Chapter V.

Several interesting spatial and temporal trends have been identified in these model results. These results need to be evaluated against observations before their significance can be discussed. Comparisons between RASM-H and ITP data will be made in the following chapter.

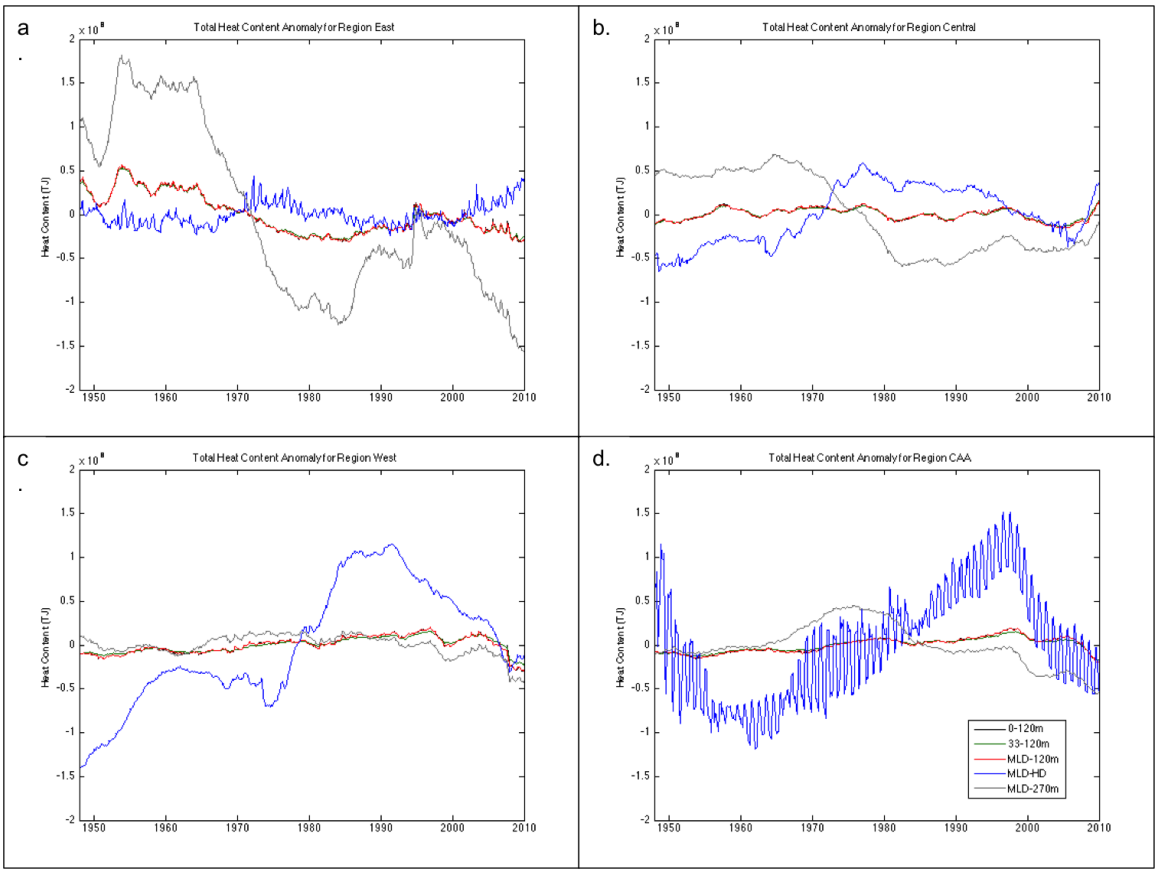

Figure 47. Heat content anomalies (heat content minus the mean annual cycle) for all five methods in each sub-region. a) East, b) Central, c) West, d) CAA.

c. RASM Heat Content Results Summary

Figures 48 and 49 summarize the variations in heat content depending on location and method. These figures show the long term mean heat content of the total basin (Figure 48) and the mean heat content per area (J/m^2) of each individual sub-region (Figure 49). In all regions, HC-5 estimates the greatest amount of heat. In all regions other than the east, HC-4 results in more heat than the three remaining methods. The eastern region has the least amount of heat in HC-4, as well as in the three methods using 120 m as a lower bound. However, it has by far the most amount of heat based on HC-5. The western and CAA regions are similar, with a large difference in heat content between HC-4 and the three shallower methods.

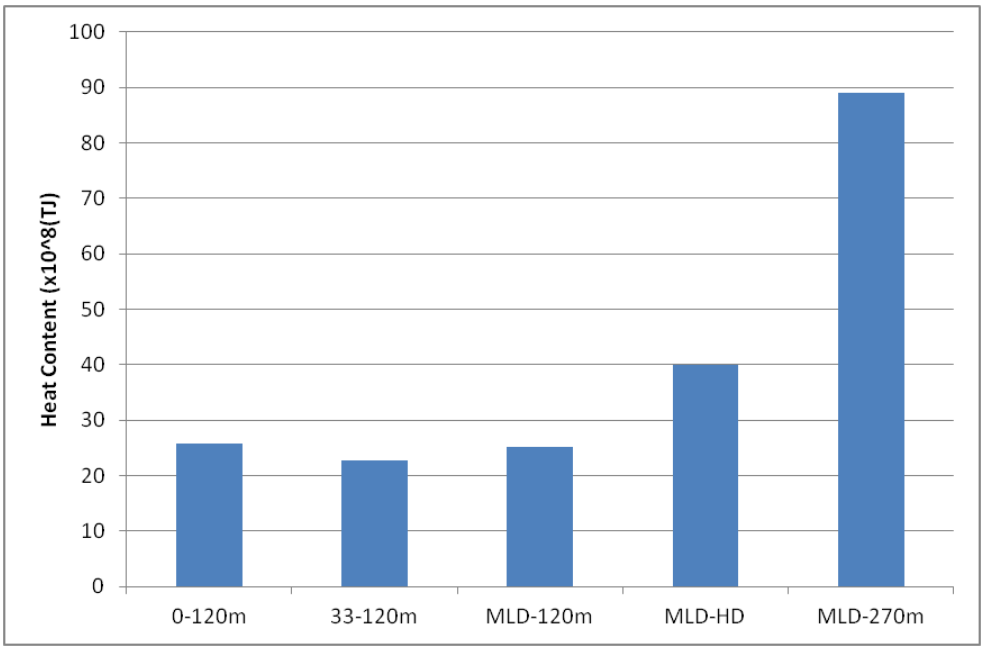

Figure 48. The long-term mean of full basin total heat content in the Arctic Ocean as determined by the five methods.

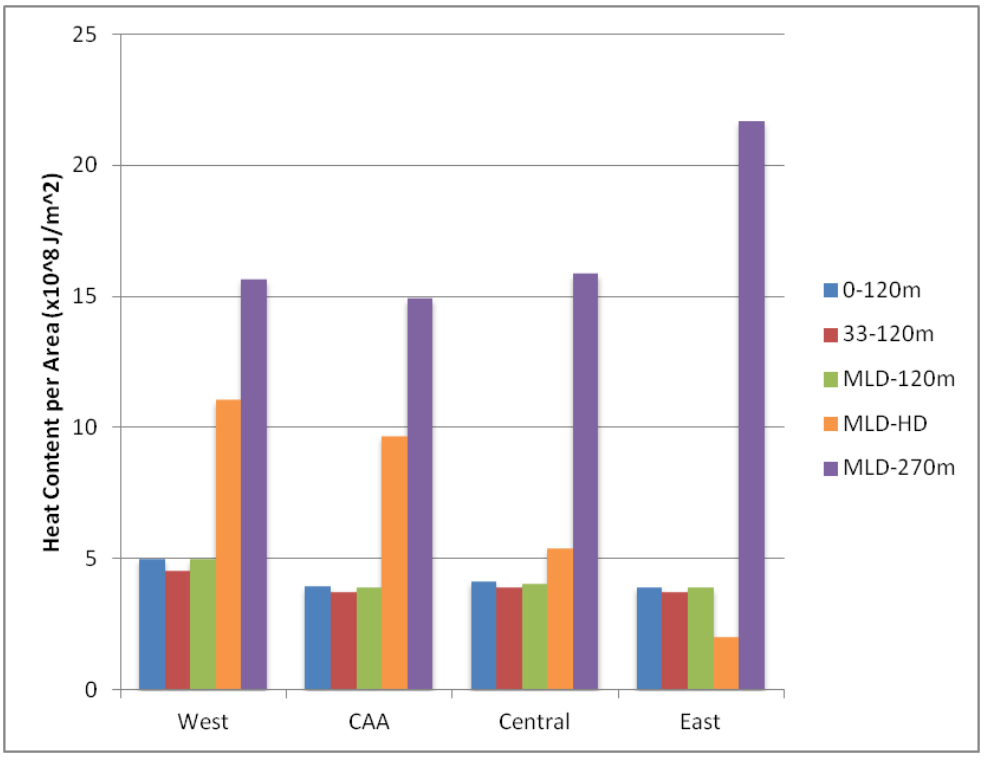

Figure 49. The long-term mean of regional heat content per area in the four sub-regions (defined in Figure 30 a.) of the Arctic Ocean as determined by the five methods.

C. OBSERVATIONAL RESULTS FROM ICE TETHERED PROFILERS

1. Mixed Layer Depth and Halocline Depth

To evaluate RASM-H results, estimates of MLD, HD, and heat content from the ITP observational data are presented here. Refer to Figure 8 and Table 1 in the Chapter III for locations and descriptions of the ITPs. The mean MLDs and HDs from each ITP are plotted in Figures 50 and 51 for ITPs located in the west and east, respectively. The mean MLDs are similar for all ITPs; eastern and western ITPs both show an average MLD of around 25-28 m. The mean halocline depth, however, is much deeper in the west than the east (160.7 m versus 120.0 m).

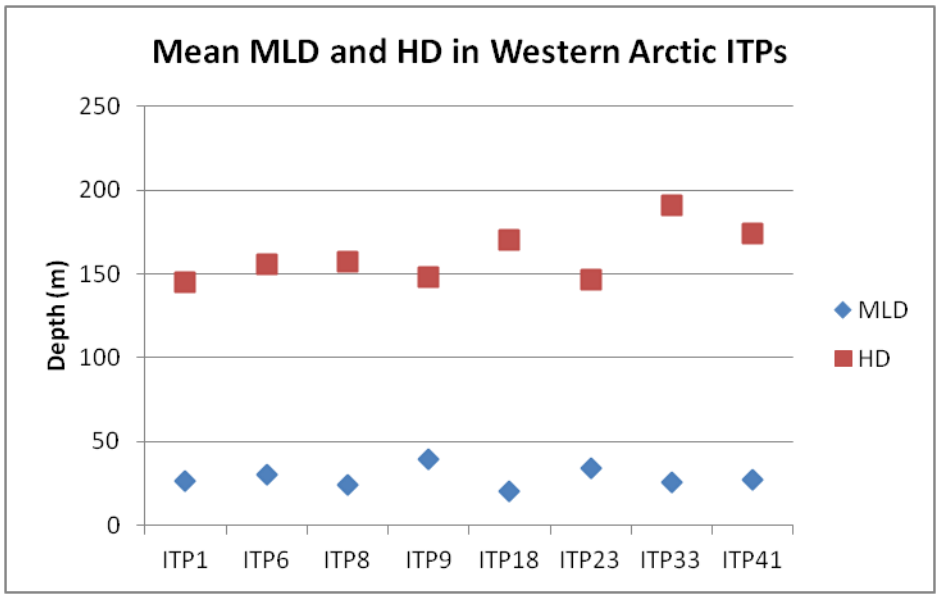

Figure 50. ITP-based estimates of MLDs and HDs in the Western Arctic. Since all ITPs are in the same region and are sequential in time, HDs appear to be deepening. ITPs 9 and 23 spend a significant portion of time near the CAA and have slightly shallower HDs and slightly deeper MLDs. See Figure 8 and Table 1 in the Methods chapter for locations and descriptions of ITPs.

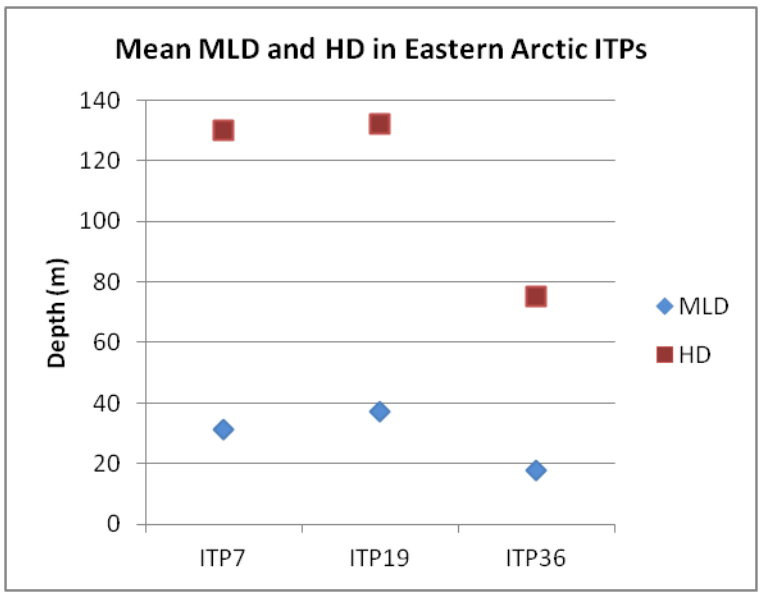

Figure 51. ITP-based estimates of MLDs and HDs in the Eastern Arctic. ITPs are not all from the same region; therefore, unlike with the western ITPs (Figure 50), we cannot say that there is a meaningful trend in MLD or HD.

Time series of ITP temperature with calculated MLD and HD are shown in Figures 52 and 53 for the western and eastern ITPs, respectively. To better visualize the heat content of these profiles, Figures 54 and 55 show the same time series but for the freezing point elevation (temperature minus freezing temperature, which can serve as a proxy of the heat content). ITP1 shows a typical seasonal development of the mixed layer (top left, Figures 52 and 54). In the October through January time frames, the MLD deepens to around 40 m where it remains until March. Then it begins to shoal to as low as 9 m in September. The HD generally deepens during the 18-month lifespan of the ITP, but is slightly deeper in the winter months. Its shallowest depth is 113 m in October of 2006, and deepest depth is 167 m in January of 2007.

In all western ITPs, summer Pacific water advected through Bering Strait (Jackson et al. 2011) can be seen as a warm band at around 80 m depth. A near surface temperature maximum (NSTM), which is a result of local solar insolation as described by Jackson et al. (2011), is visible just below the MLD in some, but not all, profiles. The NSTM is more easily identified in the freezing point elevation figures. The halocline

depth aligns with the minimum temperature associated with the winter Pacific water (Steele and Boyd 1998) at around 150 m. The HD varies in time and location, but is generally deeper than 120 m and shallower than 270 m. Notice that heat from the summer Pacific water can often be found below 120 m and heat from the Atlantic layer can usually be found shallower than 270 m. In the eastern ITPs (Figures 53 and 55), the HD is at or above 120 m. Even though there is very little heat above the HD there, any inclusion of the Atlantic layer below HD dominates estimates of heat content. It is also worth pointing out that ITP 36, from the Laptev Sea region, has a HD consistently shallower than 120 m, with a very strong Atlantic layer heat signature just below it.

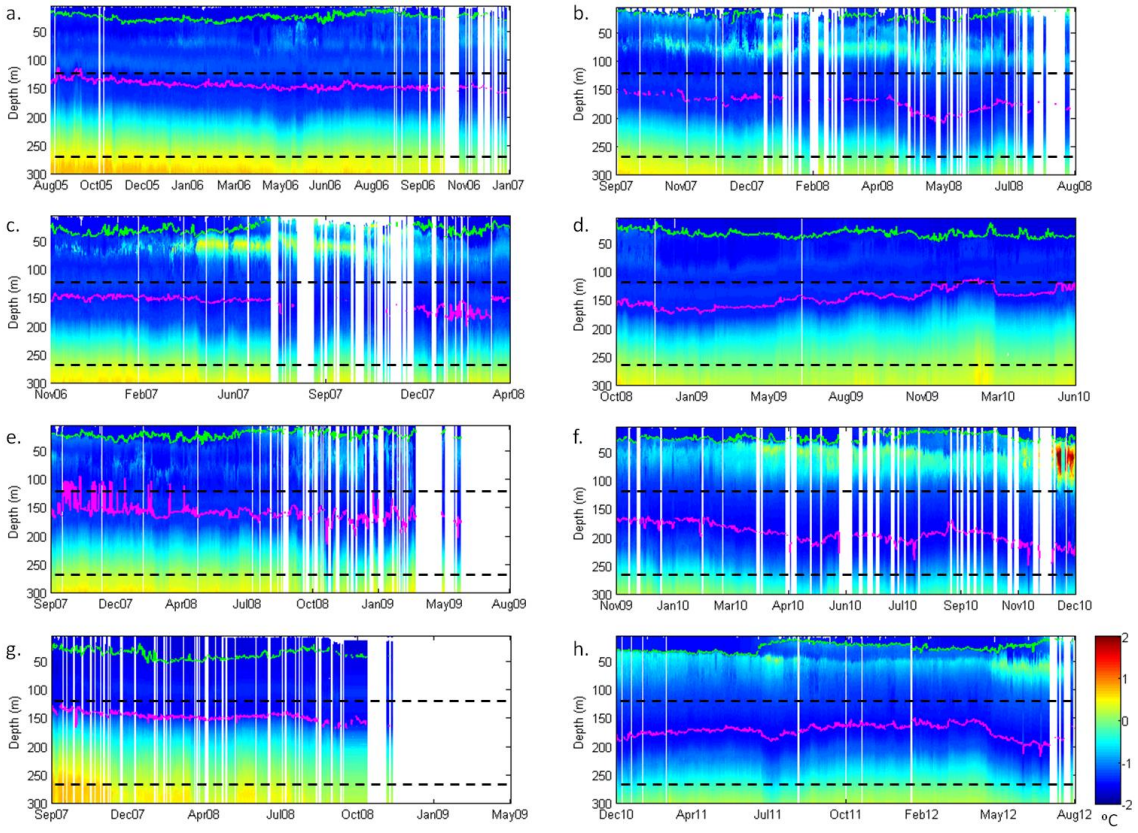

Figure 52. Temperature profiles with time for the eight western ITPs. The calculated MLD (green) and HD (magenta) are indicated. Also, dashed lines indicating 120 m and 270 m are shown for reference. The temperature scale is -2 to +2°C.

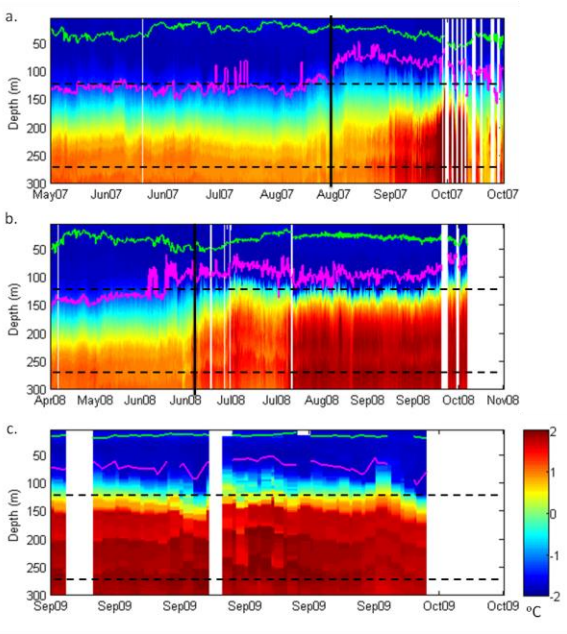

Figure 53. Same as Figure 52, but for eastern ITPs. Vertical black dashed line in ITPs 7 and 19 indicate approximate location where the ITP drifted out of the Arctic Ocean via the Fram Strait. Data after this time are ignored for analysis below.

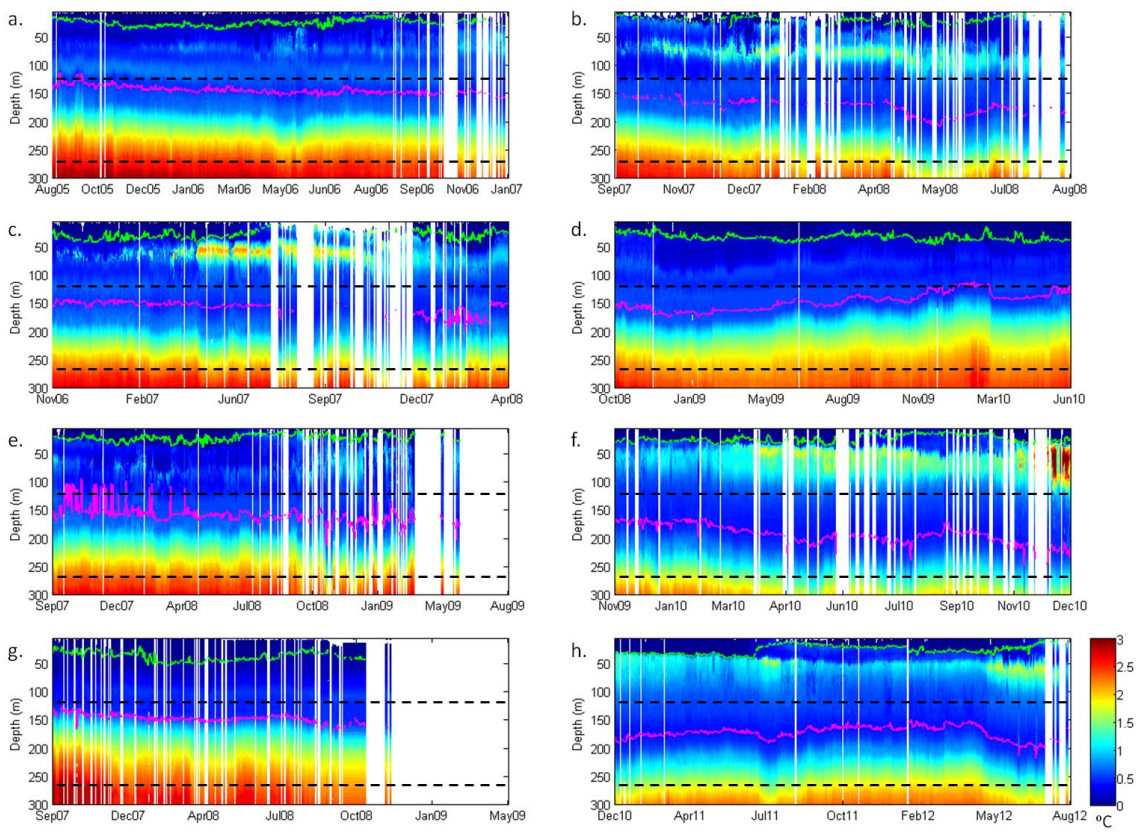

Figure 54. Same as Figure 52, but plotting freezing point elevation calculated as temperature minus the freezing temperature. The temperature scale is 0 to +3 ^{o}C.

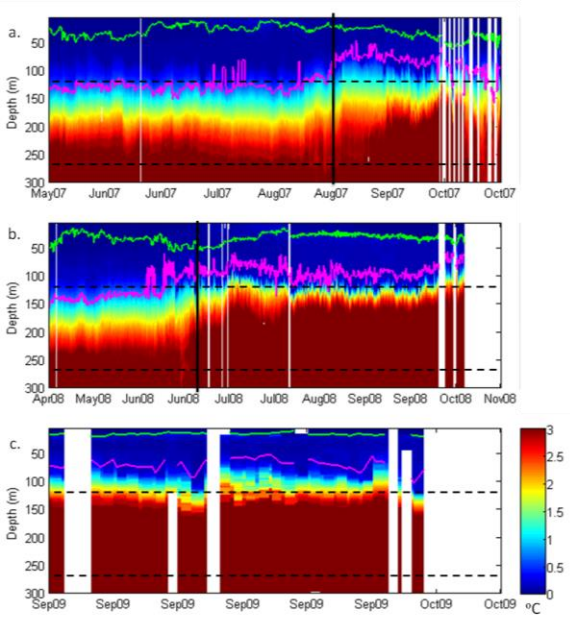

Figure 55. Same as 54, but for eastern ITPs.

2. Heat Content

As with the RASM calculations, the same five methods of calculating heat content from the ITP data are used. These are surface to 120 m (HC-1), 33 m to 120 m (HC-2), MLD to 120 m (HC-3), MLD to HD (HC-4), and MLD to 270 (HC-5; see Table 5). Figure 56 shows the MLD and HD (top panel) and heat content for the five different methods for ITP 1. Figure 57 shows the same information, but for ITP 7. Figures for all other ITPs are included in the Appendix.

The middle panel of Figure 56 (ITP 1) shows all five heat content calculations on the same scale. There is an approximate order of magnitude more heat in the HC-5 method than in any of the other methods. This is due to the fact that 270 m is deeper than the observed HD and is including heat from the Atlantic Layer. The bottom panel of Figure 56 excludes this method so the other four methods can be better compared. The remaining four methods produce results of similar magnitude and variability. The three methods that use 120 m as the lower limit produce almost identical results, indicating that there is little to no effect of adjusting the upper bound, and that heat near the surface is insignificant. Considering that for practical reasons ITPs are deployed in thick ice to

enhance platform survival (WHOI 2014), it is reasonable to expect that near-surface water is very close to freezing temperature throughout all seasons. The brief period between July and October 2006 goes against this trend, with an identifiable, albeit small, amount of heat between the surface and 33 m. After this period, however, heat in all levels increases as ITP 1 drifted south and reached its end of life.

For these analyses, heat content is calculated as heat content per area (J/m^2) around the ITP rather than attempting any sort of spatial extrapolation. For a large portion of the ITP life, the MLD-HD layer contains approximately 1 $x10^5$ J/m^2, or 50%, more heat than the methods bounded by 120 m. There is about 7 $x10^5$ J/m^2 more heat between the HD and 270 m, which is more than double the amount of heat above the HD.

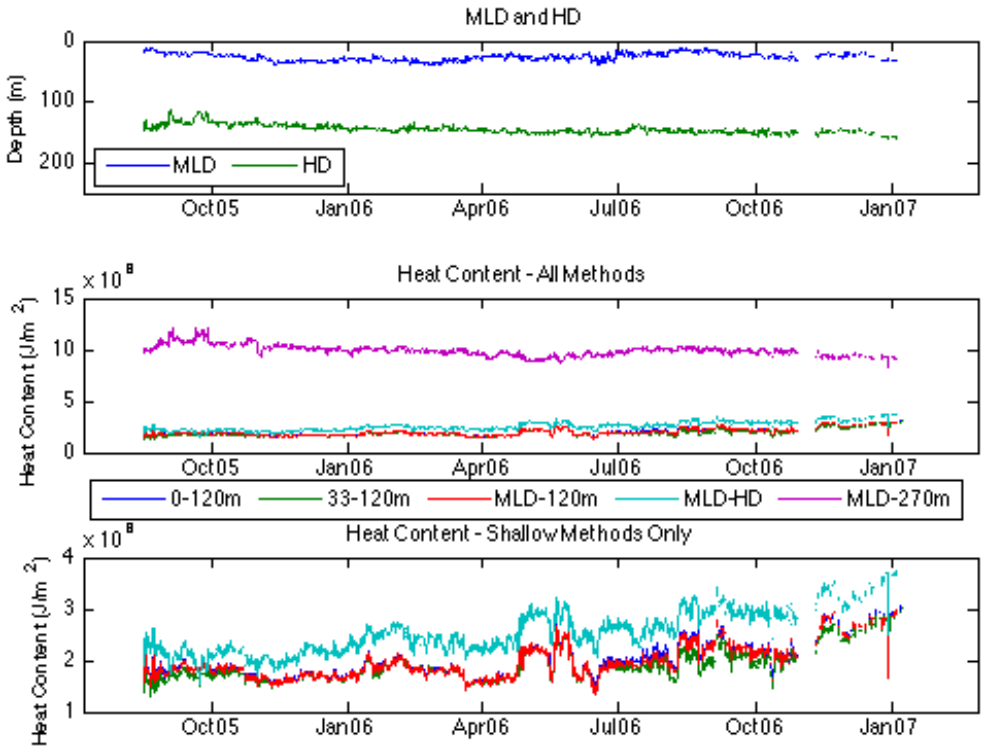

Figure 56. MLD and HD (top), and heat content per area (middle and bottom) for ITP1. The bottom plot has a smaller scale than the middle plot to better illustrate the differences between methods.

Figure 57 shows the same information as Figure 56, but for ITP7 in the east. Again, there is more heat in the MLD-HD layer than in any of the shallower than 120 m methods.

However, the magnitude of difference is much smaller. There is only about 0.25 $x10^5$ J/m^2 more heat between 120 m and the halocline, but the percent increase is still high at around 40%. The depths between the HD and 270 m contain a vastly greater amount of heat at around 14 $x10^5$ J/m^2, more than an order of magnitude more heat than is present above the halocline.

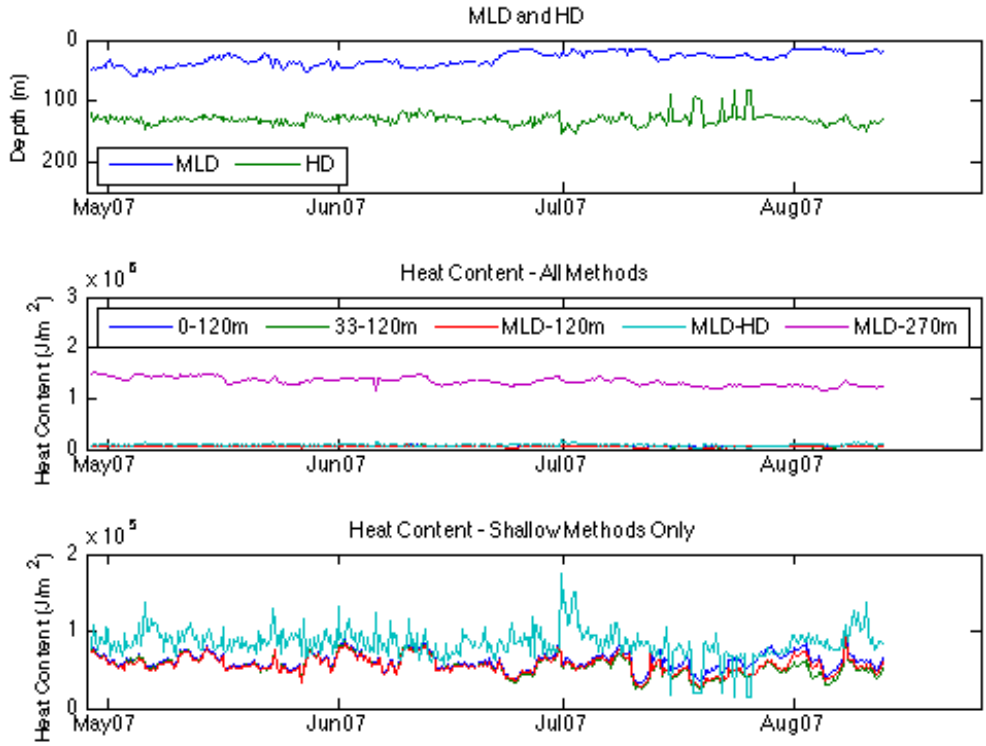

Figure 57. Same as Figure 56, but for ITP 7.

Figure 58 is a histogram of mean heat content per area for each ITP, comparing all five methods of calculating heat content, similarly as it was done for the model results (Fig. 49). Western ITPs have more heat in the shallower methods (surface to 120 m, 33 m to 120 m , MLD to 120 m, and MLD to HD) than the eastern ITPs. However, eastern ITPs have much higher mean heat contents in the MLD to 270 m layer. It can also be seen that the MLD-270 m method produces much more heat than any of the other methods. Also, the MLD-HD method identifies additional heat that is below 120 m in all ITPs except for ITP

36. From Figures 53 and 55, it can be seen that the halocline is shallower than 120 m in the eastern ITPs; therefore, less heat is found in the MLD-HD layer.

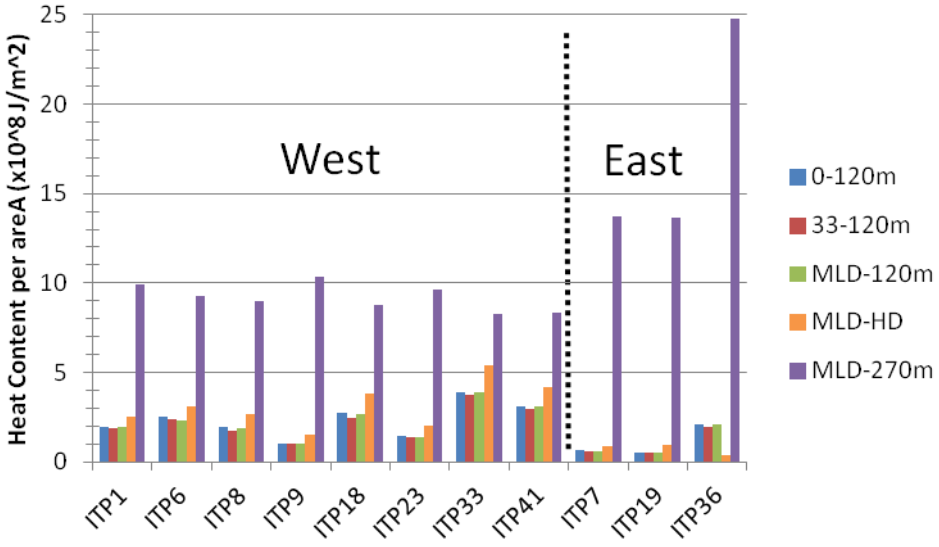

Figure 58. Histogram of mean heat content per profile of each ITP. All five methods are displayed.

Because the ITPs are operating sequentially in time from 2005 to 2010, a crude time series for that period can be constructed. From Figure 58, it can be seen that heat content in the first four methods has increased during this period. Figure 59 shows the MLD-HD heat content of all western ITPs to better illustrate this trend. The sample size is too small to claim any statistical significance, but the data is suggestive of an increasing amount of heat above the halocline. Another interesting trend that can be seen in Figure 64 is a slight decrease of heat content in the MLD to 270 m depth range.

These trends, their significance, and comparisons to RASM results will be further discussed in Chapter V.

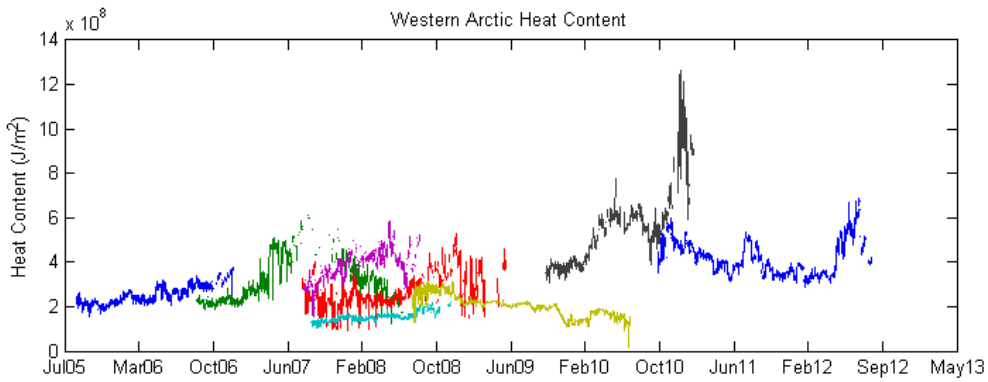

Figure 59. Heat content per area (J/m^2) between the MLD and HD for all western ITPs during the period of summer 2005 to summer 2010.

D. SUMMARY OF RESULTS

In this chapter, modeled and observed mixed layer depths, halocline depths, and ocean heat content were analyzed for spatial and temporal trends. Values and spatial patterns of MLD and HD were similar between the ITP data set and RASM-H. A 62-year hind-cast from RASM-H showed that the halocline has deepened since 1948, and the deepening was most significant in the west. Five ways to calculate heat content were compared using ITPs and RASM-H. Each method produced different amounts of heat content, and each method was characterized by different spatial and temporal patterns. These general patterns found by RASM-H are qualitatively similar to the patterns found in the observed record. Overall, the method of calculating heat content that uses the mixed layer depth and halocline depth as limits of integration best eliminates the Atlantic heat signature. In the next chapter, this method will be used to analyze how upper ocean heat content is distributed across the Arctic Ocean and how it has changed on seasonal, inter-annual, and decadal time scales.

V. DISCUSSION: UNDERSTANDING SPATIOTEMPORAL CHANGES IN UPPER OCEAN HEAT CONTENT IN THE ARCTIC FROM 1948 TO 2009

A. OVERVIEW

The purpose of this study is to estimate the magnitudes and variability of heat content in the upper Arctic Ocean, defined as the ocean layer below the surface mixed layer and above the halocline, from local to basin-wide and from seasonal to multi-decadal scales, in order to advance understanding of potential contributions of oceanic forcing to 21st century decline in the Arctic sea ice cover. Summary of the results presented in the previous chapter yields three primary findings:

- Significant differences exist among the five methods used to calculate heat content in the upper Arctic Ocean.
- The mean annual cycle of heat content is not spatially uniform.
- Significant spatial and temporal trends exist in upper ocean heat content.

Each of these findings will be discussed in greater detail in this chapter.

B. DIFFERENCES AMONG THE FIVE METHODS OF ESTIMATING HEAT CONTENT IN THE UPPER ARCTIC OCEAN

1. Comparing RASM-H and ITP Data Sets

Prior to conducting any comparisons between the modeled and observed data sets, there are a few important details to point out. Recall from Chapter III that ITPs are Lagrangian sensors, moving with the ice and sampling different locations along the drift track during its lifetime. The model results used, however, are in the Eularian grid. Also, the rate at which ITPs drift and sample (twice daily) leads to a horizontal resolution on the order of tens of meters. The ocean model component of RASM-H, on the other hand, has a horizontal resolution of about 9 km. Vertical resolutions are different as well. ITPs sample at 1 m vertical resolution, while RASM-H has vertical resolution ranging from 5 m at near the surface to 300 m at depth (see Table 3 in Chapter III). Finally, and most importantly, RASM-H outputs monthly mean values of temperature and salinity, from

which heat content was calculated. ITPs are measuring temperature and salinity twice daily. Finally, the two data sets are used differently to characterize spatial differences. Results from the ITPs are lumped into one of two regions, east or west, while 50 x 50 model grid cell sub-regions were defined in RASM-H. The model regions chosen are similar to, but not precisely identical to, the observed locations. Considering all of these differences, it would be unrealistic to expect the RASM-H temperatures and heat contents to be the same as those from ITPs. To produce meaningful comparisons, we look at long-term means of regional model subsets that are co-located with groups of ITPs. For RASM-H output, heat content per area (m^2) is used, while for ITP data, heat content per profile (per sampled point) is used. The magnitudes of heat content are not the same, but some general characteristics, e.g., trends, can be compared.

2. MLD as an Upper Limit

Consistent across all times and places, using the MLD as an upper depth limit for heat content calculations produces a different result than any fixed depth. This is true for both model output as well as observational data. Many of the RASM-H results presented above support this finding, but it is most easily understood when looking at the mean annual cycle of heat content presented in Figure 44. In the top panels of this figure, the three methods that use 120 m as a lower depth boundary to calculate the full Arctic mean annual cycle of heat content are compared. Considering the surface upper boundary method as a control, it can be seen that the other two methods produce less heat, as expected. Method HC-2, which uses a fixed top depth of 33m, shows a highly dampened annual cycle, with much less heat being accounted for during the summer months than in the others methods. This indicates that the atmospheric and solar radiation heat signal does not penetrate deeper than 33 m. While removing this heat is desirable, the arbitrarily set depth of 33 m may exclude significant sources of heat near the surface such as the NSTM and possibly summer Pacific water. Also, as seen in Figures 29, 33, and 35, there are too many spatial and temporal variations in MLD to consider 33 m a suitable estimate of MLD. Method HC-3, which uses the calculated MLD as the top depth limit, has a slightly dampened annual cycle, but not nearly as much as the 33 m method. This shows

that the influence of solar and atmospheric heat fluxes is not completely removed, which is actually good as solar insolation below the mixed layer is retained.

While this specification is important when looking at variability on the annual scale, it is less important when looking at the inter-annual and multi-decadal time scales. As seen in Figure 42, there is little long-term variation among the three methods that use 120 m as a lower depth limit. To quantify these differences, the long term mean of heat content per area produced by method HC-3 is subtracted from methods HC-1 and HC-2 and plotted in Figure 60. There is less than 0.1 $x10^8$ J/m^2 additional heat between the MLD and the surface, and 0.1 to 0.42 $x10^8$ J/m^2 less heat between the MLD and 33 m. This value is about three orders of magnitude smaller than the total amount of heat or total variation of heat in these layers.

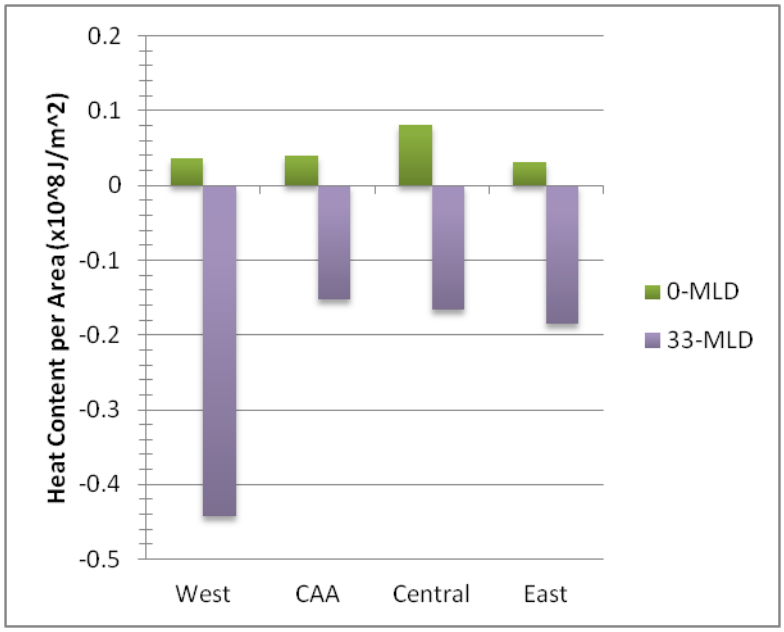

Figure 60. Differences between long-term mean estimates of heat content per area in the near-surface layers from RASM-H model output using methods HC-1, HC-2 and HC-3. The difference between the heat content from method HC-1 (surface to 120 m) and method HC-3 (MLD to 120 m) is in green, and the difference between method HC-2 (33 to 120 m) and method HC-3 (MLD to 120 m) is in purple.

The differences between these methods in RASM-H are small, but what about in observations? There is an almost imperceptible difference among the three 120 m methods presented in Figures 56, 57, and 58, but Figure 61 shows the exact differences. The differences range from 0.04 to 0.24 x10^8 J/m^2, which is of similar magnitude to the RASM-H results.

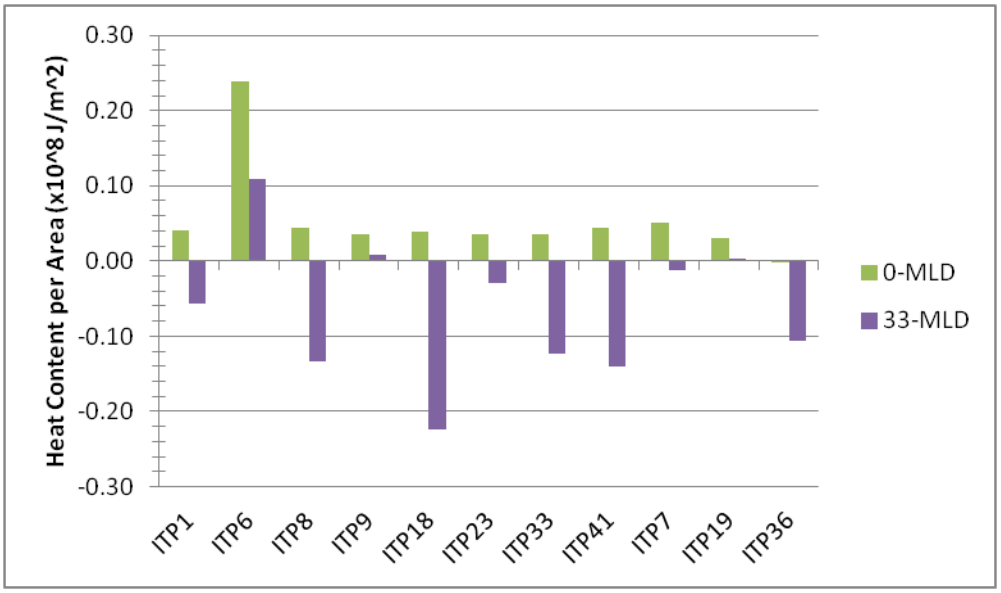

Figure 61. Differences between long-term mean estimates of heat content per area in near-surface layers in ITPs using methods HC-1, HC-2 and HC-3.

3. HD as a Lower Limit

RASM-H shows that in every region other than the east, the MLD to HD layer holds more heat in it than any of the methods that use 120 m as a bottom limit. This can be seen in the spatial patterns of heat content of Figures 37 through 41, or in the heat content time series of Figure 46. The histogram of long-term mean heat content estimated by each method shown in Figure 49 is a very simple comparison of the five methods showing these differences. To quantify them, Figure 62 shows the differences between heat content per area derived from method HC-4 and methods HC-3 and HC-5. It can be seen that in the three regions west of the Lomonosov Ridge, there is 6 x 10^8 J/m^2 of additional heat exists below 120 m that is still above the halocline. Typical magnitudes of

this ‘extra’ heat are on the same order of magnitude as the total heat content in that layer, hence represent a significant amount of heat. In the eastern Arctic, however, the difference is positive, indicating that setting a lower depth limit of 120 m is too deep, and includes excess heat from the Atlantic layer on the order of 50% of the total heat above the halocline.

Equally important is the finding that in all regions, setting a depth of 270 m as a lower limit accounts for too much heat from the Atlantic layer, which we are trying to exclude in our analyses. This is easily seen in the heat content maps (Figures 37 through 41), the heat content time series (Figure 46), and the long-term mean heat content histograms (Figures 48 and 49). Figure 62 plots the differences in mean heat content per area between methods HC-4 and HC-3 (blue), and HC-4 and HC-5 (red). The additional heat between the halocline and 270 m vary regionally, with the smallest difference in the west where the halocline is deepest and a very large difference in the east where the halocline is shallowest. The differences vary between 0.4 and 20 x 10^8 J/m^2. This represents anywhere from a 50% increase in heat content to almost ten times the amount of heat estimated in the upper ocean.

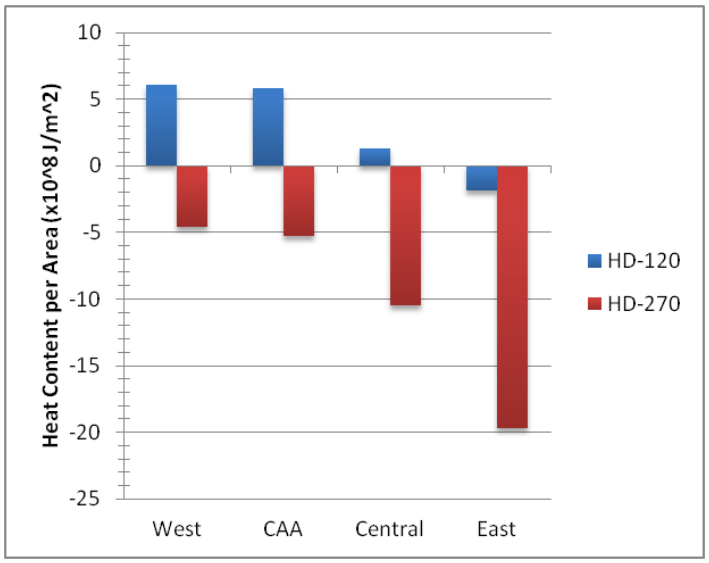

Figure 62. Differences between long-term mean estimates of heat content by region from RASM-H model output using methods HC-4, HC-3 and HC-5. The difference between methods HC-4 and HC-3 is in blue; the difference between methods HC-4 and HC-5 is in red.

A similar result is found in the ITP data, and is shown in Figure 63. The amount of heat below 120 m, but above the halocline depth is approximately 1 to 3 x10^8 J/m^2 for all ITPs other than ITP 36, where halocline is shallower than 120m. Using a depth limit of 120 m misses approximately 10 to 40% of the total heat above the halocline with the eastern ITPs representing the lower end of the spectrum. All of the ITPs measure a substantial amount of excess heat when 270 m is used as a lower bound. This holds true for RASM-H results as well. The amount of heat between the HD and 270 m accounts for roughly 50% of the total heat above 270 m in the west, and up to 98% in the east. This shows that, as measured by the ITPs, the heat below the halocline (i.e., heat from the Atlantic layer) overwhelmingly dominates the total heat content between the surface and 270 m. Clearly, using a fixed depth of 270 m as a lower limit overestimates upper ocean heat content, regardless whether using model output or observations.

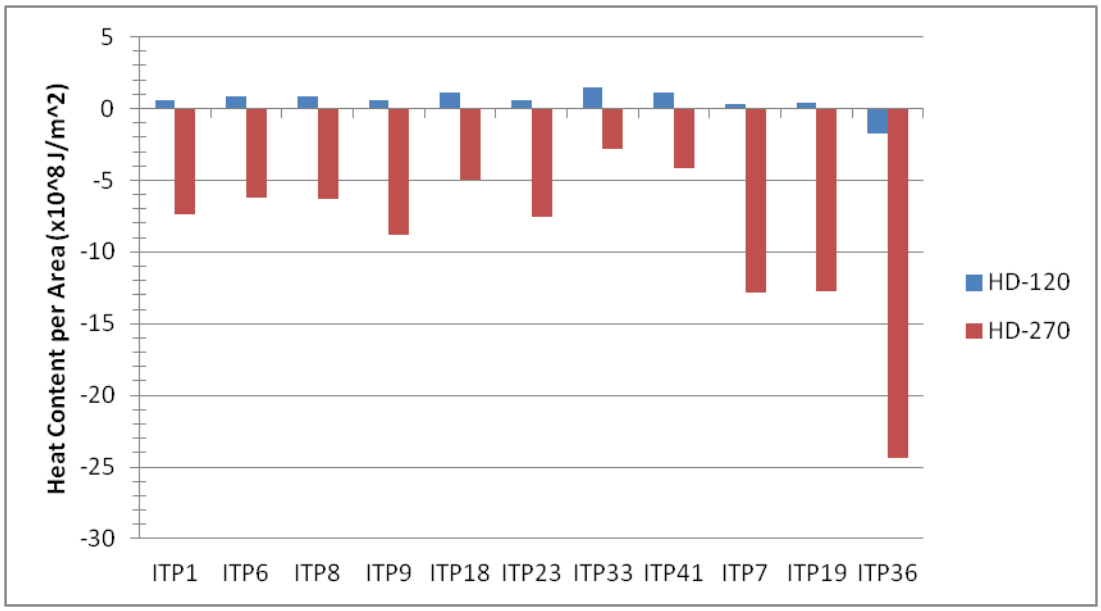

Figure 63. Same as Figure 62, but for data from ITPs.

Although it is difficult to make a direct comparison between the model and ITP because RASM-H is dealing with monthly means over a large area, while the ITPs are measuring at a much higher spatial and temporal resolution, the overall pattern and magnitudes of differences are remarkably similar. The similarities between RASM-H

output and ITP data allows us to safely proceed with using the model to analyze ocean heat content across long time series, and wide regional variations. These results also support the hypothesis that using a dynamically varying halocline depth as the lower bound produces a significantly different result, which more accurately reflects the stratification and processes governing upper ocean heat, which in turn contributes to understanding the role of oceanic forcing of sea ice melt.

C. THE ANNUAL CYCLE OF HEAT CONTENT

One of the outcomes of this study is the finding that the mean annual cycle of heat content between the mixed layer and the Atlantic layer, using a dynamically varying lower depth limit, is dramatically different from the mean annual cycle estimated using fixed depth limits. This can be seen in Figure 46.

The four methods that use a fixed lower limit produce annual cycles of similar shape. Heat content is highest in late summer and early fall when ice fraction is lowest and atmospheric temperatures are highest, and heat content is least at the end of the cold and dark winter. However, the MLD to HD method produces a significantly different result. Heat content is highest from December through May, then sharply decreases during the summer months. This variation is not insignificant. The difference between maximum and minimum heat content values is approximately 0.4×10^8, or about 10% of the total heat content. This is the same order of magnitude of change as identified in the other methods, but the timing is different. Because the only difference between this method and the others is the lower depth limit, the cause of this shape must be the variations in halocline depth. Figure 34 shows the mean annual cycles of MLD and HD for the full Arctic basin as well as the individual sub-regions.

The basin-wide mean HD is deepest in April and shallowest in August. This seasonal variation is strongest in the CAA region, and weakest in the western region. Figures 64 through 68 allow for a correlation between heat content and halocline depth by plotting the mean annual cycle of heat content (MLD to HD) on the top panel and the mean annual cycle of HD on the bottom panel. Each figure represents a different region. Figure 69 plots all regions on the same axes for ease of comparison.

Figure 64 compares the mean annual cycles of total heat content in the MLD to HD layer in the full Arctic Ocean to the mean annual cycle of the basin-wide average halocline depth. As shown above, the halocline depth varies substantially from region to region. Each region will be analyzed separately to identify their relative contributions to the full basin mean annual signal. For the full basin, heat content ranges from about 3.75 to 4.15 x 10^9 TJ, or by about 0.4 x 10^8 TJ annually. The seasonal change is roughly 15% of the total amount of heat. One of the most important results is the fact that a substantial amount of modeled heat remains in the upper ocean through winter, similarly as in observations (Jackson et al. 2010). This layer could act as a reservoir of heat that can be tapped during entrainment events such as storms, transient eddies, upwelling along the continental slope and submarine features, ice deformation and other mesoscale features yet to be fully determined.

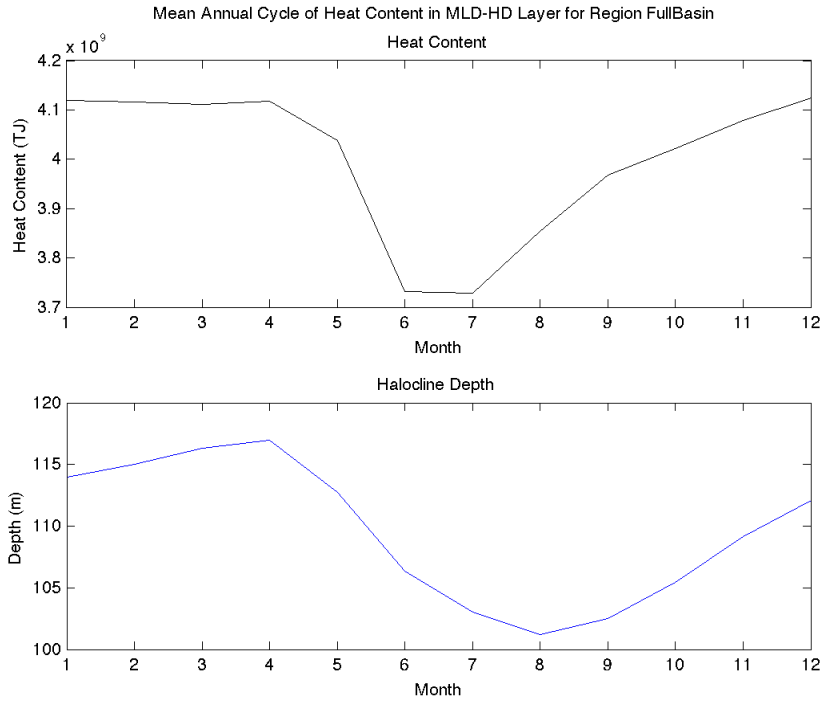

Figure 64. Mean annual cycle of total basin heat content in HC-4 (top) and of mean basin-wide halocline depth (bottom) for the full Arctic Ocean.

Figures 64 through 67 compare the same annual cycles, but for the sub-regions defined previously. Starting with the east (Figure 71), we can see that the total amount of heat in this region ranges from 4.2 to 5.15 x 10^7, or about 20% of the total heat. It is also apparent that the two cycles are almost perfectly correlated. High heat content exists in spring at the same time as the halocline is deepest. It should be noted that the total amount of heat in this layer is quite small, so variations in it may have a large effect within this region but a small impact on the total basin heat content.

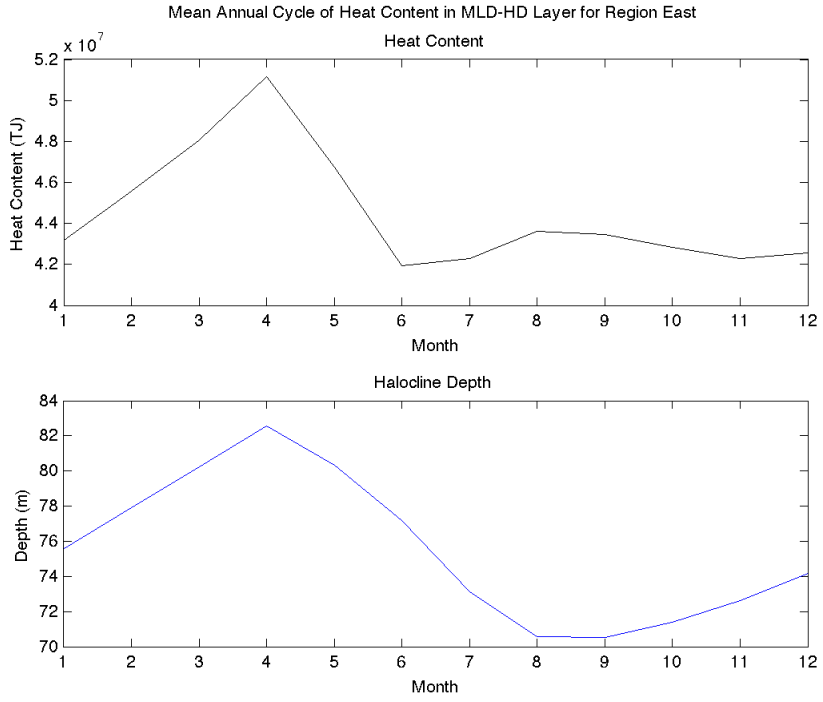

Figure 65. Same as Figure 64, but for the eastern sub-region.

Next to be discussed is the western region. There is almost an order of magnitude more heat in this region than in the east, and it follows the expected pattern of more heat in the late summer. However, the seasonal variability is roughly 0.08 x 10^8 TJ, only 3.5 % of the total. This is consistent with the relatively weak seasonal variability in the HD, which is only about 2 meters.

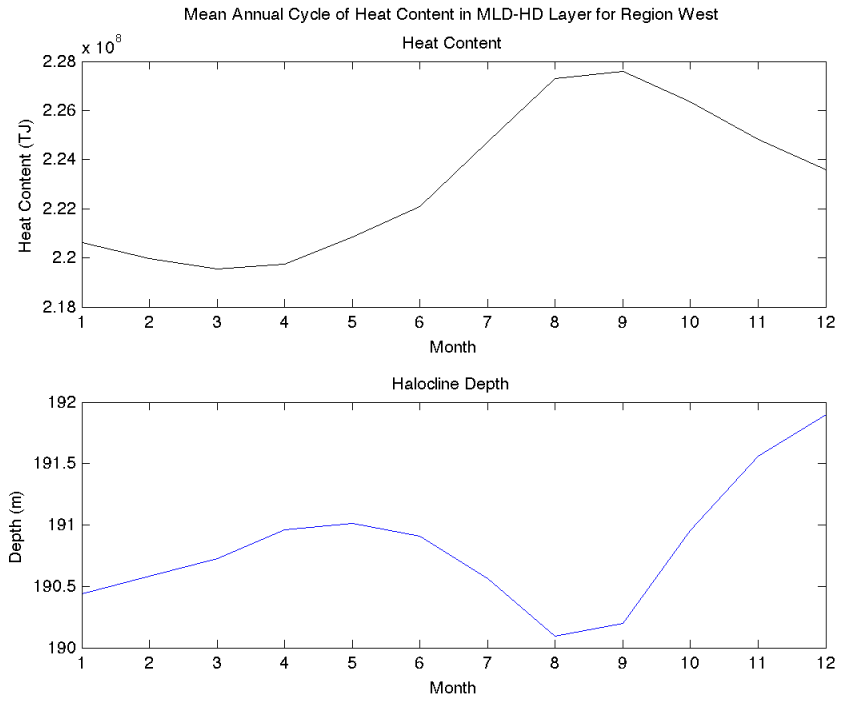

Figure 66. Same as Figure 64, but for the western sub-region.

The central region is very similar to the western region in most respects. The total heat content and halocline depth are both somewhat less in the central region, though of similar magnitudes. The seasonal variability of both parameters are also similar to those in the west.

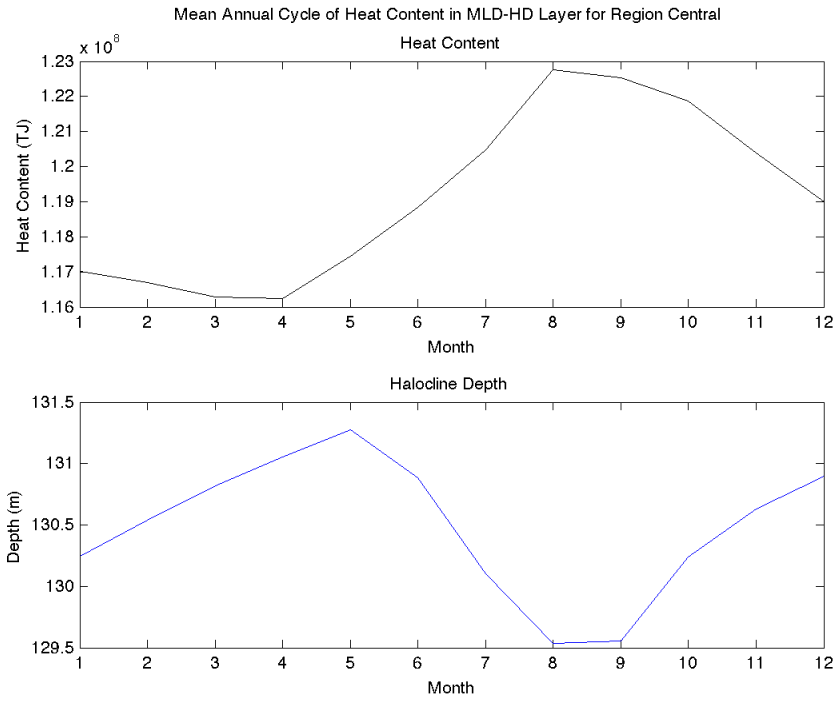

Figure 67. Same as Figure 64, but for the central sub-region.

The CAA region, however, is quite different than the other regions. While the magnitude of heat content is roughly the same as the western and central regions, approximately 2 x 10^8 TJ, its shape and range of variability are significantly different. The heat content varies by 0.6 x 10^8 TJ, approximately 30% of the average heat content, and is close to an order of magnitude greater change than in any other region. Because the heat content varies much more in the CAA region than any other, the heat content variability of CAA is the dominant factor in full Arctic basin heat content variability.

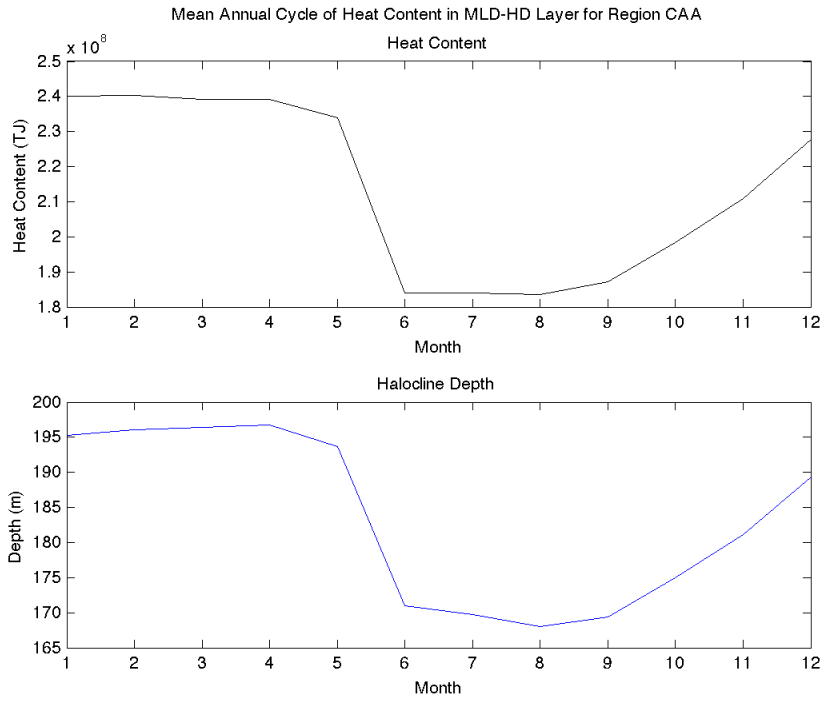

Figure 68. Same as Figure 64, but for the CAA sub-region.

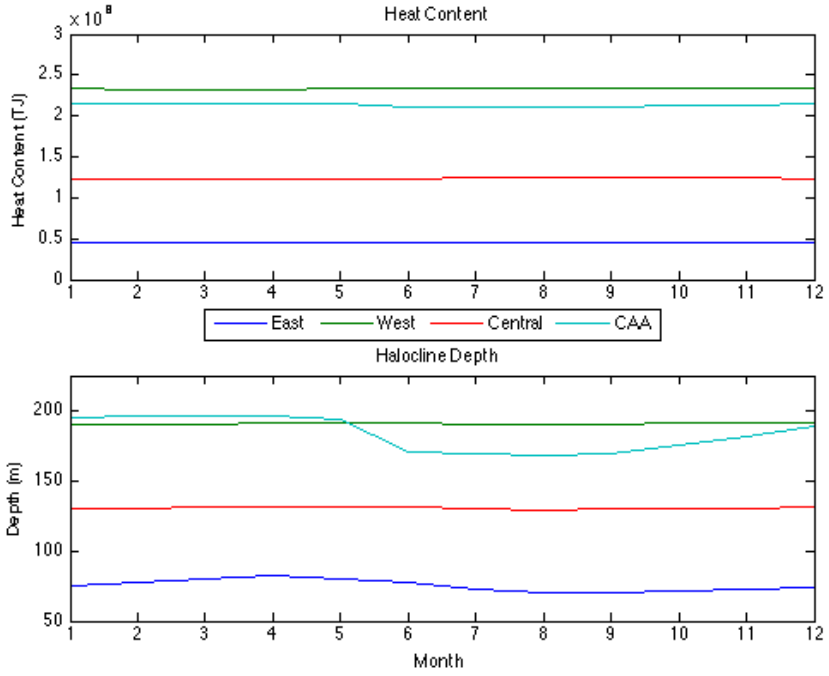

Figure 69. Same as Figure 64, but with all four sub-regions plotted simultaneously.

A deeper HD would increase the total depth range used in calculating heat content, but is this amount of heat significant? As discussed above, the layer between MLD and HD is stratified, though weakly, and heat close to the HD may not readily participate in occasional entrainment events. To better understand this, a set of sample temperature profiles from the arbitrarily chosen year of 1979 are plotted in Figure 70 along with the freezing temperature. The difference between temperature and freezing temperature gives a rough estimate of how much heat is in that model level. It is easily seen that the temperature around the halocline depth is approximately 1 degree Celsius above freezing, which represents approximately 7 x 10^7 J of heat, which is not an insignificant amount of heat. For thoroughness, profiles from other time periods were similarly analyzed and the results were consistent.

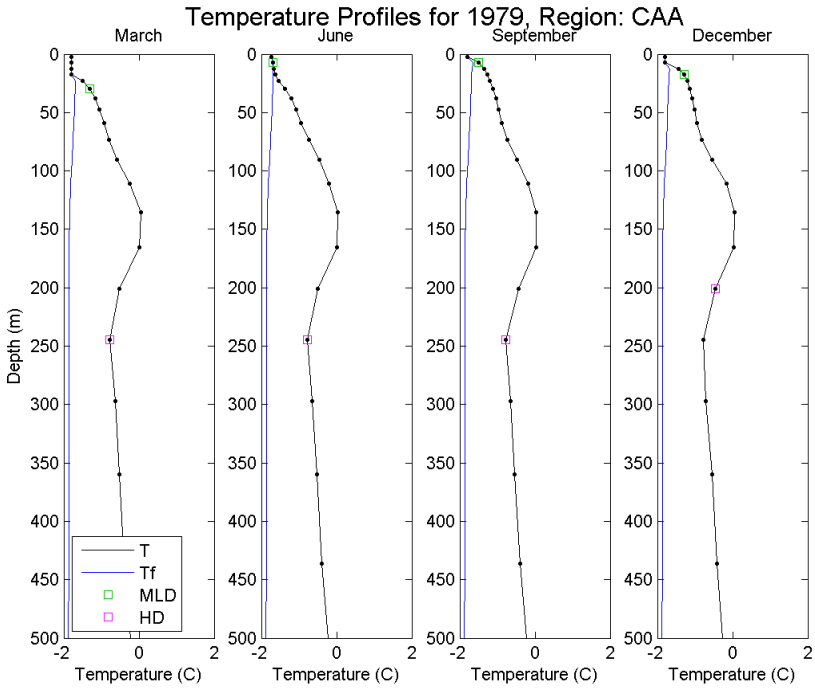

Figure 70. Profiles of model temperature (black) and freezing temperature (blue) for March, June, September, and December, 1979 for a point in the CAA sub-region. The black dots indicate model values at each discrete level, and the black line is a linear interpolation between model levels for ease of viewing. The MLD and HD for that profile are marked in green and magenta, respectively.

To verify this sensitivity of heat content to halocline depth, sample profiles from ITP 1 are plotted in Figure 71. At the depth of halocline, the freezing point elevation is approximately 1 degree Celsius, which supports the findings from RASM results.

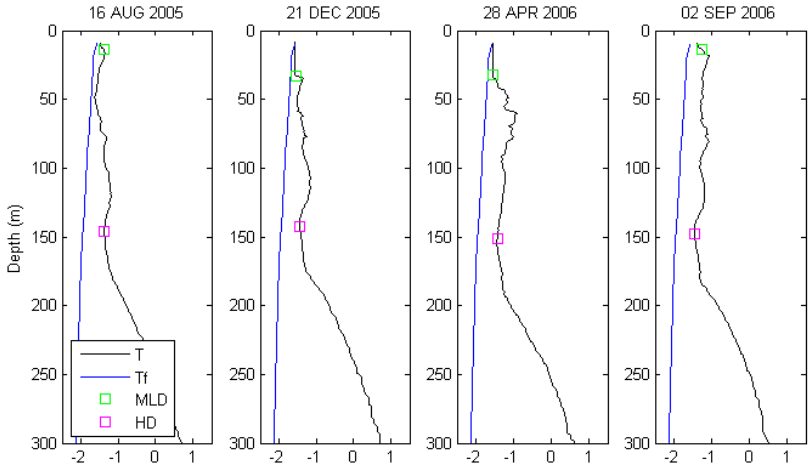

Figure 71. Profiles of temperature (black) measured by ITP 1 with calculated freezing temperature (blue) from four different time. Calculated MLD and HD are indicated in green and magenta, respectively.

To summarize this result, the mean annual cycle of heat content between the mixed layer and the Atlantic layer is not the same in all regions. The heat content at a point is very sensitive to the calculated depth of the halocline, especially considering the discretization of model depths.

D. SPATIOTEMPORAL TRENDS IN UPPER OCEAN HEAT CONTENT

The central purpose of this study is to determine what, if any, trends exist in upper ocean heat content in the Arctic, which may affect and help explain the continues decline of the Arctic sea ice cover for the past decades. To address this, the total heat content between the mixed layer and the Atlantic layer for the Arctic Ocean and for the above-defined sub-regions were calculated for all RASM monthly mean outputs. These time series are plotted in Figure 72. To better quantify the variations, deviations from the mean annual cycles are plotted in Figure 73. The heat content of this layer increases by

approximately 1.5 x 10^9 TJ, or 40%, from 1948 to 1990. It decreases by about 0.25 x 10^9 TJ, or about 6%, in the 1990s, but then increases again by a similar amount in the 2000s.

This heat increase is not uniform across all regions. The eastern region does show an increase in heat content of about 0.5 x 10^8 TJ, about 25%, but only in the time range of 1990 to 2010. The central region showed a larger increase of heat content, 1 x 10^8 TJ, almost doubling. A large increase came between 1964 and 1976, and another large increase between 2005 and 2010. The largest increase in heat content is in the west and in CAA regions. Both regions experienced increases of over 2 x 10^8 TJ before 1990. The CAA region decreased during the first 10 years, though. Heat content decreased in both of these regions from 1990-2010 to about 1.5 x 10^8 TJ. From 1960 to 2010, heat content in every region increases.

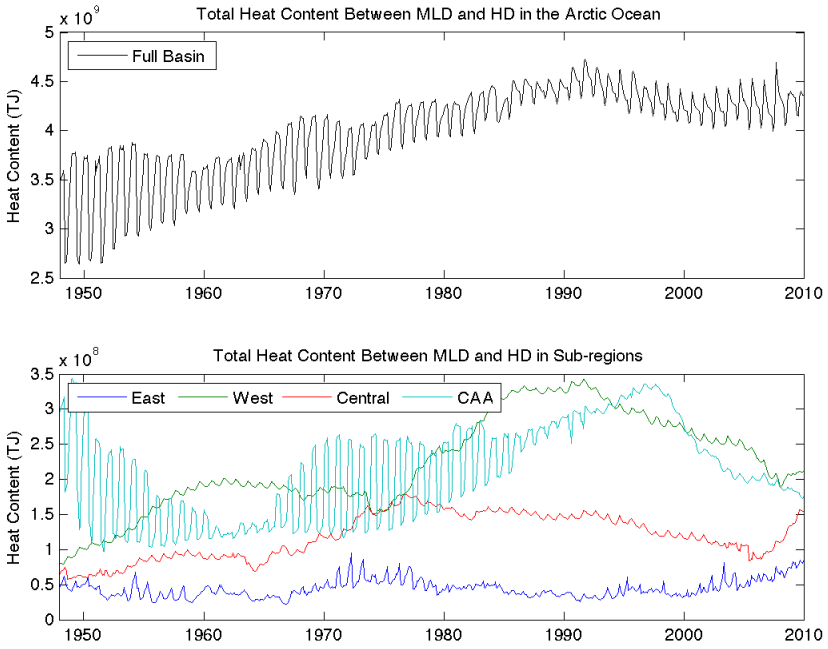

Figure 72. Time series of heat content between the MLD and HD for the full Arctic Ocean (top) and the individual sub-regions (bottom).

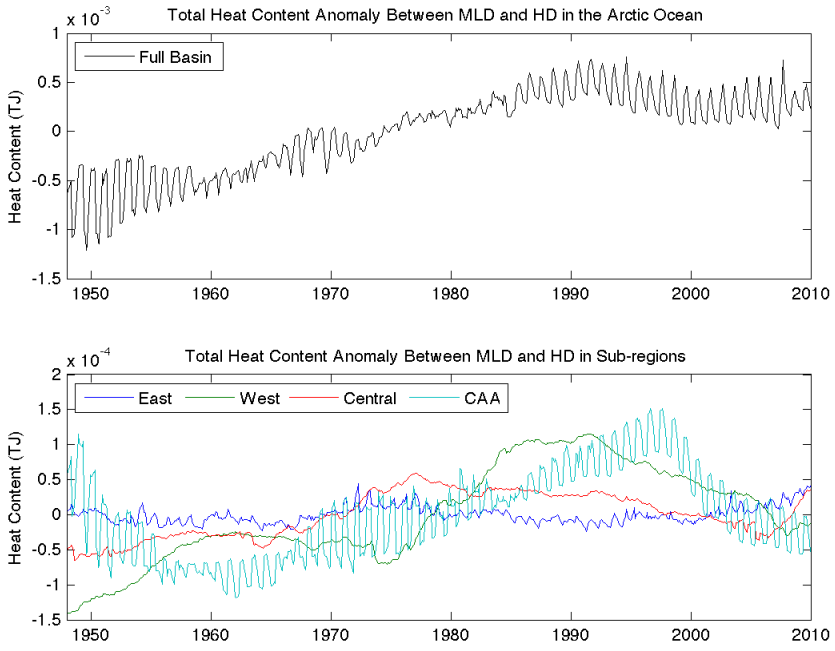

Figure 73. Anomalies of heat content for the Arctic Ocean (top) and individual sub-regions (bottom).

There is a time period where data from both ITP observations and RASM output exist, from 2005 to the end of 2009. While a direct comparison of heat content magnitudes is difficult due to previously discussed reasons, trends can be compared. Figure 74 shows the total heat content and heat content anomalies for the sub-regions East, West, and Central for the time period when model results and observations both exist. The CAA region has been excluded because none of the selected ITPs spent any significant time in that region. In both the western and central regions, there is a significant increase in modeled heat content. Heat content decreases from 2004 to 2008 in the eastern region, but then increases again in the final two years. For comparison, refer to Figure 59 in Chapter IV, which plots heat content derived from western Arctic ITP measurements. Hence, there is a positive trend in western Arctic heat content in both observations and RASM.

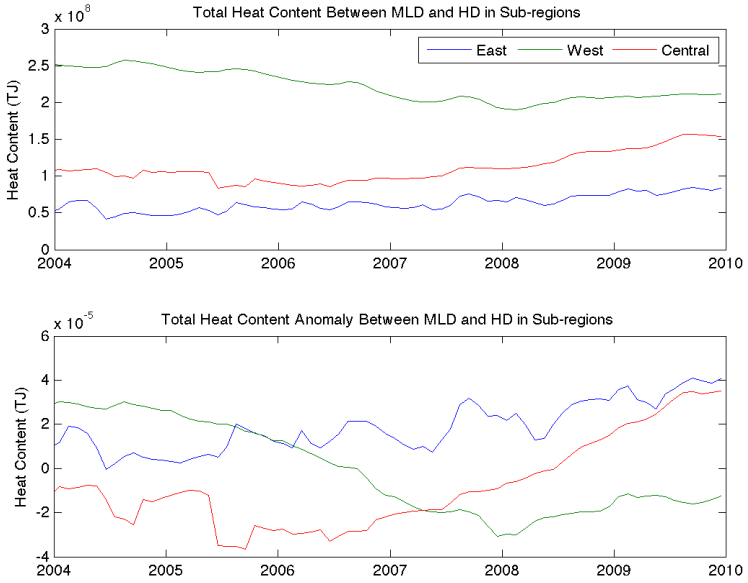

Figure 74. Modeled regional heat content (top) and heat content anomalies (bottom) for the eastern, western, and central sub-regions of RASM for the period 2004 through 2009.

Another way to examine spatial patterns of heat content change is by looking at maps of mean heat content for various time periods. The period from 1948 to 1979 is considered as a control or a reference period. Heat content per model grid cell are averaged for each of the decades of 1980 to 1989, 1990 to 1999, and 2000 to 2009, and then the difference between those decades and the control period are plotted in Figures 75 and 76. It can be easily seen in Figure 81 that there is significantly more heat in the western Arctic. The heat is concentrated along the slope regions from the Chukchi Sea through the Beaufort Sea to the Canadian Arctic Archipelago, and along the southern edges of the deep basin in the western Arctic. The eastern regions of the Arctic experience little change in heat content over the decades, while the western regions show significant increases in heat content. In particular, the upper ocean heat content was highest in the 1990s in the western Arctic, which is coincident with the shift in sea ice thickness and extent as discussed in Maslowski et al. (2012) and Stroeve et al. (2011b).

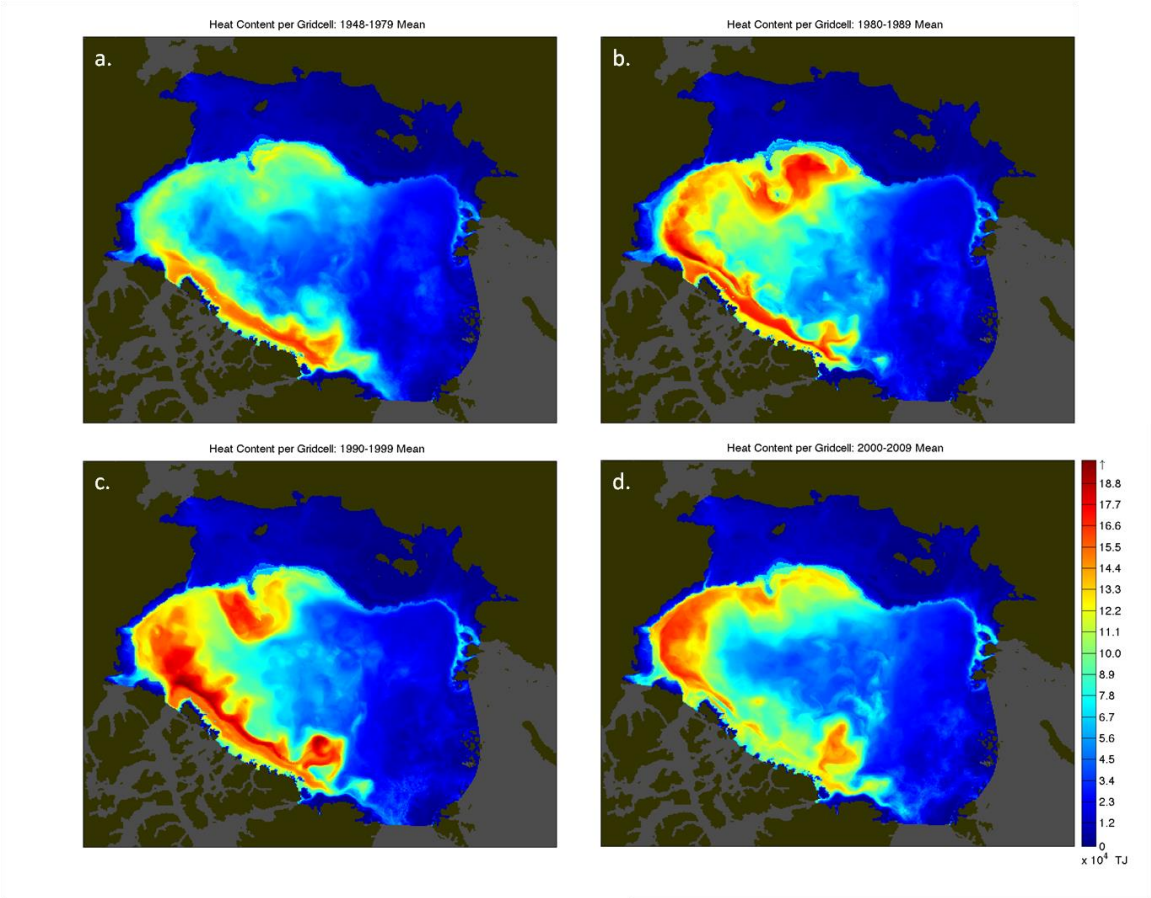

Figure 75. Modeled heat content between MLD and HD, per model grid cell, and averaged for 1948 to 1979 (a), 1980 to 1989 (b), 1990 to 1999 (c), and 2000 to 2009 (d). All figures have the same color scale.

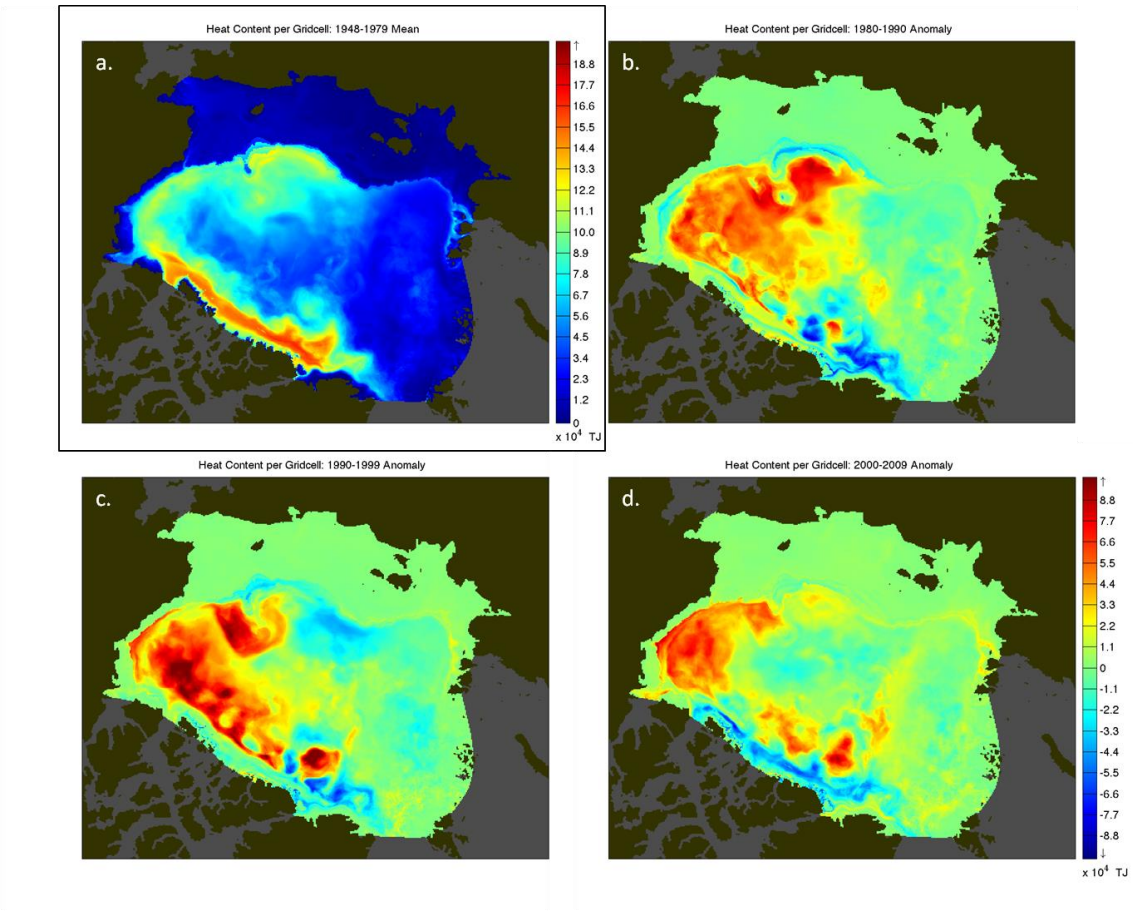

Figure 76. Modeled MLD-HD heat content decadal anomalies (decadal mean minus long term mean of 1948 to 1979, a) for 1980-1989 (b), 1990-1999 (c), and 2000-2009 (d). Panels b, c, and d share the same scale. For the anomalies, warm colors indicate positive anomalies (greater heat content than the long term mean) while cool colors indicate negative anomalies (less heat content than the long term mean). Green color indicates values of heat content that are similar to those of the long term mean.

THIS PAGE INTENTIONALLY LEFT BLANK

VI. CONCLUSIONS AND RECOMMENDATIONS FOR FUTURE STUDIES

A. CONCLUSIONS

In this thesis, it has been shown that there is a significant quantity of heat in the Arctic Ocean just below the mixed layer both in a regional model and based on in-situ profiles scattered across the Arctic Ocean. If this at least some of this heat is entrained into the mixed layer, it may significantly alter the surface heat balance at the air-ocean-ice boundary and could have already contributed to the continuous decline of Arctic sea ice volume during the satellite era.

This result is sensitive to the choice of the top/bottom depths in which heat content is estimated and considered able to affect sea ice. This sensitivity is very small for the upper depth, as the differences between using the surface, 33 m, and a dynamic mixed layer depth, are small at all regions and on all time scales. The choice of lower depth limit, however, makes a major difference. This is due to the fact that the halocline, the upper limit of the warm Atlantic layer, varies in depth across the Arctic Ocean. Because the strong density gradient across the halocline inhibits vertical mixing, heat from the Atlantic layer has little or no influence on the heat content above. Therefore, it is recommended that only heat content from above the halocline should be considered as available for entrainment into the surface mixed layer. Heat content in this layer (defined as the upper ocean) remains present throughout winter, it has increased in recent decades, especially in the western Arctic, and it may limit ice growth in winter and help melt sea ice during the summer season. The bulk magnitudes of heat content calculated from monthly mean temperature and salinity fields simulated by the ice-ocean component of the Regional Arctic System Model closely match the values of heat content estimates from observations made by Ice Tethered Profilers.

Upper ocean heat content is not uniformly distributed across the Arctic Ocean. Excluding the contributions of heat content from the Atlantic layer, there is significantly more subsurface ocean heat content in the western Arctic Ocean, especially in the Beaufort Sea, over the Chukchi Plateau region, and along the northern slope of the

Canadian Arctic Archipelago. This spatial distribution of heat content was reported based on both observational and modeled data sets.

According to the RASM-H ice-ocean model hind-cast, there has been a substantial increase in subsurface ocean heat content, especially prior to 1992, and after 2000. Observations from ITPs, available since 2005, also show an increase in upper ocean heat content. This change has not been spatially uniform. Not only do the western regions of the Arctic Ocean contain more heat content, but they have experienced the largest changes in heat content as well. According to the model, heat content below the mixed layer but above the halocline in the western Arctic Ocean has approximately doubled during the period of 1948 to 1990. This increase in western Arctic Ocean heat content may be partly responsible for the preconditioning and the rapid reduction of sea ice cover in the west.

There was a slight decline in upper ocean heat content in the 1990s. It is possible that some of this ocean heat was used for melting ice or removed to the atmosphere through the increasing areal fraction of first-year sea ice, which would offset the trend of increasing heat content. As sea ice became younger and thinner, it was able to drift more swiftly, deform more, and permit greater surface momentum and turbulent heat fluxes. This would allow for increased heat transfer out of the ocean and into the atmosphere. Process studies of heat exchanges between the atmosphere, sea ice, and ocean are needed to support this hypothesis.

B. RECOMMENDATIONS FOR FUTURE STUDY

This study provided objective estimates of the total amount of heat in the Arctic Ocean, which is readily available for entrainment into the mixed layer, for the past six decades. This thesis does not investigate ways in which this heat may be entrained into the mixed layer, and we leave this area of investigation for subsequent study. Future studies should further investigate such processes as mesoscale eddies, transient wind-driven mixing events, sea ice deformation and shelf-basin interactions. One significant contributor of sea ice loss may be synoptic-scale storms. Studies have shown that storms cause significant ice deformation and loss over time scales of a few days (Overeem et al.

2011; Asplin et al. 2012; Simmonds and Rudeva 2012). However, these studies focus on mechanical break-up and redistribution of ice and do not address the possibility of heat entrainment from below the mixed layer as a source of reduced ice growth in winter and increased sea ice melt in summer. Another process worth investigating is vertical mixing induced by internal waves. Although large-scale mean internal wave energy in the Arctic is small when compared to lower latitudes, it has been observed that it may dominate vertical mixing on local and seasonal scales (Rainville and Woodgate 2009).

To further study these processes, we will need more observations in the pan-Arctic region of not just the ocean, but also ice, atmosphere, and the land. This lack of observations is a known issue among the scientific community. A recent report by the National Research Council (2012) states a lack of observations of ice-ocean conditions is a key challenge in advancing predictive capability in the Arctic System. According to this report, there are several initiatives under way that will help overcome this challenge. One of these initiatives is the Defense Research Initiative in the Marginal Ice Zone (MIZ), sponsored by the Office of Naval Research, is currently underway and includes a large field project during the spring and summer of 2014. The MIZ project will collect data from ITPs, Autonomous Ocean Flux Buoys, Ice Mass Balance buoys, wave buoys, floats, autonomous weather stations, and more, to collect information from the air, sea, and ice in the western Arctic. These data should enable process studies to investigate mechanisms for transferring heat between the atmosphere, sea ice, and ocean (Office of Naval Research [ONR] 2014). Another proposed field study in the Arctic is the Multidisciplinary drifting Observatory for the Study of Arctic Climate (MOSAiC), initiated by the Atmospheric Working Group of the International Arctic Science Committee (IASC). The goals of this project are to deploy an array of atmospheric, ice, and oceanographic observing sensors on a variety of platforms in a network "specifically designed to characterize the important processes within the atmosphere-ice-ocean system that impact the sea-ice mass and energy budgets" (IASC 2014). The MIZ and MOSAiC initiatives are only two field studies of many underway or planned, and all of these will be of great benefit to our understanding of the Arctic System.

It was also shown in this study that heat content calculations are sensitive to the depth of the halocline. Other ways to determine the halocline depth should be explored, verified *in-situ* and analyzed for sensitivity. It is possible that the configuration of the ocean component of RASM used in this study is misplacing the halocline or may be misrepresenting the temperatures at the level of the halocline. Other, possibly higher resolution, model configurations should be investigated to see if the halocline depth and temperature could be better simulated. Such configurations could include various vertical mixing parameterizations, increased vertical resolution, or more physical formulation of the vertical coordinate in the ocean model. It is possible that the way that this configuration, H-case, handles freshwater inflow via climatological restoration may be affecting the results. Other configurations of the ocean component, such as RASM G-case, which replaces the surface restoration to climatological salinity with a realistic freshwater forcing (including river runoff and precipitation minus evaporation fluxes), should be compared to verify these potential impacts. It would also be worthwhile to explore alternative vertical coordinate systems. The ocean component of RASM uses a fixed height coordinate system, but there also exists terrain following coordinate models, isentropic or isopycnal models, and scaled height (z*) models (Adcroft and Campin 2003). These alternate coordinate systems, or hybrid combinations of two or more of them, would likely affect the results of this study.

The analysis of heat content indicated the presence of strong spatial and temporal trends. Spectral analysis of the heat content time series and empirical orthogonal analysis of the spatial patterns should be conducted to better identify spatial as well as seasonal, inter-annual, and multi-decadal patterns. These types of analyses may also offer insight into physical processes that may be forcing the Arctic on longer time scales such as the Arctic Oscillation or Pacific-North American/Pacific Decadal Oscillations. Notwithstanding, the time series analysis in this thesis is a necessary precursor toward understanding the issues at hand.

This study used the stand-alone ice-ocean components of RASM and lays the foundation for expanding this type of analysis to the fully coupled RASM model results. This would allow greater degrees of freedom, permitting the study of how cross-

component processes, such as river runoff and bio-chemical processes, can affect the geo-physical components. By using a coupled regional model for the next stage of this work, we are taking a step towards evaluating and improving the ability of ESMs to resolve ocean heat content and its effects on sea ice. Improving our understanding of processes and feedbacks between ocean heat, the atmosphere, and sea ice, is a requirement for better forecasting future sea ice and Arctic climate conditions. These efforts will reduce uncertainty and provide government, commercial, and military policy makers the information they need to make better decisions now.

THIS PAGE INTENTIONALLY LEFT BLANK

APPENDIX. ADDITIONAL FIGURES

A. ADDITIONAL RASM HEAT CONTENT TIME SERIES FIGURES

The following figures are full time series heat content calculated by using the five different sets of depth limits, for each of the four sub-regions defined in Chapter IV.

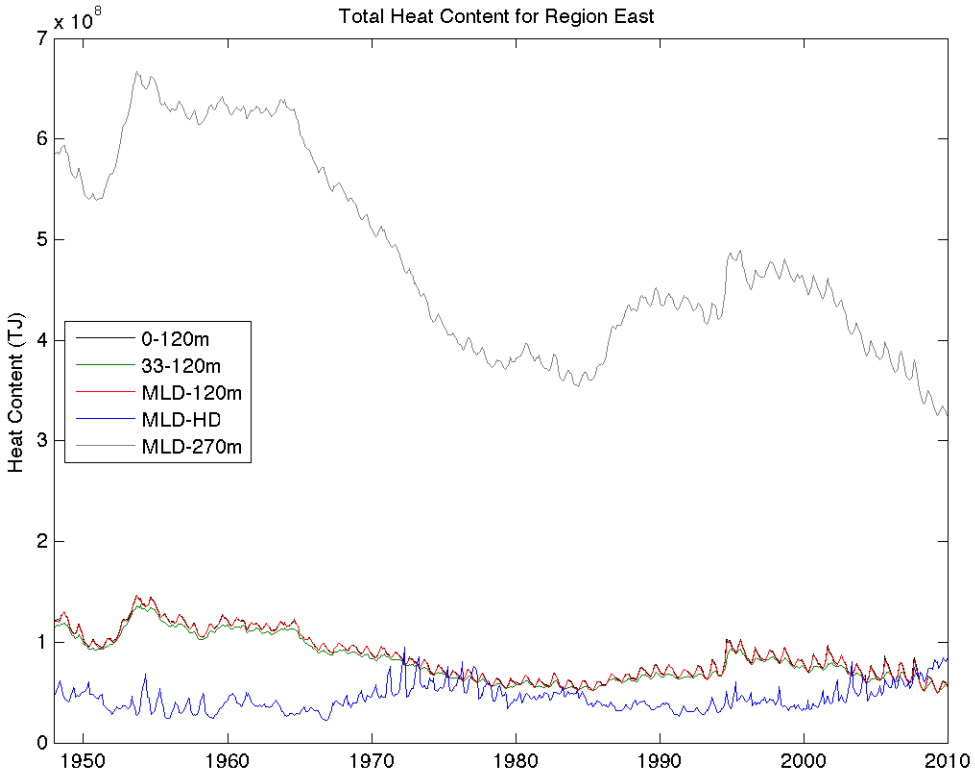

Figure 77. Full time series of heat content calculated five ways for eastern sub-region.

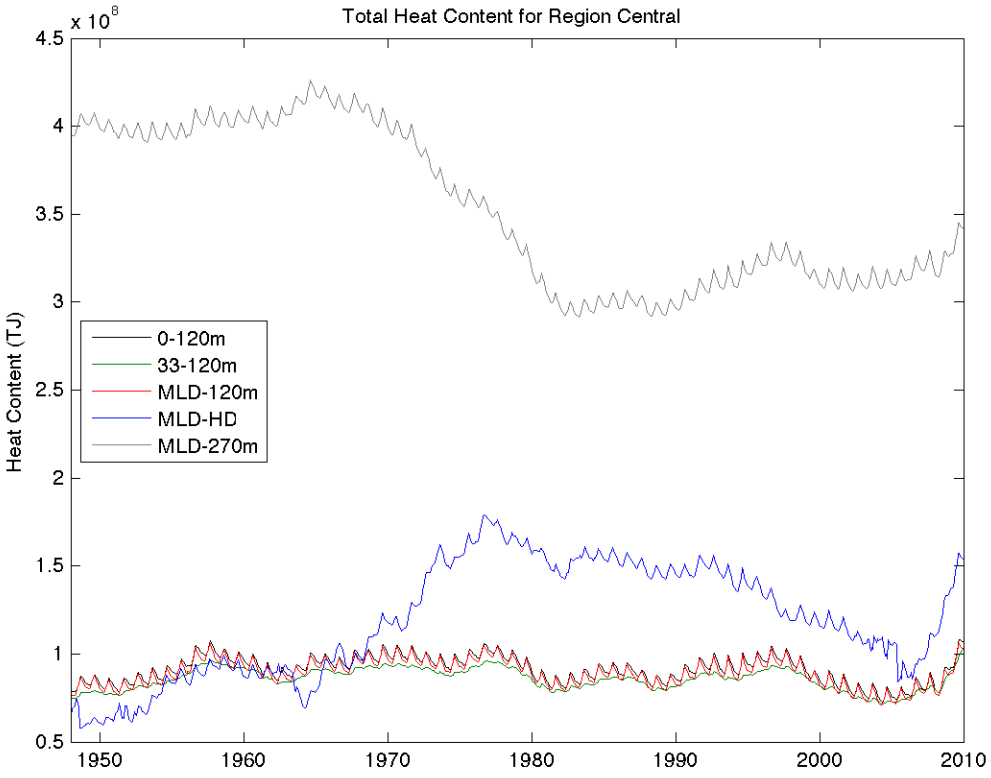

Figure 78. Same as Figure 77, but for the central sub-region.

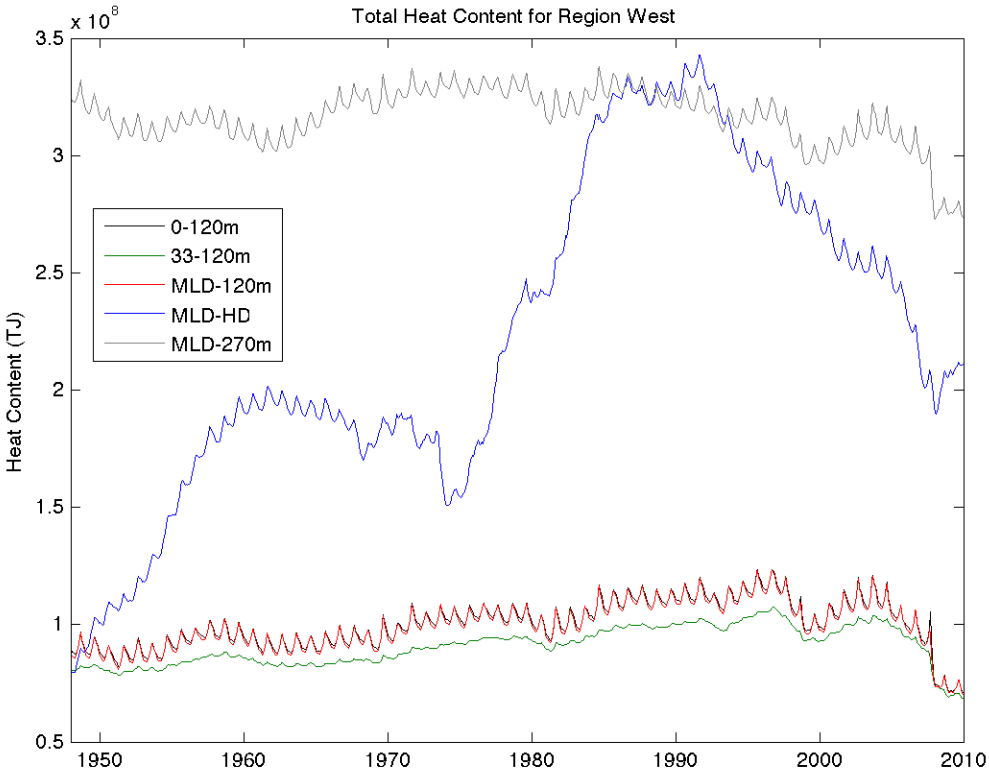

Figure 79. Same as Figure 77, but for the western sub-region.

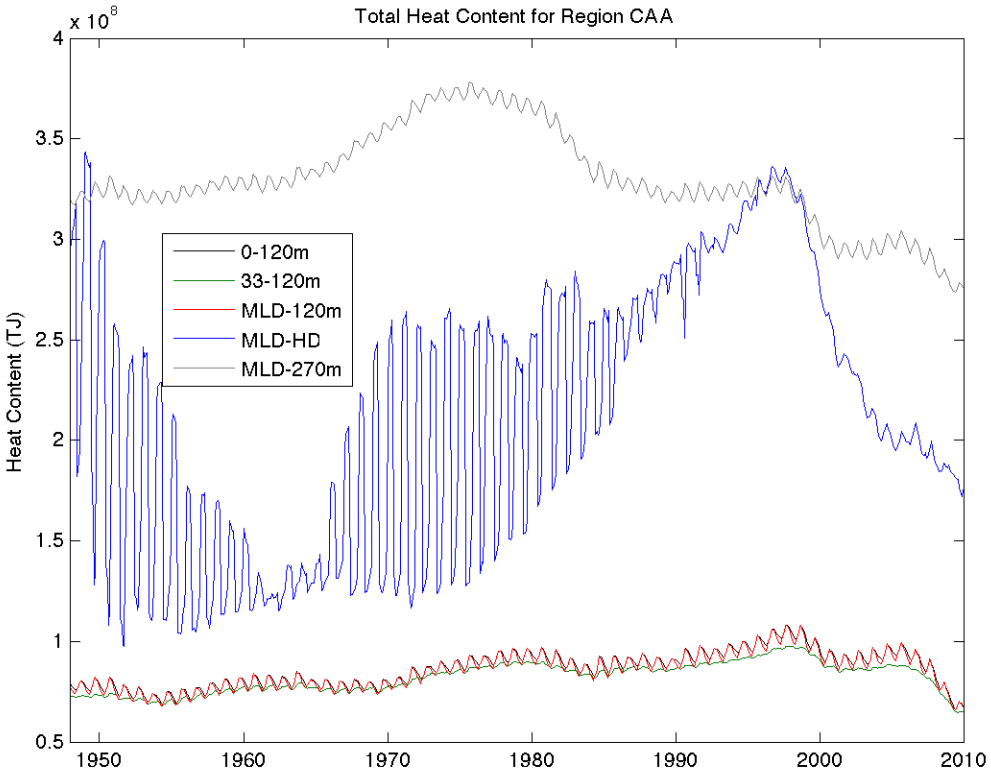

Figure 80. Same as Figure 77, but for the Canadian Arctic Archipelago sub-region.

B. ADDITIONAL ITP HEAT CONTENT TIME SERIES FIGURES

The following figures contain similar MLD, HD, and heat content time series for the ITPs analyzed in this study that are not shown in Chapter 4. These data are summarized in the histograms included in Chapter IV.

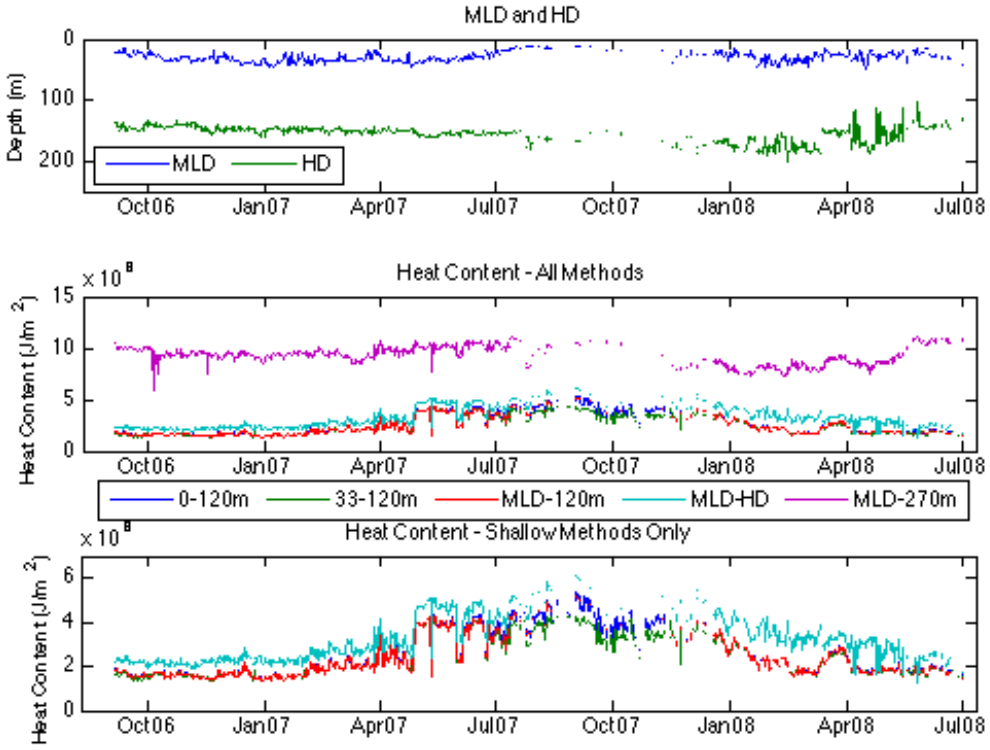

Figure 81. MLD and HD (top panel), heat content computed in five ways (middle panel), and heat content computed in four ways (bottom panel) for ITP 6.

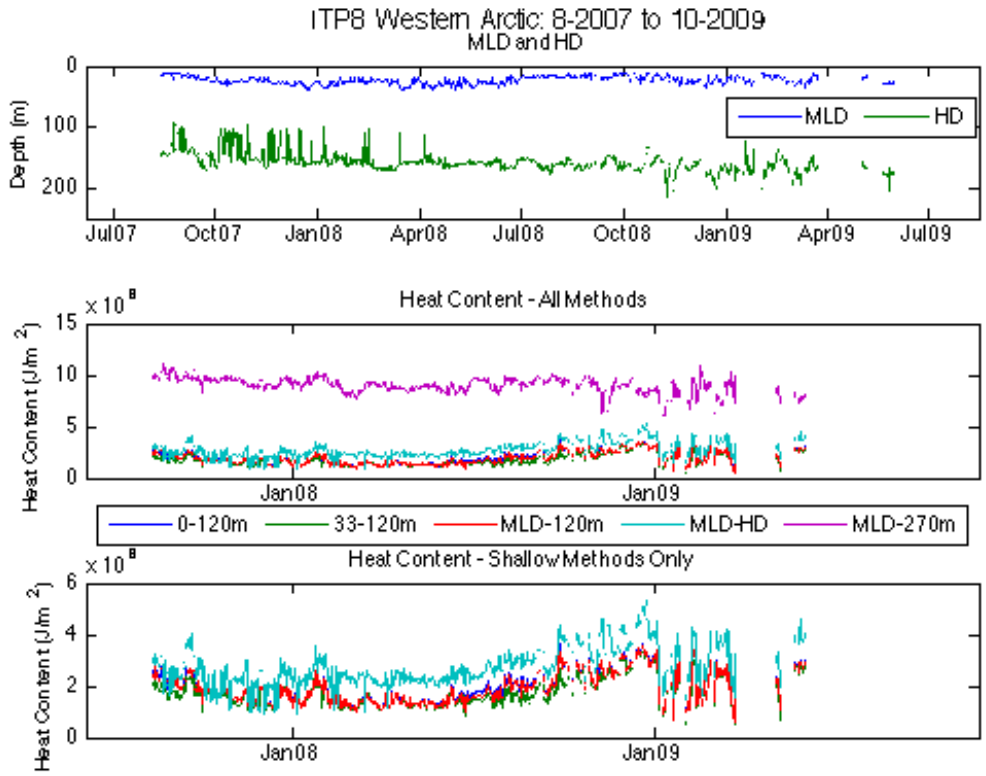

Figure 82. Same as Figure 81, but for ITP 8.

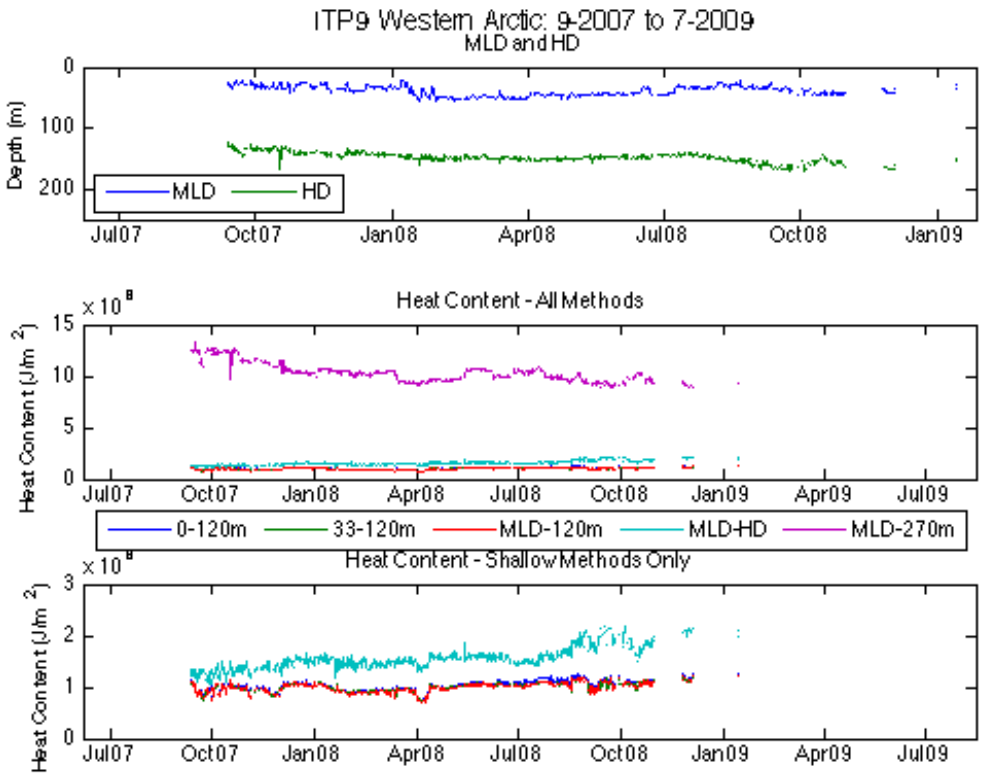

Figure 83. Same as Figure 81, but for ITP 9.

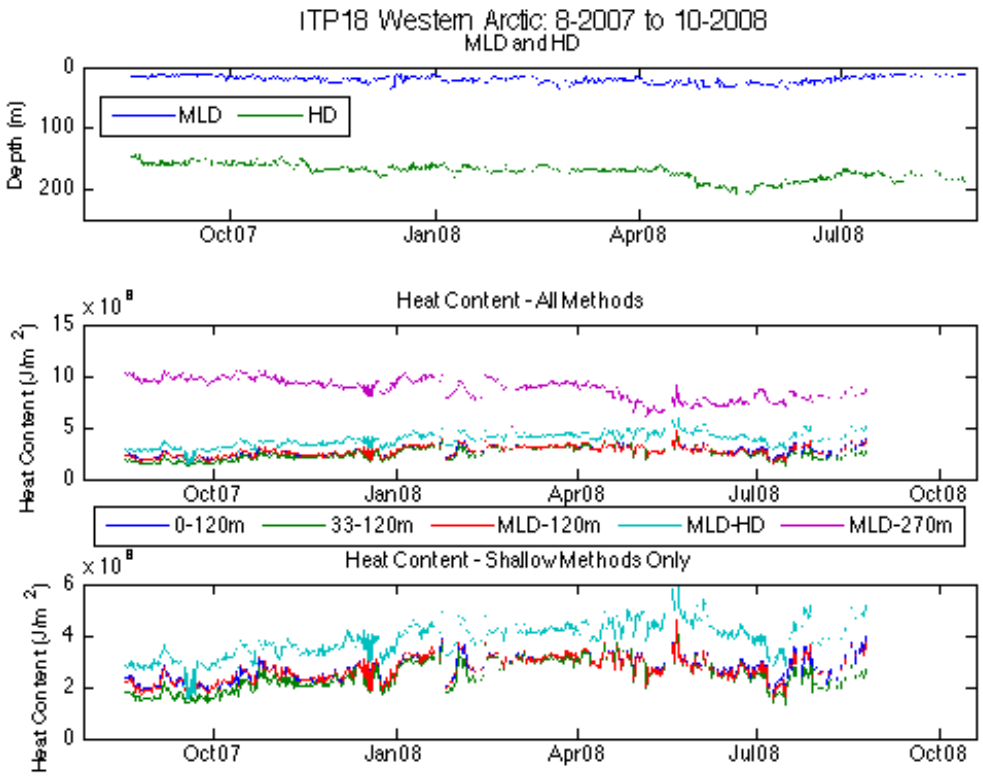

Figure 84. Same as Figure 81, but for ITP 18.

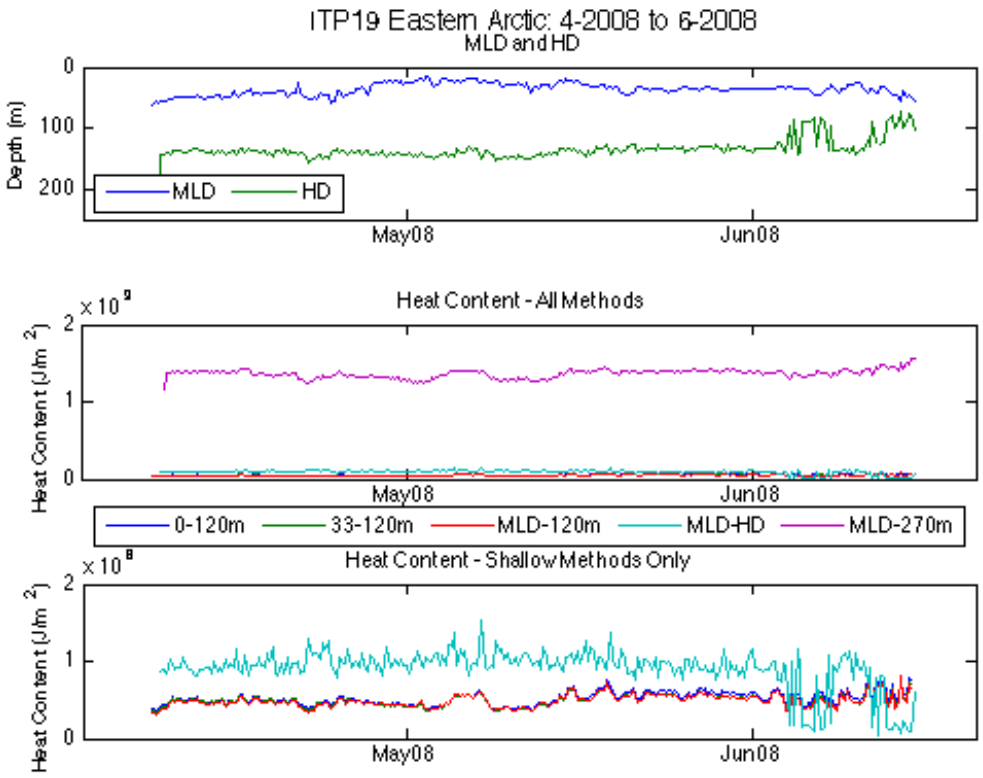

Figure 85. Same as Figure 81, but for ITP 19.

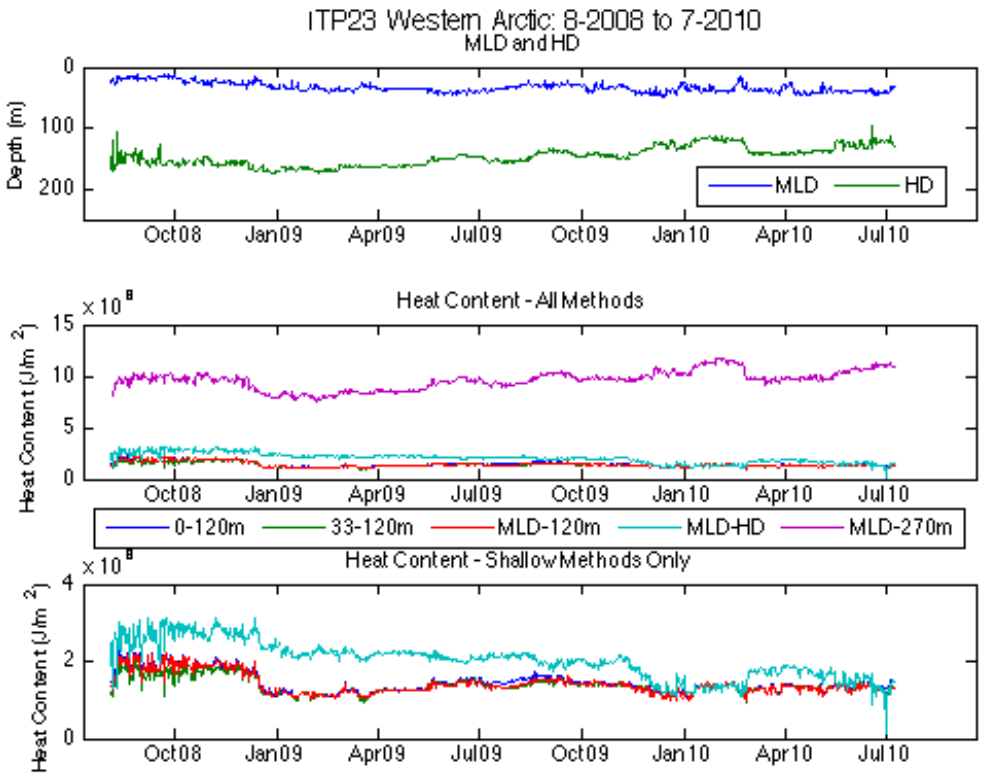

Figure 86. Same as Figure 81, but for ITP 23.

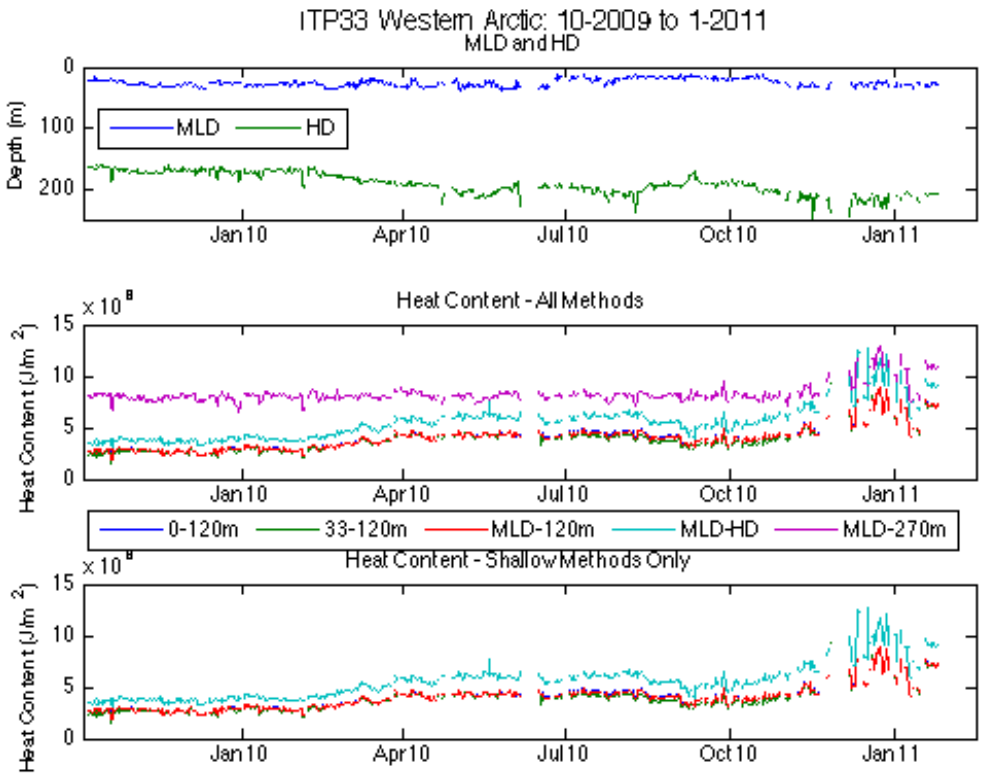

Figure 87. Same as Figure 81, but for ITP 33.

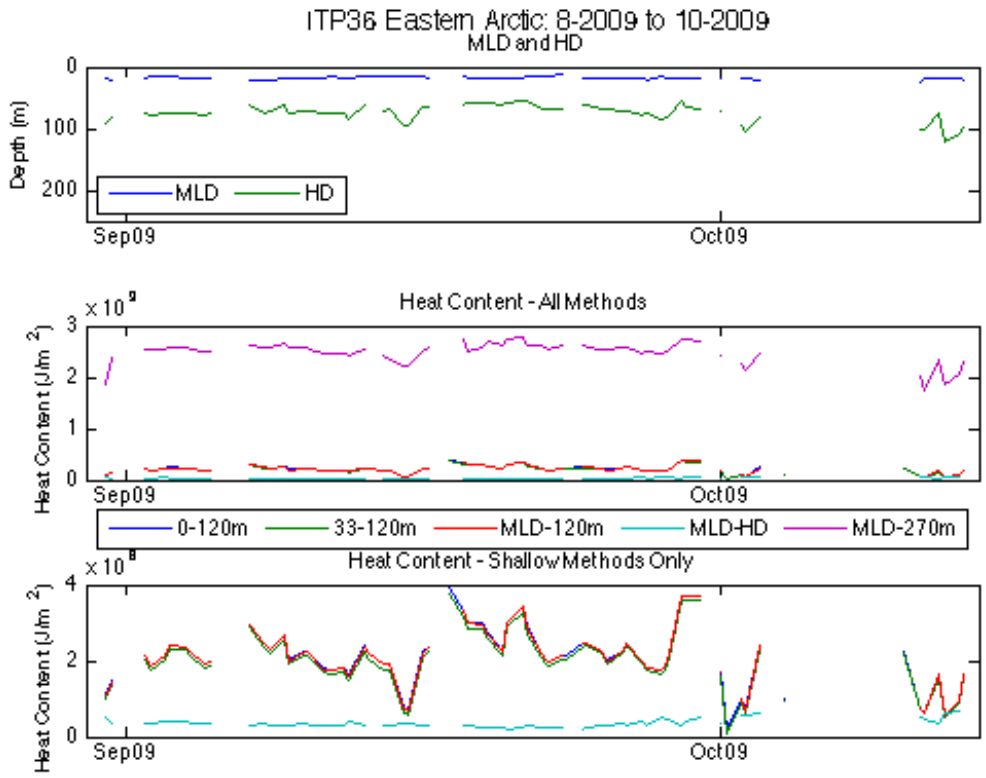

Figure 88. Same as Figure 81, but for ITP 36.

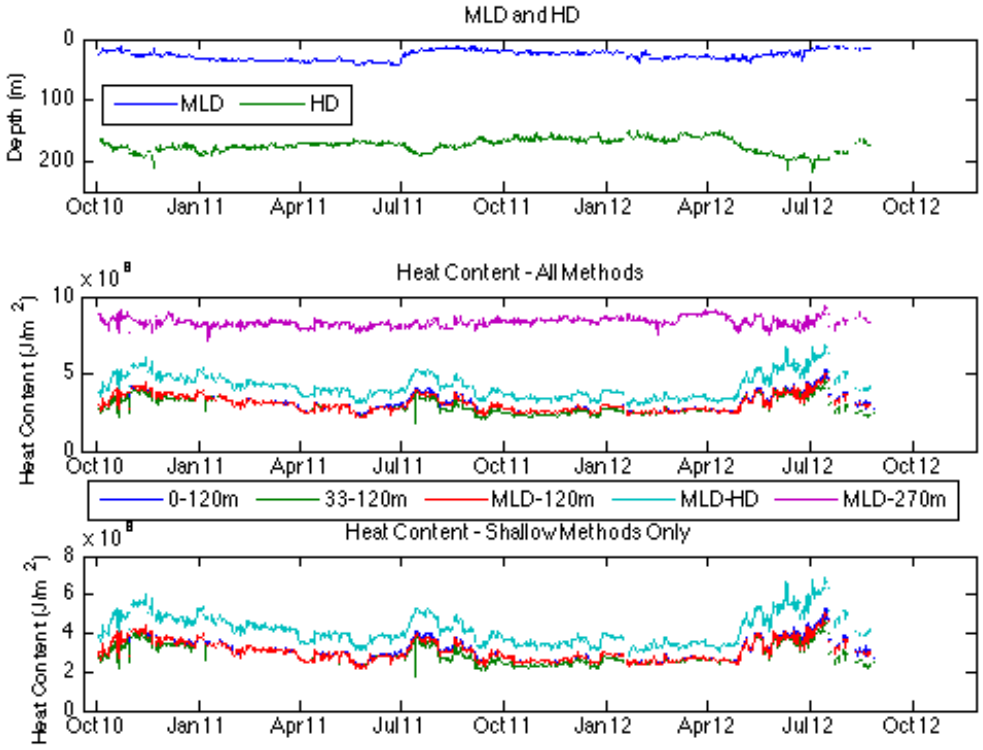

Figure 89. Same as Figure 81, but for ITP 41.

THIS PAGE INTENTIONALLY LEFT BLANK

LIST OF REFERENCES

Adcroft, A., and J. Campin, 2003: Rescaled height coordinates for accurate representation of free-surface flows in ocean circulation models, *Ocean Modeling*, **7**, 269–284.

Arctic Centre, cited 2014: Arctic Indigenous Peoples. [Available online at http://www.arcticcentre.org/InEnglish/SCIENCE-COMMUNICATIONS/Arctic-region/Arctic-Indigenous-Peoples].

Arctic Council, 2009: *Arctic Marine Shipping Assessment 2009 Report.* Arctic Council, Norwegian Chairmanship, Oslo, Norway, 290 pp.

Arctic Council, cited 2014: About the Arctic Council. [Available online at http://www.arctic-council.org/index.php/en/about-us/arctic-council/about-arctic-council].

Argo, cited 2014: Argo – part of the integrated global observation strategy. [Available online at http://www.argo.ucsd.edu].

Asplin, M. G., R. Galley, D. G. Barber, and S. Prinsenberg, 2012: Fracture of summer perennial sea ice by ocean swell as a result of Arctic storms, *J. Geophys. Res.*, **117**, C06025, doi:10.1029/2011JC007221.

Berkman, P. A., and O. R. Young, 2009: Governance and environmental change in the Arctic Ocean, *Science*, **324**, 339–340.

Briegleb, B. P., and B. Light, 2007: A Delta-Eddington multiple scattering parameterization for solar radiation in the sea ice component of the Community Climate System Model. NCAR Technical Note NCAR/TN-47, 100 pp.

Department of the Navy, Memorandum for Distribution, 2009: Task Force Climate Change. [Available online at http://greenfleet.dodlive.mil/files/2010/09/Task-Force-Climate-Change-charter.pdf].

Derksen, C., & Brown, R., 2012:. Spring snow cover extent reductions in the 2008-2012 period exceeding climate model projections. *Geophys. Res. Lett.* doi:10.1029/2012GL053387

DuVivier, A. K., and J. J. Cassano, 2013: Evaluation of WRF model resolution on simulated mesoscale winds and surface fluxes near Greenland. *Mon. Wea. Rev.*, **141**, 941–963.

Food and Agriculture Organization of the United Nations, cited 2014: Yearbook of Fishery Statistics Summary tables. [Available online at ftp://ftp.fao.org/FI/STAT/summary/default.htm].

Flato, G. M., 2011: Earth system models: an overview. WIREs Clim Change, 2, 783–800. doi: 10.1002/wcc.148.

Gent, Peter R., and Coauthors, 2011: The Community Climate System Model version 4. *J. Climate*, **24**, 4973–4991.doi: http://dx.doi.org/10.1175/2011JCLI4083.1.

Giorgi, F., 2005: Climate change prediction. *Climatic Change*, **73**, 239–265.

Haynes, J. E., cited 2010: Understanding the importance of oceanic forcing on sea ice variability. [Available online at http://calhoun.nps.edu/public/handle/10945/5078].

Holte, J., and L. Talley, 2009: A new algorithm for finding mixed layer depths with applications to Argo data and Subantarctic mode water formation, *J. Atmos. Oceanic Technol.*, **26**, 1920–1939.

Howell, S. E. L., C. R. Duguay, and T. Markus, 2009: Sea ice conditions and melt season during variability within the Canadian Arctic Archipelago: 1979–2009, *Geophys. Res. Lett.*, **36**, L 10502, doi:10.1029/2009GL037681.

Hufford, G., 2009: National Weather Service Alaska Region Sea Ice Program. *3rd Symposium on the Impacts of an Ice-Diminishing Arctic on Naval and Maritime Operations*, Annapolis, MD, U.S. National Ice Center and the U.S. Arctic Research Commission, 1-39.

Humpert, M., and A. Raspotnik, 2012: The future of Arctic shipping along the Transpolar Sea Route, *The Arctic Yearbook 2012*, 281–307. [Available online at http://www.arcticyearbook.com].

Hurrell, J. W., M. M. Holland, P. R. Gent, S. Ghan, J. E. Kay, P. J. Kushner, and S. Marshal, 2013: The Community Earth System Model: a framework for collaborative research. *Bulletin of the American Meteorological Society,* **94**, 1339–1360. doi:10.1175/BAMS-D-12-00121.1

IASC, cited 2014: MOSAiC. [Available online at http://www.mosaicobservatory.org].

IPCC, 2013: *Climate Change 2013: The Physical Science Basis: Contribution of Working Group 1 to the Fifth Assessment Report of the Intergovernmental Panel on Climate Change*, edited by T. F. Stocker, D. Qin, G.-K. Plattner, M. Tignor, S. K. Allen, J. Boschung, A. Nauels, Y. Xia, V. Bex, and P. M. Midgley, Cambridge University Press.

Jackett, D. R., T. J. McDougall, R. Feistel, D. G. Wright, and S. M. Griffies, 2006: Algorithms for density, potential temperature, conservative temperature, and the freezing temperature of seawater, *J. Atmos. & Oceanic Techno.*, **23**, 1709–1728.

Jackson, J. M., E. C. Carmack, F. A. McLaughlin, S. E. Allen, and R. G. Ingram, 2010: Identification, characterization, and change of the near-surface temperature maximum in the Canada Basin, 1993–2008. *J. Geophys. Res.,* **115**, C05021, doi:10.1029/2009/JC005265.

Jackson, J. M., S. E. Allen, F. A. McLaughlin, R. A. Woodgate, and E. C. Carmack, 2011: Changes to the near-surface waters in the Canada Basin, Arctic Ocean from 1993–2009: A basin in transition. *J. Geophys. Res.*, **116**, C10008, doi:10.1029/2011JC007069.

Jakobsson, M., L. A. Mayer, B. Coakley, J. A. Dowdeswell, S. Forbes, B. Fridman, H. Hodnesdal, R. Noormets, R. Pedersen, M. Rebesco, H.-W. Schenke, Y. Zarayskaya A, D. Accettella, A. Armstrong, R. M. Anderson, P. Bienhoff, A. Camerlenghi, I. Church, M. Edwards, J. V. Gardner, J. K. Hall, B. Hell, O. B. Hestvik, Y. Kristoffersen, C. Marcussen, R. Mohammad, D. Mosher, S. V. Nghiem, M. T. Pedrosa, P. G. Travaglini, and P. Weatherall, 2012: The International Bathymetric Chart of the Arctic Ocean (IBCAO) Version 3.0, *Geophysical Res. Lett.*, doi: 10.1029/2012GL052219.

Joint World Meteorological Organization-Intergovernmental Oceanographic Commission Technical Commission for Oceanography and Marine Meteorology, cited 2014: World Meteorological Organization (WMO) Publication No. 259 Sea Ice Nomenclature. [Available online at http://www.jcomm.info/index.php?option=com_oe&task=viewDocumentRecord&docID=4438].

Koivurova, T., and E. J. Molenaar, 2009: International Governance and Regulation of the Marine Arctic Overview and Gap Analysis. WWF International Arctic Program, Oslo, Norway, pp 44.

Krishfield, R., J. Toole, A. Proshutinsky, and M.-L. Timmermans, 2008: Automated ice-tethered profilers for seawater observations under pack ice in all seasons. J. Atmos. Oceanic Technol., **25,** 2091–2105.

Kwok R., and D. A. Rothrock. 2009: Decline in Arctic sea ice thickness from submarine and ICESat records: 1958–2008. Geophys. Res. Lett. 36:L15501

Kwok, R., G. F. Cunningham, H. J. Zwally, and D. Yi, 2007: Ice, Cloud, and land Elevation Satellite (ICESat) over Arctic sea ice: Retrieval of freeboard, *J. Geophys. Res.*, **112**, C12013, doi:10.1029/2006JC003978

Langen, P. L., and V. A. Alexeev, 2007: Polar amplification as a preferred response in an idealized aquaplanet GCM. Climate Dynamics, **29,** 305–317. doi: 10.1007/S00382-006-0221-X

Lecomte, O., T. Fichefet, M. Vancoppenolle, F. Domine, F. Massonnet, P. Mathiot, S. Morin, and P. Y. Barriat, 2013: On the formulation of snow thermal conductivity in large-scale sea ice models. *Journal of Advances in Modeling Earth Systems*, **5**, 542–557. doi:10.1002/jame.20039

Lique, C., and M. Steele, 2013: Seasonal to decadal variability of Arctic Ocean heat content: A model-based analysis and implications for autonomous observing systems, J. Geophys. Res. Oceans, **118**, 1673–1695, doi:10.1002/jgrc.20127.

Logerwell, L., 2008: Cruise Report for the 2008 Beaufort Sea Survey. NOAA, U.S. Department of Commerce, National Marine Fisheries Service, Alaska Fisheries Science Center.

Maslowski, W., J. Clement Kinney, and J. Jakacki, 2007: Toward prediction of environmental and Arctic change, *Comp. in Sci. & Eng*., **9**, 6, 29–34.

Maslowski, W., J. L. Clement Kinney, M. E. Higgins, and A. Roberts, 2012: Future of Arctic sea ice, *Annual Review of Earth and Planetary Sciences*, **40**, 625–654.

Maslowski, W., 2013: Understanding the Arctic Climate System. *International Innovation*, pp 70–72, February 2013, Research Media, UK, ISSN 2051-8528.

Maslowski, W., Kinney, J. C., Marble, D. C. and Jakacki, J, 2013: Towards eddy-resolving models of the Arctic Ocean. *Ocean modeling in an eddying regime, Geophys. Monogr. Ser.*, Vol 177, edited by M. W. Hecht and H. Hasumi, Ameri. Geophys. Union, Washington, D. C. doi: 10.1029/177GM16

Maslowski, W., J. L. Clement Kinney, S. R. Okkonen, R. Osinski, A. F. Roberts, W. Williams, 2014: The large scale ocean circulation and physical processes controlling Pacific-Arctic interaction. *The Pacific Arctic Region,* J. M. Grebmeier and W. Maslowski, Ed., Springer, p. 101–132.

McGeehan, T., and W. Maslowski, 2011: Impact of shelf-basin freshwater transport on deep convection in the western Labrador Sea, *J. Phys. Ocean.*, **41**, 2187–2210.

McPhee, M., 2008: *Air-Ice-Ocean Interaction: Turbulent Ocean Boundary Layer Exchange Processes*. Springer, 215 pp

Mills, T., cited 2012: An evaluation of sea ice deformation and its spatial characteristics from the regional arctic system model. [Available online at http://calhoun.nps.edu/public/bitstream/handle/10945/27872/12Dec_Mills_Thomas.pdf?sequence=1].

National Research Council, 2012: Seasonal-to-decadal predictions of Arctic sea ice: challenges and strategies. The National Academies Press, Washington, DC, 80 pp.

National Snow and Ice Data Center, cited 2014: State of the Cryosphere. [Available online at http://nsidc.org/cryosphere/sotc/sea_ice.html]

Northern Sea Route Information Office (NSRIO), cited 2014: Transit Statistics. [Available online at http://www.arctic-lio.com/nsr_transits].

Nguyen, A. T., R. Kwok, and D. Menemenlis, 2011: Source and pathway of the western Arctic upper halocline in a data-constrained coupled ocean and sea ice model, *J. Phys. Ocean*., **42**, 802–823.

Office of Naval Research (ONR), cited 2014: Marginal Ice Zone (MIZ) Program. [Available online at http://www.apl.washington.edu/project/project.php?id=miz].

Office of the Secretary of Defense, 2013: Arctic Strategy. [Available online at http://www.defense.gov/pubs.2013_Arctic_Strategy.pdf]

Okkonen, S. R., C. J. Ashjian, R. G. Campbell, W. Maslowski, J. L. Clement-Kinney, and R. Potter, 2009: Intrusion of warm Bering/Chukchi waters onto the shelf in the western Beaufort Sea, *J. Geophys. Res.*, **114**, C00Q11, doi:10.1029/

Osinski, R., W. Maslowski, A. Roberts, J. Clement Kinney, and A. Craig, 2014: On the sensitivity of sea ice states to variable parameter space in the Regional Arctic System Model., *Ann. Glaciol., submitted.*

Ostreng, W., 2012: Shipping and resources in the Arctic Ocean: a hemispheric perspective, *The Arctic Yearbook 2012*, 247–280. [Available online at http://www.arcticyearbook.com].

Overeem, I., R. S. Anderson, C. W. Wobus, G. D. Clow, F. E. Urban, and N. Matell, 2011: Sea ice loss enhances wave action at the Arctic coast, *Geophys. Res. Lett*., **38**, L17503, doi:10.1029/2011GL048681.

Perovich, D. K., B. Light, H. Eicken, K. F. Jones, K. Runciman, and S. V. Ngheim, 2007: Increasing solar heating of the Arctic Ocean and adjacent seas, 1979–2005: Attribution and role in the ice-albedo feedback, *Geophys. Res. Lett.*, **34**, L19505, doi:10.1029/2007GL031480.

Perovich, D. K., J.A. Richter-Menge, K. F. Jones, and B. Light, 2008: Sunlight, water, and ice: Extreme Arctic sea ice melt during the summer of 2007. *Geophys. Res Lett.*, **35**, doi:Artn L11501 Doi 10.1029/2008gl034007

Rainville, L., and R. A. Woodgate, 2009: Observations of internal wave generation in the seasonally ice-free Arctic, *Geophys. Res. Lett.*, **36**, L23604, doi:10.1029/2009GL041291.

Roberts, A. and Coauthors, 2010: A science plan for regional Arctic system modeling. International Arctic Research Center Tech. paper 10-0001, 47 pp. [Available online at www.iarc.uaf.edu/publications/reports/IARCTP10-0001.pdf].

Roberts, A., A. P. Craig, W. Maslowski, R. Osinski, A. DuVivier, M. Hughes, B. Nijssen, J. Cassano, M. Brunke, 2014: Simulating transient ice-ocean Ekman transport in the Regional Arctic System Model and Community Earth System Model, *Ann. Glaciol,. In review.*

Rudels, B., E. Jones, U. Schauer, and P Eriksson, 2004: Atlantic sources of the Arctic Ocean surface and halocline waters, *Polar Res.,* **23**, 181–203.

Schneider, N., and P. Muller, 1990: The meridional and seasonal structures of the mixed-layer depths and its diurnal amplitude observed during the Hawaii-to-Tahiti Shuttle experiment. *J. Phys. Oceanogr.*, **20**, 1395–1404.

Screen, J. A., & Simmonds, I., 2010:. The central role of diminishing sea ice in recent Arctic temperature amplification. *Nature*, **464**, 1334–1337. doi: 10.1038/Nature09051

Shimada, K., E. Carmack, K. Hatakeyama, and T. Takizawa, 2006: Varieties of shallow temperature maximum waters in the Western Canadian Basin of the Arctic Ocean, *Geophys. Res. Lett.* **28**, 3441–3444.

Showstack, R., 2013: Pentagon Strategy Recognizes Need for Increased Research in the Arctic, *Eos*, **94**, 485–486.

Sigler, M., 2009: Climate Change and Arctic Fisheries. *3rd Symposium on the Impact of an Ice-Diminishing Arctic on Naval and Maritime Operations*, Annapolis, MD, U. S. National Ice Center and the U. S. Arctic Research Commission, 1–28.

Simmonds, I., and I. Rudeva, 2012: The great Arctic cyclone of August 2012, *Geophs. Res. Lett.*, **39**, L23709, doi:10.1029/2012GL054259.

Steele, M., and T. Boyd, 1998: Retreat of the cold halocline layer in the Arctic Ocean, *J. Geophys. Res.*, **103**, 10,419–10,435.

Steele, M., J. Morison, W. Ermold, I. Rigor, M. Ortmeyer, and K. Shimada, 2004: Circulation of summer Pacific halocline waters in the Arctic Ocean, *J. Geophys. Res.*, **109**, C02027, doi:10.1029/2003JC002009.

Stroeve, J.C., M. C. Serreze., M. M. Holland, J. E. Kay, J. Maslanik, and A. P Barrett, 2011b: The Arctic's rapidly shrinking sea ice cover: a research synthesis, *Clim Change,* doi 10.1007/s10584-011-0101-1

Task Force Climate Change /Chief of Naval Operations, 2014: U.S. Navy Arctic Roadmap 2014–2030, 43 pp.

Thomson, R. E., and I. V. Fine, 2003: Estimating mixed layer depth from oceanic profile data, *J. Atmos Oceanic Technol.,* **20**, 319–329.

Timmermans, M.-L., S. Cole, and J. Toole, 2012: Horizontal density structure and restratification of the Arctic Ocean surface layer, *J. Phys. Ocean.*, **42**, 659–668.

Toole, J. M., M.-L. Timmermans, D. K. Perovich, R. A. Krishfield, A. Proshutinsky, and J. A. Richter-Menge, 2010: Influences of the ocean surface mixed layer and thermohaline stratification on Arctic Sea ice in the central Canada Basin, *J. Geophys. Res.*, **115**, C10018, doi:10,1029/2009JC005660.

Treat, C. C., & Frolking, S. (2013). Carbon Storage: A permafrost carbon bomb? *Nature Climate Change*, **3**, 865–867, doi:10.1038/nclimate2010

Turner, J., E. A. Rasmussen, and A. M. Carleton, 2003: Introduction. *Polar Lows - Mesoscale Weather Systems in the Polar Regions*, E. A. Rasmussen and J. Turner, Eds., Cambridge University Press, 1–51.

United Nations Office of Legal Affairs, cited 2014: United Nations Convention on the Law of the Sea of 10 December 1982 Overview and full text. [Available online at http://www.un.org/depts/los/convention_agreements/convention_overview_convention.htm.]

United States Coast Guard, cited 2013: United States Coast Guard Arctic strategy [Available online at http://www.uscg.mil/seniorleadership/DOCS/CG_Arctic_Strategy.pdf].

University of Illinois, 2014: The Cryosphere Today. [Available online at http://arctic.atmos.uiuc.edu/cryosphere/.]

USGS, 2008: Circum-Arctic resource appraisal: Estimates of Undiscovered oil and gas north of the Arctic Circle. USGS Fact Sheet 2008-3049, 4 pp.

Wadhams, P., 2000: *Ice in the ocean*. Gordon and Breach Science Publishers, 351 pp.

Wadhams, P., and N. R. Davis, 2000: Further evidence of ice thinning in the Arctic Ocean. *Geophysical Research Letters,* **27,** 3973–3975.

White House, 2010: *National security strategy.* [Available online at http://www.whitehouse.gov/sites/default/files/rss_viewer/national_security_strategy.pdf].

White House, 2013: *National strategy for the Arctic Region.* [Available online at http://www.whitehouse.gov/sites/default/files/docs/nat_arctic_strategy.pdf].

White House, 2014: *Implementation plan for the national strategy for the Arctic Region*. [Available online at http://www.whitehouse.gov/sites/default/files/docs/implementation_plan_for_the_national_strategy_for_the_arctic_region_-_fi....pdf].

Wijesekera, R. W., and M. C. Gregg, 1996: Surface layer response to weak winds, westerly bursts, and rain squalls in the western Pacific warm pool, *J. Geophys. Res.***, 101**, 977–997.

Woods Hole Oceanographic Institution, cited 2014: Ice-tethered profiler. [Available online at http://www.whoi.edu/itp]

WHOI, cited 2014: Arctic ocean circulation. [Available online at http://www.whoi.edu/main/topic/arctic-ocean-circulation]

Woodgate, R., K. Aagaard, J. H. Swift, K. K. Falkner, and W. M. Smethie Jr., 2005: Pacific ventilation of the Arctic Ocean's lower halocline by upwelling and diapycnal mixing over the continental margin, *Geophys. Res. Lett.*, **32**, L18609, doi:10.1029/2005/GL023999.

INITIAL DISTRIBUTION LIST

1. Defense Technical Information Center
   Ft. Belvoir, Virginia

2. Dudley Knox Library
   Naval Postgraduate School
   Monterey, California